NASA-TP-2501 19860010879

NASA Technical Paper 2501

December 1985

Flight Measurements of Surface Pressures on a Flexible Supercritical Research Wing

Clinton V. Eckstrom

NASA

NASA Technical Paper 2501

1985

Flight Measurements of Surface Pressures on a Flexible Supercritical Research Wing

Clinton V. Eckstrom

Langley Research Center
Hampton, Virginia

National Aeronautics and Space Administration

Scientific and Technical Information Branch

SUMMARY

A flexible supercritical research wing, used for both demonstration of active-control technology and evaluation of aerodynamic loads, was flight-tested as part of the NASA Drones for Aerodynamic and Structural Testing (DAST) Program. The wing, designated as ARW-1 (aeroelastic research wing), was geometrically similar to the wing of the F-8 supercritical wing (SCW) airplane but was smaller, as appropriate for the modified drone aircraft on which it was flown. The conditions for design cruise were a Mach number of 0.98 and a lift coefficient of 0.36 at an altitude of 45 000 ft. Aerodynamic loads, in the form of wing surface pressure measurements, were obtained for off-design flight test conditions during flights at altitudes of 15 000, 20 000, and 25 000 ft at Mach numbers from 0.70 to 0.91. Surface pressure coefficients determined from pressure measurements at 80 orifice locations are presented individually as a nearly continuous function of angle of attack for constant values of Mach number. Nonlinear variations of surface pressure coefficients with angle of attack (for Mach numbers ≥0.85) suggested the presence and movement of pressure gradients as angle of attack was varied. The surface pressure coefficients are also presented individually as a function of Mach number for an angle of attack of 2.0°. The nearly continuous values of the pressure coefficient clearly show details of the pressure gradient, which occurred in a rather narrow Mach number range. The effects of changes in angle of attack, Mach number, and dynamic pressure are also shown by chordwise pressure distributions for the range of test conditions experienced. Results for changes in dynamic pressure indicate the wing experienced an increase in twist (leading edge down) for the higher dynamic pressures. Reynolds numbers for the tests ranged from 5.7 to 8.4×10^6. Limited comparisons with F-8 SCW data indicate local differences, but overall the data were reasonably close.

INTRODUCTION

The aeroelastic research wing (ARW-1) was flight-tested as part of the NASA Drones for Aerodynamic and Structural Testing (DAST) Program (refs. 1 and 2). The objectives of the ARW-1 flight test operations were to evaluate an active-control flutter suppression system (FSS) and to evaluate the effects of flexibility on wing aerodynamic loading. The ARW-1 was a supercritical wing of shape (airfoil, twist, droop, etc.) and planform similar to the wing of the F-8 supercritical wing (SCW) airplane (ref. 3) but is smaller, as appropriate for the BQM-34F drone aircraft on which it was flown. A special feature of the ARW-1 was that it was designed to flutter within the drone flight envelope, thereby providing the desired instability for active-control evaluation (refs. 4 to 7). Unfortunately, because of an improper gain setting in the FSS, uncontrolled flutter developed resulting in loss of the wing early in the flight test program (ref. 8). Although the flight tests performed did not achieve all the planned goals, data were obtained from a sufficient range of test conditions to accomplish part of the aerodynamic loads evaluation.

This paper presents results from aerodynamic loads measurements on the DAST ARW-1 at subcritical Mach numbers. The results are in the form of wing surface pressure coefficients for pressure measurements taken at four semispan stations. Sufficient data were obtained to allow presentation of the surface pressure coefficients for individual orifice locations as nearly continuous functions of angle of attack, Mach number, and dynamic pressure. Conventional chordwise pressure distributions are also presented for a range of Mach numbers, angles of attack, and dynamic pressures. In addition, a limited comparison of these data with data for the F-8 SCW is presented.

WING AND INSTRUMENTATION

Research Wing

The ARW-1 was an early version of a supercritical wing that was designed for cruise at a high transonic speed (M = 0.98). (A list of symbols and abbreviations used in this paper appears after the references.) Photographs of the drone aircraft with the ARW-1 taken during flight testing are presented in figures 1(a) and 1(b). The general arrangement of the BQM-34F drone aircraft with the ARW-1 is presented in figure 2. The basic wing planform, which was defined by extending the straight line portions of the wing leading and trailing edges to the fuselage centerline, had (1) a reference area S of 30 ft^2, (2) a span b of 171.0 in., (3) a root chord length c_r of 36.99 in., (4) a taper ratio λ of 0.365, (5) a leading-edge sweep angle of 44.32° (40.0° sweep at the 50-percent-chord line), (6) an aspect ratio of 6.8, and (7) an mac of 27.06 in. In the inboard region (YF < 33 in.), the wing was modified by glove fairings designed to give the same drag rise Mach number for the wing root sections as for its outboard sections (ref. 9). For FSS test purposes there were hydraulically actuated control surfaces on the outboard wing panels, as shown in figure 2. The control-surface hinge line was at the 77-percent-chord line, with the control surface extending from η = 0.788 to 0.905.

The wing was constructed in a tooling fixture whose shape accounted for the predicted wing structural deflection due to aerodynamic loading at the cruise conditions (M = 0.98, h = 45 000 ft, q_∞ = 207 psf, and C_L = 0.36). The wing structural deflection at cruise was estimated by applying the F-8 SCW model wind-tunnel-measured pressure distributions to the wing analytical finite-element structural model. The resulting incremental wing deflections were then subtracted from the wing cruise shape to give the tooling fixture shape. The design cruise shape was defined in reference 10, and the ordinates for the wing tooling fixture shape are presented in table I. The differences between the design cruise shape and the tooling fixture shape expressed in terms of the wing leading- and trailing-edge vertical locations z and the wing twist ε are presented in figures 3 and 4, respectively.

The wing structure consisted of a wing center section, the right and left wing panels, which had removable leading and trailing edges, and the wing-tip sections. The wing center section was machined from a thick aluminum plate to a configuration that provided a high degree of stiffness without consideration of minimum weight. The joining surface between the wing center section and each wing panel was in a plane normal to the 25-percent-chord line (front spar centerline) for that wing panel.

The structure of the wing panels consisted of a front spar located at the 25-percent-chord line, a rear spar located at the 60-percent-chord line, upper and lower stringers located midway between the front and rear spars, and ribs that were positioned perpendicular to the front spar and located every 12 in. along the span. A special streamwise rib located near the wing tip functioned as the outboard end fitting for the front and rear spars and as the attachment location for the removable wing-tip sections. The fiberglass skins between the front and rear spars were riveted to the spar and rib flanges to form a single-cell box beam. The fiberglass skins that formed the leading- and trailing-edge sections and the tip section were attached to the spar and rib flanges with screws to allow for access to instrumentation and hydraulic system components. Details of the wing structural arrangement are shown in figure 5.

Measurements of the wing airfoil shape were made after wing fabrication was completed. The leading-edge and center-section surface deviations from the template airfoil shapes (tooling fixture ordinates) were generally less than ±0.020 in. The trailing-edge surface deviations from the template airfoil shapes were larger because the trailing-edge section skins had a tendency to curl (trailing edge down) as the fiberglass cured, resulting in a slight increase in camber at the cusp region of the airfoil. A listing of the deviations of the wing leading- and trailing-edge vertical locations from the tooling fixture shape are presented in table II. A comparison of airfoil ordinates at a typical wing station (YF = 37.11 in.) for both the left and right semispans is presented in table III. All screw and rivet heads and the gaps between the wing skin sections were filled with body putty and smoothed, and a final coat of paint was applied before flight-testing started.

The ARW-1 was similar in shape and planform to the wing on the F-8 supercritical wing (SCW) airplane except for a few significant differences. These were: (1) the ARW-1 had a 0° wing incidence angle (at the aircraft centerline), whereas the F-8 SCW had a 1.5° wing incidence angle; (2) in the region immediately adjacent to and overlapping the drone fuselage, the glove chord length was reduced to keep the upper surface of the glove contour from rising above the fuselage profile; (3) the drone fuselage did not have area-ruled fairings; and (4) different wing deformations were developed at flight conditions other than for cruise due to differences in the tooling fixture shape and in the structural stiffness of the two wings.

Instrumentation

The right wing panel was instrumented for measurement of chordwise surface pressures at four semispan stations. (See table IV and fig. 6.) The installation of outboard trailing-edge control surfaces, which were required for the implementation of the FSS, precluded use of orifice tubing aft of the 60-percent-chord line (rear spar location) on orifice rows 3 and 4.

The surface pressure for each orifice location was measured with a separate miniature pressure transducer. All the pressure transducers were located in two insulated, temperature-controlled compartments that were located inside the leading edge near the wing root. The transducer temperatures were controlled to help minimize measurement errors which could result from large temperature changes. Pressure transducers capable of measuring to ±3.5 psi and ±2.0 psi were used in these measurements. Each pressure transducer range was kept small to improve measurement resolution. The ±3.5 psi pressure transducers were used to measure surface pressures at orifices located on the wing upper surface from the leading edge to the 50-percent-chord line and on the wing lower surface at the 3-percent-chord line, where the largest surface pressure measurements were expected. For the remaining orifices, the pressure transducers had a range of ±2.0 psi. The static pressure measured in the wing center section (fuselage area) was used as the reference pressure for all the surface pressure transducers. A measurement was also made of the difference between the aircraft pitot-probe static pressure and the wing reference static pressure. Surface pressure measurements were corrected through use of the measured difference in static pressure for the two locations.

Onboard pressure measurements were transmitted to the ground receiving station by means of a 9-bit pulse-code modulation (PCM) telemetry system with a main frame sampling rate of 300 samples per second. The surface pressure measurements were on subcommutated channels, with each pressure transducer being sampled at a rate of 30 samples per second. Measurements of flight conditions (aircraft angle of attack, dynamic pressure, etc.) were transmitted to the ground station by means of a separate 10-bit PCM system with a sampling rate of 500 samples per second. The flight data needed for the analyses for this report were on subcommutated channels that were sampled at either 50 or 100 samples per second. Both PCM systems transmitted data to the ground receiving station for recording on magnetic tape continuously throughout each flight test.

PRESENTATION OF RESULTS

The results of this investigation are presented in the following figures:

Figure

Test data:
- Flight-test conditions 7

Surface pressure coefficients:
- Variations of wing surface pressure coefficients with angle of attack for flight 10 8
- Variations of wing surface pressure coefficients with angle of attack for flight 11 9
- Variations of wing surface pressure coefficients with Mach number for flight 10 10
- Variations of wing surface pressure coefficients with Mach number for selected orifice locations 11
- Variations of wing surface pressure coefficients with dynamic pressure 12

Chordwise pressure distributions:
- Chordwise pressure distributions for flight 10 13
- Chordwise pressure distributions for flight 11 14
- Variations of chordwise pressure distributions for different Mach numbers but approximately equal dynamic pressures 15
- Variations of chordwise pressure distributions for equal Mach numbers but different dynamic pressures 16
- Variations of chordwise pressure distributions with combined changes in Mach number and dynamic pressure for flight 10 17
- Variations of chordwise pressure distributions with combined changes in Mach number and dynamic pressure for flight 11 18
- Variations of chordwise pressure distributions from flight tests of DAST ARW-1 and F-8 SCW 19
- Variations of chordwise surface pressure distributions from DAST ARW-1 flight tests and F-8 SCW scaled-model wind-tunnel results 20

DISCUSSION OF RESULTS

Test Data

The DAST ARW-1 surface pressure measurements presented herein were obtained from two flight tests designated as flights 10 and 11. The flight-test conditions for flights 10 and 11 are presented in figure 7. Flight 10 was flown at nominal altitudes of 20 000 and 25 000 ft, and flight 11 was flown at a nominal altitude of 15 000 ft. The ranges of Mach number and dynamic pressure at which the majority of the data were acquired are shown by the rectangular symbols in figure 7. Some data were also acquired at other test conditions since the instrumentation system recorded data on a continuous basis. Eight of the test conditions were selected for the primary data analysis. The eight primary test conditions are shown in figure 7 by the closed symbols. The number of data samples, the mean Mach number and dynamic pressure and their standard deviations, and the Reynolds number for each of the eight primary test conditions are listed in table V. The number of data samples for each test condition resulted from the use of only 2 samples per second of the available 30 samples per second.

Surface Pressure Coefficients

Effects of changes in angle of attack.- The variations of wing surface pressure coefficients with angle of attack are presented in figures 8 and 9 for flights 10 and 11, respectively. The data presented are for Mach numbers of 0.75, 0.80, 0.85, 0.875, and 0.90 at an altitude of 25 000 (flight 10) and for Mach numbers of 0.70, 0.75, and 0.80 at an altitude of 15 000 (flight 11). These are the primary test conditions indicated in figure 7 by the closed symbols. It should be noted that both dynamic pressure and Mach number changed when the flights were at constant altitude. The data are presented in a stacked format in figures 8 and 9, with the data set for each Mach number having a different origin point on the vertical axis. The number of data samples in each data set is listed in table V. The line (or curve) through each data set represents a least-squares second-degree polynomial equation fit to that data set.

The data in figures 8 and 9 show that the variations of pressure coefficient with angle of attack are nearly linear for Mach numbers from 0.70 to 0.80. At Mach numbers from 0.85 to 0.90, there are several pronounced nonlinear variations of pressure coefficient with angle of attack. These nonlinear variations are most noticeable on the upper surface at orifice row 1 from $x/c = 0.30$ to 0.61 (fig. 8(a)) and on the lower surface at orifice row 4 from $x/c = 0.03$ to 0.15 (fig. 8(h)). The nonlinear variations of pressure coefficient with angle of attack are attributed to the presence of weak pressure gradients which moved relative to the orifice locations as the angle of attack was changed.

The data also show that the slopes (i.e., the sensitivities) of the upper-surface pressure coefficients relative to angle of attack are generally positive and that the slopes of the lower-surface pressure coefficients relative to angle of attack are generally negative. This indicates that the respective local flow velocities increased and decreased with increasing angle of attack. The slope of the pressure coefficients relative to angle of attack is largest for the orifice locations near the wing leading edge. At the more downstream orifice locations, the sensitivity of pressure coefficients to angle of attack is reduced considerably to small or negligible values.

In general, the data of figures 8 and 9 indicate an expected variation with and sensitivity to angle of attack. Also indicated are nonlinearities which suggest the presence and movement of pressure gradients as angle of attack was varied.

Effects of changes in Mach number.- Variations of wing surface pressure coefficients that occurred with changes in Mach number for flight 10 at an angle of attack of 2.0° are presented in figure 10. The data were obtained while flying at a constant altitude of 25 000 ft; therefore, both dynamic pressure and Mach number were changing as shown on figure 7. The nearly continuous form of the data results from including measurements obtained both at and between the test conditions noted in figure 7 (for $M \geq 0.80$). The surface pressure coefficients increase significantly with increasing Mach number at some orifice locations. The increases, which are most pronounced for the upper-surface orifices at row 1 (fig. 10(a)) at $x/c = 0.20$ to 0.70, indicate the presence and movement of a pressure gradient (recompression wave) on the wing upper surface as the Mach number was varied from about 0.82 to 0.92.

For the lower-surface orifices at row 1 (fig. 10(b)), there is evidence of a recompression wave at $x/c = 0.40$ for $M = 0.90$, and this wave moved back to $x/c = 0.50$ for $M \approx 0.92$. For the upper-surface orifices at row 2 (fig. 10(c)), there is evidence of a recompression wave located at $x/c = 0.80$ for $M \approx 0.89$. For orifice rows 3 and 4, the recompression wave effects are most clearly shown on the lower surface (figs. 10(f) and 10(h)) at $x/c = 0.15$.

Variations of wing surface pressure coefficients with Mach number are presented in a stacked arrangement in figure 11 for selected orifice locations on the upper surface at row 1. The data for an angle of attack of 2.0° (fig. 11(a)) are a replot of those presented in figure 10(a) for $x/c = 0.20$ to 0.70. Similar data for an angle of attack of 2.5° are presented in figure 11(b). These data show the significant effect that small changes in Mach number can have on the surface pressure coefficients when a recompression wave is present. The data also show that the recompression wave moved downstream as Mach number was increased. The largest change in the surface pressure coefficient was approximately 0.30, which occurred at $x/c = 0.40$ for Mach numbers from 0.87 to 0.89 (fig. 11(a)). The recompression wave was located farther downstream for the same Mach numbers when the angle of attack was increased from 2.0° to 2.5° (fig. 11(b)). The nearly continuous data presented in figure 11 clearly define the details of the pressure coefficient variations associated with the recompression wave that occur in a relatively narrow Mach number range.

Effects of changes in dynamic pressure.- The variations of wing surface pressure coefficients that occurred with changing dynamic pressure are presented in figure 12 for a Mach number of 0.75 and an angle of attack of 2.0°. Data from flights 10 and 11 are shown on the same plot to increase the range of dynamic pressures. The data from flight 10 were acquired when the aircraft was flying initially at an altitude of 20 000 ft and then while climbing to and flying at an altitude of 25 000 ft. (See fig. 7.) The data from flight 11 were acquired while flying at an altitude of 15 000 ft. The data of figure 12 indicate that near the leading edge of the wing and outboard on the span (orifice rows 3 and 4), the upper-surface pressure coefficients become more positive as dynamic pressure was increased. Likewise, for the lower surface the pressure coefficients become more negative with increased dynamic pressure. This indicates that the local angles of attack became more negative as dynamic pressure was increased (i.e., the wing was twisted negatively along the span).

Variations in surface pressure coefficients have been presented for changes in angle of attack, in Mach number, and in dynamic pressure. In each case, as the test condition was changed the wing loading and, therefore, the twist distribution for the wing also changed. As a result the surface pressure coefficient variations presented in figures 8 to 12 represent the combined effects of test condition changes and concurrent wing-twist-distribution changes. For dynamic pressure (fig. 12), the changes in surface pressure coefficients are believed to be primarily due to wing-twist-distribution changes resulting from changes in aerodynamic loading.

Chordwise Pressure Distributions

Surface pressure coefficients used to generate chordwise pressure distributions were obtained primarily from the curves fit to the data of figures 8 and 9. The curves represent least-squares second-degree polynomial equations fit to the data sets. The equations, which represent the data sets, were also used to compute surface pressure coefficients for each orifice location at angle-of-attack increments of 0.5° within the original data range. Surface pressure data arrays were formed for each Mach number (figs. 8 and 9). Results from figures 10 and 11, which more clearly define surface pressure variations with Mach number, were then used to modify the surface pressure data arrays where there was significant scatter in the data sets of figures 8 and 9. All chordwise pressure distributions presented in the following sections are based on results listed in the surface pressure coefficient data arrays of tables VI to XIII.

Chordwise pressure distributions for flights 10 and 11 are presented in figures 13 and 14, respectively. The pressure distributions from flight 10 are for angle-of-attack increments of 0.5° from 1.5° to 4.0° for $M = 0.75$ (fig. 13(a)) and from 2.0° to 3.0° for $M = 0.80$ to 0.90 (figs. 13(b) to 13(c)). The pressure distributions from flight 11 are for angle-of-attack increments of 0.5° from 2.0° to 3.0° for $M = 0.70$ to 0.80 (figs. 14(a) to 14(c)). These angles of attack are representative of the range of angles of attack for which data were acquired for each primary test condition.

The pressure distributions presented in figures 13 and 14 for orifice row 1 show that a lifting pressure developed essentially along the entire chord length for all angles of attack and Mach numbers. For orifice rows 2, 3, and 4, the pressure distributions indicate that the region near the wing leading edge experienced some down loading (the surface pressure on the wing lower surface was more negative than the surface pressure on the upper surface) for most angles of attack and Mach numbers. The down loading was largest for the lowest angles of attack shown. Since the airfoil shape from the leading edge to the midchord was essentially symmetric, the pressure distributions with down loading near the leading edge indicate that the local angle of attack was negative. This effect is to be expected because of the large negative twist that was built into the wing (fig. 4). The only test condition for which lifting pressures were developed along the entire span was for an angle of attack of 4.0° at a Mach number of 0.75 (fig. 13(a)). Note that the pressure distributions in the cusp region of the airfoil (aft of $x/c = 0.70$, measured at orifice rows 1 and 2) do not change significantly with angle of attack. In general, the chordwise pressure distributions show that the outboard portion of the wing leading edge was subjected to varying degrees of down loading for most of the test conditions evaluated.

Effects of changing Mach number.- Variations of chordwise pressure distributions obtained at different Mach numbers but at essentially the same dynamic pressures are presented for comparison in figure 15. In figure 15(a), a comparison may be made of chordwise pressure distributions for $M = 0.70$ and 0.85, for which the respective mean values of dynamic pressure were 410 and 406 psf. A similar comparison may be made in figure 15(b) for $M = 0.75$ and 0.90, for which the respective mean values of dynamic pressure were 466 and 456 psf. Comparisons of the data show that an increase in lifting pressure occurred on the wing upper surface at row 1 ($x/c = 0.20$) when going from $M = 0.70$ to 0.85 and that a larger increase in lifting pressures occurred when going from $M = 0.75$ to 0.90 (for $x/c = 0.20$ to 0.40). The other noticeable change occurred on the lower surface at orifice row 4 where there was an increase in down loading for the higher Mach numbers.

Effects of changing dynamic pressure.- Variations of chordwise pressure distributions for equal Mach numbers but different dynamic pressures are presented for comparison in figure 16. Data are presented in figure 16(a) for a Mach number of 0.75 and dynamic pressures of 320 and 466 psf. Similar data for a Mach number of 0.80 and dynamic pressures of 360 and 533 psf are presented in figure 16(b). Section normal-force coefficients are presented in table XIV for comparison of the loadings. These data show the primary effect of increasing the flight dynamic pressure by approximately 50 percent was a reduction in loading for comparable Mach numbers and angles of attack.

The significance of the change in dynamic pressure on local wing twist can be evaluated by noting that for orifice row 4 the c_n' value for flight 10 at $\alpha = 2.0°$ was essentially the same as for flight 11 at $\alpha = 3.0°$. Thus, the effect of the increase in dynamic pressure was about the same as if the angle of attack at orifice row 4 decreased by 1.0°.

Combined effects of changes in Mach number and dynamic pressure.- The variations in chordwise pressure distributions that occurred with combined changes in Mach number and dynamic pressure for flights 10 and 11 are presented in figures 17 and 18. The combinations of Mach number and dynamic pressure are the primary test conditions for flights 10 and 11 as noted in figure 7. The data show the combined effects of changes in both Mach number and dynamic pressure for angles of attack of 2.0° (figs. 17(a) and 18(a)) and 3.0° (figs. 17(b) and 18(b)).

The pressure distributions for orifice row 1 at an angle of 2.0° indicate the development and downstream movement of a pressure gradient on the wing upper surface as Mach number and dynamic pressure were increased. This effect was reported in the previous discussion on the effects of Mach number on the surface pressure coefficients (fig. 10(a)). The pressure distributions for orifice row 1 at an angle of attack of 3.0° (fig. 17(b)) were similar to those for 2.0° (fig. 17(a)) except that the pressure gradient was located farther downstream for equivalent Mach numbers. For orifice row 2 the pressure distributions remained relatively unchanged for both angles of attack as Mach number increased. For orifice rows 3 and 4 at an angle of attack of 2.0° the steep pressure gradient on the wing lower surface between $x/c = 0.10$ and 0.15 indicates that a recompression wave was located between these two orifice locations. This finding is consistent with the surface pressure coefficient data presented in figures 10(f) and 10(h). At an angle of attack of 3.0°, the large negative pressures (down loading) and the steep pressure gradients on the lower surface that were evident at 2.0° were considerably reduced. For the limited Mach number range of flight 11 (fig. 18), the measured surface pressure data are quite similar. The most noticeable differences in pressure distributions occurred outboard on the wing at orifice rows 3 and 4. These differences were probably more a result of wing twist due to increased dynamic pressure (i.e., increased wing torsion loadings) than a result of Mach number changes.

Comparison of DAST ARW-1 Pressure Distributions With F-8 SCW Pressure Distributions

Comparison with F-8 SCW flight-test data.- The Mach numbers and angles of attack for which measured wing surface pressure data are available for the F-8 SCW airplane (ref. 9) are different than the Mach numbers and angles of attack tested with the DAST vehicle. To obtain a comparison of the pressure distributions, the results for the DAST ARW-1 (flight 10) at a Mach number of 0.80 (angle-of-attack range from 1.0° to 3.2°) were extrapolated to obtain data for an angle of attack of 3.73°, which was the lowest comparable angle of attack for which F-8 SCW results were available. The extrapolation was accomplished by means of the least-squares second-degree polynomial equations described in the section entitled "Chordwise Pressure Distributions." (Note that 1.5° must be added to the angle of attack for the F-8 SCW to account for the difference in incidence angle (wing mounting) between the DAST ARW-1 and the F-8 SCW.)

Flight-measured wing surface pressure distributions for the DAST ARW-1 and the F-8 SCW are presented for comparison in figure 19. The data indicate several areas of reasonable agreement as well as areas of differences. Pressure distributions are presented for four semispan stations η that were at slightly different locations on either wing. The semispan location of each orifice row is noted in the figure. At orifice row 1, the upper-surface pressure distributions show good agreement whereas the ARW-1 lower-surface pressure distribution is generally more positive than that for the F-8 SCW.

The comparison of pressure distributions for orifice row 2 indicates good agreement for the wing upper surface over most of the chord length except that F-8 SCW data near the trailing edge indicate a second velocity peak from about $x/c = 0.60$ to 0.90. The pressure coefficients for the wing lower surfaces show similar trends, but the ARW-1 pressure coefficients are again generally more positive than those of the F-8 SCW.

The F-8 SCW upper- and lower-surface pressure coefficients for orifice row 3 are nearly equal for about the first 15 percent of the wing local chord. Since the airfoil is approximately symmetrical for the leading edge of the wing, the results indicate that the local angle of attack was near 0°. In contrast, the ARW-1 results for row 3 show a large difference between the upper- and lower-surface pressure coefficients in the leading-edge region, indicating that ARW-1 experienced a positive local angle of attack at orifice row 3. The surface pressure coefficients near the leading edge of orifice row 4 indicate that there was a slightly negative local angle of attack for the F-8 SCW and a positive angle of attack for the ARW-1.

The data of figure 19 indicate that the ARW-1 and the F-8 SCW surface pressure distributions agree reasonably well. The differences that exist occurred at the two outboard orifice rows and indicate that the ARW-1 probably had slightly higher local angles of attack than the F-8 SCW at the outboard regions of the wing.

Comparison with F-8 SCW model data.- Wing surface pressure distributions from the DAST ARW-1 flight test and from the F-8 SCW scaled-rigid-model wind-tunnel test are presented for comparison in figure 20 for Mach numbers of 0.80 and 0.90. The data compare reasonably well at a Mach number of 0.80 (fig. 20(a)). The most significant difference in the two sets of data occurs at the aft end of the chord line for orifice rows 1 and 2. The difference in wing surface pressure coefficients between the upper and lower surfaces is generally greater for the ARW-1 than for the F-8 SCW model.

There are additional differences in the data for the ARW-1 and the F-8 SCW model for a Mach number of 0.90 (fig. 20(b)). The most significant difference at this Mach number is a region of higher lifting pressure on the upper surface between $x/c = 0.15$ and 0.60 at orifice row 1 for ARW-1. Also, the upper-surface pressures at orifice rows 1 and 2 for ARW-1 indicate a second velocity peak near the trailing edge ($x/c = 0.80$).

CONCLUDING REMARKS

A flexible supercritical research wing (ARW-1) was used for both active-control technology demonstration and evaluation of aerodynamic loads. The design cruise conditions for the wing were a Mach number M of 0.98 at an altitude of 45 000 ft. Aerodynamic loads, in the form of wing surface pressure measurements, were obtained for off-design conditions during flight tests at altitudes of 15 000, 20 000, and 25 000 ft at Mach numbers from 0.70 to 0.91. The wing surface pressure measurements, which were converted to coefficient form were presented for individual orifice locations and as chordwise pressure distributions. The analysis of these results indicated the following:

1. The variation of surface pressure coefficient with angle of attack for $M \leq 0.80$ was quite linear, with the largest sensitivity being near the wing leading edge. There were several nonlinear variations of surface pressure coefficient with angle of attack for $M \geq 0.85$; these variations suggested the presence and movement of pressure gradients as angle of attack was varied.

2. The nearly continuous data for variations of surface pressure coefficient with Mach number clearly showed the details of large pressure variations that were associated with a recompression wave which occurred in a relatively narrow Mach number range.

3. Variations of surface pressure coefficient with dynamic pressure indicated that as dynamic pressure was increased the wing twisted along the span (leading edge down).

4. The chordwise pressure distributions for orifice row 1 indicated that a lifting pressure was developed along the entire chord length for the range of angles of attack, Mach numbers, and dynamic pressures reported herein. The chordwise pressure distributions for orifice rows 2, 3, and 4 indicated that the region near the wing leading edge experienced some down loading for most of the test conditions evaluated.

5. Comparisons of chordwise pressure distributions for equal dynamic pressures and angles of attack but different Mach numbers indicated the existence and growth of a region of higher lifting pressures on the wing upper surface at orifice row 1 for the higher Mach numbers.

6. Comparisons of chordwise pressure distributions for equal Mach numbers and angles of attack but different dynamic pressures indicated the wing experienced an increase in twist (leading edge down) for the higher dynamic pressures.

7. A limited comparison of results from the ARW-1 flight test with the measurements from the F-8 supercritical wing (SCW) airplane flight tests and with results from the F-8 SCW model tests indicated that there were some local differences, but overall the data were reasonably close.

NASA Langley Research Center
Hampton, VA 23665-5225
July 15, 1985

REFERENCES

1. Murrow, H. N.; and Eckstrom, C. V.: Drones for Aerodynamic and Structural Testing (DAST) - A Status Report. J. Aircr., vol. 16, no. 8, Aug. 1979, pp. 521-526.

2. Kotsabasis, Alexandros: The DAST-I Remotely Piloted Research Vehicle Development and Initial Flight Testing. NASA CR-163105, 1981.

3. Supercritical Wing Technology - A Progress Report on Flight Evaluations. NASA SP-301, 1972.

4. Abel, Irving; Perry, Boyd, III; and Murrow, Harold N.: Two Synthesis Techniques Applied to Flutter Suppression on a Flight Research Wing. J. Guid. & Control, vol. 1, no. 5, Sept.-Oct. 1978, pp. 341-346.

5. Edwards, John W.: Flight Test Results of an Active Flutter Suppression System Installed on a Remotely Piloted Research Vehicle. AIAA/ASME/ASCE/AHS 22nd Structures, Structural Dynamics and Materials Conference and AIAA Dynamics Specialists Conference - A Collection of Technical Papers, Part 2, Apr. 1981, pp. 778-789. (Available as AIAA-81-0655.)

6. Newsom, Jerry R.; and Pototzky, Anthony S.: Comparison of Analysis and Flight Test Data for a Drone Aircraft With Active Flutter Suppression. AIAA/ASME/ASCE/AHS 22nd Structures, Structural Dynamics and Materials Conference and AIAA Dynamics Specialists Conference - A Collection of Technical Papers, Part 2, Apr. 1981, pp. 644-653. (Available as AIAA-81-0640.)

7. Bennett, Robert M.; and Abel, Irving: Application of a Flight Test and Data Analysis Technique to Flutter of a Drone Aircraft. AIAA/ASME/ASCE/AHS 22nd Structures, Structural Dynamics and Materials Conference and AIAA Dynamics Specialists Conference - A Collection of Technical Papers, Part 2, Apr. 1981, pp. 811-820. (Available as AIAA-81-0652.)

8. Murrow, Harold N.: Status and Future Plans of the Drones for Aerodynamic and Structural Testing (DAST) Program. Advanced Aerodynamics and Active Controls - Selected NASA Research, NASA CP-2172, 1981, pp. 21-36.

9. Montoya, Lawrence C.; and Banner, Richard D.: F-8 Supercritical Wing Flight Pressure, Boundary-Layer, and Wake Measurements and Comparisons With Wind Tunnel Data. NASA TM X-3544, 1977.

10. Byrdsong, Thomas A.; and Hallissy, James B.: Longitudinal and Lateral Static Stability and Control Characteristics of a 1/6-Scale Model of a Remotely Piloted Research Vehicle With a Supercritical Wing. NASA TP-1360, 1979.

11. Harris, Charles D.: Wind-Tunnel Measurements of Aerodynamic Load Distribution on an NASA Supercritical-Wing Research Airplane Configuration. NASA TM X-2469, 1972.

SYMBOLS AND ABBREVIATIONS

b reference wing span, in.

c local streamwise chord length, in.

C_L lift coefficient

c_n wing-section normal-force coefficient, full chord length, $\int_0^1 \left(C_{p,l} - C_{p,u}\right) d(x/c)$

c'_n wing-section normal-force coefficient, partial chord length, $\int_0^{.55} \left(C_{p,l} - C_{p,u}\right) d(x,c)$

C_p pressure coefficient, $(p - p_\infty)/q_\infty$

FS fuselage station

h altitude, ft

LE leading edge

M free-stream Mach number

$\bar{M}$ mean value of Mach number for test condition

mac mean aerodynamic chord length, in.

p local static pressure, psf

p_∞ free-stream static pressure, psf

q_∞ free-stream dynamic pressure, psf

$\bar{q}_\infty$ mean value of dynamic pressure for test condition, psf

R Reynolds number based on mac

S wing reference area, ft^2

TE trailing edge

x streamwise distance measured from local wing leading edge, in.

Y_F spanwise distance measured normal to fuselage centerline, in.

Y_W distance along wing 25-percent-chord line measured from plane of symmetry, in.

z vertical distance from wing reference plane, in.

α angle of attack, deg

Δ increment

ε angle of twist of local airfoil section (angle between wing reference plane and a line through wing leading edge and a point midway between the upper and lower surfaces at the airfoil maximum thickness), deg

η semispan location, $Y_F/(b/2)$

λ wing taper ratio, c_t/c_r

σ standard deviation

Subscripts:

l lower

r wing root

t wing tip

u upper

TABLE I.- ORDINATES FOR WING TOOLING FIXTURE SHAPE

(a) Y_F = 10.00 in.; leading edge at FS = 210.0479 in.

x/c	x, in.	Upper-surface z, in.	Lower-surface z, in.
0.000000	0.0000	1.5999	1.5999
.000625	.0408	1.8503	1.3454
.001250	.0817	1.9562	1.2401
.002500	.1634	2.1018	1.0925
.003750	.2451	2.2122	.9803
.005000	.3268	2.3055	.8868
.007500	.4903	2.4608	.7302
.010000	.6537	2.5895	.5982
.015000	.9805	2.7983	.3831
.020000	1.3074	2.9702	.2100
.025000	1.6343	3.1172	.0632
.037500	2.4514	3.4158	-.2210
.050000	3.2685	3.6617	-.4411
.075000	4.9028	4.0657	-.7816
.100000	6.5371	4.3776	-1.0327
.150000	9.8057	4.8388	-1.3863
.175000	11.4400	5.0064	-1.5019
.200000	13.0742	5.1394	-1.5881
.250000	16.3428	5.3029	-1.6949
.300000	19.6113	5.3466	-1.7255
.350000	22.8799	5.3023	-1.6794
.400000	26.1484	5.1957	-1.5493
.450000	29.4170	5.0556	-1.3381
.500000	32.6855	4.8942	-1.0647
.550000	35.9540	4.7144	-.7336
.600000	39.2225	4.5199	-.3510
.650000	42.4910	4.2953	.0706
.700000	45.7596	4.0470	.5129
.750000	49.0281	3.7727	.9694
.800000	52.2966	3.4780	1.3867
.850000	55.5651	3.1449	1.6759
.900000	58.8337	2.7201	1.7775
.925000	60.4681	2.5138	1.7665
.950000	62.1024	2.2834	1.7092
.975000	63.7367	2.0219	1.6143
.991300	64.8023	1.8188	1.5156
1.000000	65.3711	1.4540	1.4540

TABLE I.- Continued

(b) Y_F = 15.00 in.; leading edge at FS = 210.0479 in.

x/c	x, in.	Upper-surface z, in.	Lower-surface z, in.
0.000000	0.0000	1.4937	1.4937
.000625	.0319	1.7011	1.2864
.001250	.0638	1.7898	1.1975
.002500	.1275	1.9148	1.0719
.003750	.1912	2.0094	.9766
.005000	.2550	2.0870	.8975
.007500	.3825	2.2154	.7667
.010000	.5100	2.3222	.6583
.015000	.7649	2.4931	.4842
.020000	1.0199	2.6277	.3432
.025000	1.2749	2.7415	.2239
.037500	1.9123	2.9738	-.0066
.050000	2.5497	3.1613	-.1803
.075000	3.8246	3.4623	-.4380
.100000	5.0994	3.6883	-.6148
.150000	7.6491	4.0092	-.8449
.175000	8.9239	4.1201	-.9194
.200000	10.1988	4.2037	-.9734
.250000	12.7485	4.3066	-1.0290
.300000	15.2982	4.3472	-1.0260
.350000	17.8479	4.3393	-.9587
.400000	20.3975	4.2980	-.8288
.450000	22.9472	4.2326	-.6469
.500000	25.4969	4.1533	-.4309
.550000	28.0466	4.0558	-.1784
.600000	30.5963	3.9273	.1046
.650000	33.1460	3.7720	.4285
.700000	35.6957	3.6022	.7724
.750000	38.2454	3.4008	1.1383
.800000	40.7951	3.1909	1.4875
.850000	43.3448	2.9667	1.7451
.900000	45.8945	2.6675	1.8708
.925000	47.1693	2.5135	1.8882
.950000	48.4441	2.3406	1.8592
.975000	49.7190	2.1567	1.7991
.991300	50.5502	2.0198	1.7325
1.000000	50.9938	1.6836	1.6836

TABLE I.- Continued

(c) Y_F = 20.00 in.; leading edge at FS = 239.2395 in.

x/c	x, in.	Upper-surface z, in.	Lower-surface z, in.
0.000000	0.0000	1.3261	1.3261
.000625	.0246	1.4943	1.1590
.001250	.0491	1.5673	1.0865
.002500	.0981	1.6717	.9819
.003750	.1471	1.7497	.9025
.005000	.1961	1.8132	.8375
.007500	.2941	1.9169	.7332
.010000	.3922	2.0011	.6491
.015000	.5882	2.1347	.5136
.020000	.7843	2.2343	.4053
.025000	.9804	2.3174	.3154
.037500	1.4705	2.4861	.1414
.050000	1.9607	2.6141	.0169
.075000	2.9410	2.8064	-.1532
.100000	3.9213	2.9533	-.2639
.150000	5.8820	3.1644	-.3870
.175000	6.8623	3.2412	-.4259
.200000	7.8427	3.3026	-.4528
.250000	9.8033	3.4036	-.4666
.300000	11.7640	3.4815	-.4323
.350000	13.7247	3.5269	-.3618
.400000	15.6854	3.5443	-.2594
.450000	17.6461	3.5314	-.1323
.500000	19.6069	3.4929	.0192
.550000	21.5676	3.4383	.2036
.600000	23.5283	3.3519	.4187
.650000	25.4890	3.2594	.6801
.700000	27.4498	3.1665	.9620
.750000	29.4105	3.0485	1.2635
.800000	31.3712	2.9239	1.5623
.850000	33.3319	2.7720	1.8036
.900000	35.2926	2.5880	1.9416
.925000	36.2730	2.4717	1.9671
.950000	37.2533	2.3491	1.9522
.975000	38.2336	2.2182	1.9028
.991300	38.8728	2.1278	1.8416
1.000000	39.2140	1.7985	1.7985

TABLE I.- Continued

(d) Y_F = 25.00 in.; leading edge at FS = 248.5600 in.

x/c	x, in.	Upper-surface z, in.	Lower-surface z, in.
0.000000	0.0000	1.0929	1.0929
.000625	.0203	1.2214	.9676
.001250	.0405	1.2776	.9111
.002500	.0811	1.3564	.8308
.003750	.1217	1.4148	.7722
.005000	.1622	1.4621	.7262
.007500	.2434	1.5371	.6533
.010000	.3245	1.5978	.5927
.015000	.4868	1.7007	.4925
.020000	.6490	1.7847	.4172
.025000	.8113	1.8560	.3558
.037500	1.2169	1.9966	.2373
.050000	1.6226	2.1056	.1493
.075000	2.4339	2.2797	.0291
.100000	3.2452	2.4135	-.0569
.150000	4.8680	2.6072	-.1732
.175000	5.6794	2.6854	-.2037
.200000	6.4908	2.7546	-.2207
.250000	8.1136	2.8649	-.2194
.300000	9.7366	2.9396	-.1884
.350000	11.3596	2.9851	-.1322
.400000	12.9826	3.0103	-.0501
.450000	14.6057	3.0135	.0513
.500000	16.2289	2.9924	.1755
.550000	17.8521	2.9624	.3293
.600000	19.4753	2.9307	.5186
.650000	21.0985	2.8900	.7505
.700000	22.7217	2.8446	1.0151
.750000	24.3449	2.7798	1.3047
.800000	25.9680	2.6998	1.5871
.850000	27.5910	2.5926	1.8098
.900000	29.2138	2.4558	1.9310
.925000	30.0252	2.3648	1.9450
.950000	30.8365	2.2599	1.9180
.975000	31.6479	2.1378	1.8456
.991300	32.1768	2.0480	1.7661
1.000000	32.4591	1.7163	1.7163

TABLE I.- Continued

(e) Y_F = 30.00 in.; leading edge at FS = 255.0596 in.

x/c	x, in.	Upper-surface z, in.	Lower-surface z, in.
0.000000	0.0000	.8949	.8949
.000625	.0181	1.0134	.7789
.001250	.0363	1.0597	.7321
.002500	.0725	1.1289	.6632
.003750	.1088	1.1778	.6139
.005000	.1451	1.2167	.5753
.007500	.2176	1.2800	.5133
.010000	.2902	1.3306	.4646
.015000	.4353	1.4125	.3888
.020000	.5804	1.4811	.3324
.025000	.7255	1.5407	.2862
.037500	1.0883	1.6613	.1966
.050000	1.4511	1.7573	.1262
.075000	2.1766	1.9109	.0224
.100000	2.9021	2.0306	-.0519
.150000	4.3532	2.2123	-.1429
.175000	5.0788	2.2842	-.1627
.200000	5.8043	2.3458	-.1741
.250000	7.2554	2.4426	-.1723
.300000	8.7065	2.5139	-.1422
.350000	10.1575	2.5641	-.0914
.400000	11.6086	2.5964	-.0178
.450000	13.0596	2.6129	.0716
.500000	14.5106	2.6195	.1852
.550000	15.9615	2.6199	.3268
.600000	17.4124	2.6171	.5050
.650000	18.8632	2.6031	.7291
.700000	20.3140	2.5782	.9954
.750000	21.7647	2.5346	1.2844
.800000	23.2153	2.4761	1.5616
.850000	24.6659	2.3964	1.7608
.900000	26.1164	2.2776	1.8527
.925000	26.8416	2.2000	1.8498
.950000	27.5668	2.1050	1.8031
.975000	28.2919	1.9867	1.7077
.991300	28.7647	1.8957	1.6154
1.000000	29.0171	1.5639	1.5639

TABLE I.- Continued

(f) Y_F = 33.00 in.; leading edge at FS = 258.1945 in.

x/c	x, in.	Upper-surface z, in.	Lower-surface z, in.
0.000000	0.0000	.8019	.8019
.000625	.0175	.9198	.6854
.001250	.0349	.9638	.6411
.002500	.0698	1.0319	.5742
.003750	.1047	1.0791	.5262
.005000	.1396	1.1165	.4882
.007500	.2094	1.1780	.4268
.010000	.2792	1.2270	.3804
.015000	.4188	1.3031	.3111
.020000	.5584	1.3653	.2586
.025000	.6980	1.4196	.2152
.037500	1.0469	1.5319	.1307
.050000	1.3959	1.6212	.0645
.075000	2.0939	1.7605	-.0344
.100000	2.7918	1.8703	-.1027
.150000	4.1877	2.0414	-.1754
.175000	4.8857	2.1075	-.1897
.200000	5.5836	2.1626	-.1984
.250000	6.9796	2.2518	-.1957
.300000	8.3755	2.3245	-.1632
.350000	9.7714	2.3803	-.1124
.400000	11.1673	2.4185	-.0413
.450000	12.5632	2.4416	.0437
.500000	13.9591	2.4594	.1531
.550000	15.3550	2.4704	.2899
.600000	16.7509	2.4717	.4629
.650000	18.1468	2.4630	.6830
.700000	19.5427	2.4428	.9463
.750000	20.9386	2.4038	1.2296
.800000	22.3345	2.3512	1.4996
.850000	23.7304	2.2780	1.6891
.900000	25.1264	2.1647	1.7704
.925000	25.8243	2.0899	1.7622
.950000	26.5223	1.9987	1.7108
.975000	27.2202	1.8836	1.6114
.991300	27.6753	1.7946	1.5183
1.000000	27.9182	1.4675	1.4675

TABLE I.- Continued

(g) Y_F = 40.00 in.; leading edge at FS = 265.0309 in.

x/c	x, in.	Upper-surface z, in.	Lower-surface z, in.
0.000000	0.0000	.5758	.5758
.000625	.0163	.6821	.4698
.001250	.0325	.7227	.4290
.002500	.0650	.7850	.3676
.003750	.0975	.8284	.3239
.005000	.1300	.8625	.2888
.007500	.1950	.9176	.2328
.010000	.2600	.9619	.1909
.015000	.3900	1.0316	.1282
.020000	.5200	1.0888	.0801
.025000	.6499	1.1383	.0405
.037500	.9749	1.2408	-.0372
.050000	1.2999	1.3224	-.0959
.075000	1.9498	1.4488	-.1801
.100000	2.5997	1.5488	-.2377
.150000	3.8996	1.7049	-.2972
.175000	4.5495	1.7658	-.3080
.200000	5.1994	1.8177	-.3127
.250000	6.4993	1.9037	-.3030
.300000	7.7992	1.9741	-.2693
.350000	9.0990	2.0311	-.2207
.400000	10.3989	2.0746	-.1548
.450000	11.6987	2.1053	-.0752
.500000	12.9986	2.1304	.0270
.550000	14.2984	2.1467	.1536
.600000	15.5983	2.1552	.3156
.650000	16.8982	2.1543	.5191
.700000	18.1980	2.1422	.7642
.750000	19.4979	2.1127	1.0284
.800000	20.7977	2.0668	1.2743
.850000	22.0976	1.9982	1.4510
.900000	23.3975	1.8914	1.5221
.925000	24.0474	1.8193	1.5107
.950000	24.6973	1.7314	1.4609
.975000	25.3472	1.6200	1.3642
.991300	25.7710	1.5317	1.2744
1.000000	25.9972	1.2220	1.2220

TABLE I.- Continued

(h) Y_F = 50.00 in.; leading edge at FS = 274.7971 in.

x/c	x, in.	Upper-surface z, in.	Lower-surface z, in.
0.000000	0.0000	.1852	.1852
.000625	.0146	.2749	.0941
.001250	.0291	.3106	.0583
.002500	.0582	.3645	.0049
.003750	.0872	.4026	-.0329
.005000	.1163	.4318	-.0638
.007500	.1744	.4778	-.1119
.010000	.2326	.5155	-.1474
.015000	.3488	.5763	-.2006
.020000	.4651	.6262	-.2423
.025000	.5814	.6691	-.2765
.037500	.8720	.7578	-.3444
.050000	1.1627	.8285	-.3922
.075000	1.7440	.9368	-.4550
.100000	2.3253	1.0230	-.4968
.150000	3.4880	1.1586	-.5367
.175000	4.0693	1.2125	-.5420
.200000	4.6506	1.2601	-.5408
.250000	5.8133	1.3424	-.5201
.300000	6.9759	1.4103	-.4839
.350000	8.1386	1.4701	-.4377
.400000	9.3012	1.5220	-.3783
.450000	10.4639	1.5646	-.3052
.500000	11.6265	1.6010	-.2124
.550000	12.7892	1.6260	-.0992
.600000	13.9518	1.6461	.0481
.650000	15.1145	1.6575	.2291
.700000	16.2771	1.6581	.4494
.750000	17.4397	1.6434	.6873
.800000	18.6024	1.6082	.9000
.850000	19.7650	1.5475	1.0599
.900000	20.9277	1.4515	1.1178
.925000	21.5090	1.3839	1.1027
.950000	22.0903	1.3015	1.0557
.975000	22.6717	1.1959	.9636
.991300	23.0507	1.1091	.8789
1.000000	23.2530	.8247	.8247

TABLE I.- Continued

(i) Y_F = 60.00 in.; leading edge at FS = 284.5634 in.

x/c	x, in.	Upper-surface z, in.	Lower-surface z, in.
0.000000	0.0000	-.2614	-.2614
.000625	.0128	-.1877	-.3383
.001250	.0256	-.1570	-.3690
.002500	.0512	-.1115	-.4144
.003750	.0769	-.0807	-.4462
.005000	.1025	-.0540	-.4727
.007500	.1538	-.0166	-.5130
.010000	.2051	.0148	-.5422
.015000	.3076	.0669	-.5864
.020000	.4101	.1098	-.6216
.025000	.5127	.1463	-.6504
.037500	.7690	.2218	-.7081
.050000	1.0254	.2822	-.7455
.075000	1.5381	.3736	-.7890
.100000	2.0508	.4472	-.8160
.150000	3.0763	.5639	-.8368
.175000	3.5890	.6113	-.8367
.200000	4.1017	.6547	-.8298
.250000	5.1271	.7332	-.7989
.300000	6.1526	.7989	-.7598
.350000	7.1780	.8612	-.7147
.400000	8.2035	.9207	-.6600
.450000	9.2289	.9741	-.5920
.500000	10.2543	1.0211	-.5071
.550000	11.2798	1.0550	-.4059
.600000	12.3052	1.0863	-.2725
.650000	13.3306	1.1098	-.1126
.700000	14.3561	1.1231	.0835
.750000	15.3815	1.1233	.2947
.800000	16.4070	1.1003	.4764
.850000	17.4324	1.0500	.6206
.900000	18.4578	.9674	.6688
.925000	18.9705	.9059	.6520
.950000	19.4833	.8305	.6092
.975000	19.9956	.7326	.5234
.991300	20.3296	.6494	.4459
1.000000	20.5086	.3916	.3916

TABLE I.- Continued

(j) Y_F = 70.00 in.; leading edge at FS = 294.3296 in.

x/c	x, in.	Upper-surface z, in.	Lower-surface z, in.
0.000000	0.0000	-.7099	-.7099
.000625	.0111	-.6498	-.7753
.001250	.0222	-.6245	-.8011
.002500	.0444	-.5876	-.8380
.003750	.0666	-.5601	-.8638
.005000	.0888	-.5396	-.8855
.007500	.1332	-.5086	-.9182
.010000	.1776	-.4822	-.9420
.015000	.2665	-.4380	-.9788
.020000	.3553	-.4013	-1.0081
.025000	.4441	-.3704	-1.0316
.037500	.6662	-.3064	-1.0785
.050000	.8882	-.2551	-1.1088
.075000	1.3323	-.1775	-1.1425
.100000	1.7764	-.1144	-1.1604
.150000	2.6647	-.0138	-1.1681
.175000	3.1088	.0272	-1.1640
.200000	3.5529	.0653	-1.1543
.250000	4.4411	.1358	-1.1203
.300000	5.3294	.1963	-1.0809
.350000	6.2176	.2560	-1.0361
.400000	7.1058	.3156	-.9830
.450000	7.9940	.3709	-.9186
.500000	8.8823	.4208	-.8407
.550000	9.7705	.4600	-.7507
.600000	10.6587	.4965	-.6331
.650000	11.5469	.5265	-.4932
.700000	12.4352	.5471	-.3248
.750000	13.3234	.5570	-.1468
.800000	14.2116	.5464	.0066
.850000	15.0998	.5111	.1343
.900000	15.9881	.4460	.1805
.925000	16.4322	.3938	.1668
.950000	16.8763	.3285	.1307
.975000	17.3204	.2424	.0554
.991300	17.6100	.1695	-.0098
1.000000	17.7645	-.0578	-.0578

TABLE I.- Continued

(k) Y_F = 80.00 in.; leading edge at FS = 304.0958 in.

x/c	x, in.	Upper-surface z, in.	Lower-surface z, in.
0.000000	0.0000	-1.1393	-1.1393
.000625	.0094	-1.0900	-1.1963
.001250	.0188	-1.0706	-1.2174
.002500	.0376	-1.0425	-1.2453
.003750	.0563	-1.0202	-1.2650
.005000	.0751	-1.0031	-1.2814
.007500	.1127	-.9761	-1.3068
.010000	.1502	-.9532	-1.3262
.015000	.2253	-.9158	-1.3576
.020000	.3004	-.8848	-1.3814
.025000	.3755	-.8583	-1.3998
.037500	.5633	-.8038	-1.4354
.050000	.7510	-.7601	-1.4623
.075000	1.1265	-.6924	-1.4974
.100000	1.5021	-.6370	-1.5128
.150000	2.2531	-.5488	-1.5142
.175000	2.6286	-.5140	-1.5081
.200000	3.0041	-.4828	-1.4988
.250000	3.7551	-.4253	-1.4699
.300000	4.5061	-.3730	-1.4330
.350000	5.2571	-.3220	-1.3876
.400000	6.0081	-.2710	-1.3324
.450000	6.7592	-.2243	-1.2694
.500000	7.5102	-.1803	-1.1974
.550000	8.2612	-.1402	-1.1172
.600000	9.0122	-.1055	-1.0175
.650000	9.7632	-.0756	-.8963
.700000	10.5142	-.0538	-.7595
.750000	11.2653	-.0403	-.6227
.800000	12.0163	-.0380	-.4940
.850000	12.7673	-.0529	-.3837
.900000	13.5183	-.0953	-.3301
.925000	13.8938	-.1341	-.3348
.950000	14.2693	-.1856	-.3611
.975000	14.6448	-.2552	-.4212
.991300	14.8897	-.3098	-.4677
1.000000	15.0203	-.5018	-.5018

TABLE I.- Concluded

(l) Y_F = 82.37 in.; leading edge at FS = 306.4152 in.

x/c	x, in.	Upper-surface z, in.	Lower-surface z, in.
0.000000	0.0000	-1.2362	-1.2362
.000625	.0090	-1.1890	-1.2917
.001250	.0180	-1.1711	-1.3118
.002500	.0359	-1.1452	-1.3375
.003750	.0539	-1.1241	-1.3557
.005000	.0718	-1.1077	-1.3708
.007500	.1078	-1.0813	-1.3944
.010000	.1437	-1.0590	-1.4130
.015000	.2155	-1.0230	-1.4434
.020000	.2874	-.9932	-1.4661
.025000	.3592	-.9675	-1.4833
.037500	.5388	-.9150	-1.5160
.050000	.7184	-.8729	-1.5427
.075000	1.0776	-.8068	-1.5799
.100000	1.4369	-.7528	-1.5959
.150000	2.1553	-.6670	-1.5969
.175000	2.5145	-.6336	-1.5906
.200000	2.8737	-.6043	-1.5819
.250000	3.5922	-.5505	-1.5555
.300000	4.3106	-.5008	-1.5197
.350000	5.0290	-.4528	-1.4739
.400000	5.7474	-.4053	-1.4176
.450000	6.4659	-.3622	-1.3546
.500000	7.1843	-.3211	-1.2837
.550000	7.9027	-.2815	-1.2056
.600000	8.6212	-.2483	-1.1106
.650000	9.3396	-.2195	-.9935
.700000	10.0580	-.1984	-.8648
.750000	10.7764	-.1850	-.7390
.800000	11.4949	-.1795	-.6157
.850000	12.2133	-.1887	-.5096
.900000	12.9317	-.2248	-.4527
.925000	13.2910	-.2598	-.4543
.950000	13.6502	-.3074	-.4777
.975000	14.0094	-.3722	-.5335
.991300	14.2436	-.4212	-.5744
1.000000	14.3686	-.6040	-.6040

TABLE II.- DEVIATIONS OF WING LEADING- AND TRAILING-EDGE VERTICAL LOCATIONS FROM THE TOOLING FIXTURE SHAPE

y_W, in.	Left wing		Right wing	
	Δz_{LE}, in.	Δz_{TE}, in.	Δz_{LE}, in.	Δz_{TE}, in.
58.96	0.033	-0.045	-0.006	-0.009
64.96	.029	-.043	-.003	-.004
70.96	.019	-.045	-.005	-.011
76.96	.022	-.038	.006	-.005
82.96	.014	-.029	.012	-.018
88.96	.017	-.018	.011	-.023
94.96	.022	-.028	.019	-.033
100.96	.012	-.027	.008	-.020

TABLE III.- MEASUREMENTS OF FABRICATED AIRFOIL

[Y_F = 37.11 in.; c = 26.790 in.]

(a) Left semispan, upper-surface location

x/c	z, in. (nominal)	z, in. (measured)	Δz, in.
0	0.6691	0.6696	-0.0005
.00125	.8222	.8219	-.0003
.00250	.8869	.8802	-.0067
.00500	.9673	.9725	.0052
.00750	1.0251	1.0326	.0075
.01000	1.0713	1.0804	.0091
.01500	1.1436	1.1651	.0215
.02000	1.2029	1.2202	.0173
.02500	1.2544	1.2725	.0181
.05000	1.4458	1.4586	.0128
.10000	1.6815	1.6951	.0131
.15000	1.8438	1.8572	.0134
.20000	1.9600	1.9683	.0083
.25000	2.0474	2.0578	.0104
.30000	2.1187	2.1231	.0044
.35000	2.1752	2.1802	.0050
.40000	2.2165	2.2147	-.0018
.45000	2.2441	2.2412	-.0029
.50000	2.2662	2.2618	-.0044
.55000	2.2803	2.2673	-.0130
.60000	2.2858	2.2656	-.0202
.65000	2.2817	2.2575	-.0242
.70000	2.2663	2.2366	-.0297
.75000	2.2329	2.1996	-.0333
.80000	2.1842	2.1456	-.0386
.85000	2.1137	2.0768	-.0369
.90000	2.0042	1.9542	-.0500
.95000	1.8417	1.7868	-.0549
.99130	1.6990	1.6070	-.0920
1.00000	1.3233	1.2599	-.0634

TABLE III.- Continued

(b) Left semispan, lower-surface location

x/c	z, in. (nominal)	z, in. (measured)	Δz, in.
0	0.6691	0.6600	-0.0091
.00125	.5166	.5176	.0010
.00250	.4529	.4715	.0186
.00500	.3711	.3912	.0201
.00750	.3128	.3363	.0235
.01000	.2591	.2951	.0360
.01500	.2037	.2246	.0209
.02000	.1538	.1692	.0154
.02500	.1126	.1240	.0114
.05000	-.0296	-.0299	-.0003
.10000	-.1819	-.1891	-.0072
.15000	-.2468	-.2637	-.0169
.20000	-.2655	-.2822	-.0167
.25000	-.2586	-.2734	-.0148
.30000	-.2254	-.2472	-.0218
.35000	-.1759	-.2026	-.0267
.40000	-.1079	-.1362	-.0283
.45000	-.0266	-.0534	-.0274
.50000	.0790	.0521	-.0269
.55000	.2099	.1846	-.0253
.60000	.3764	.3562	-.0202
.65000	.5667	.5637	-.0230
.70000	.8393	.8127	-.0266
.75000	1.1115	1.0790	-.0325
.80000	1.3673	1.3267	-.0406
.85000	1.5493	1.4961	-.0532
.90000	1.6245	1.5654	-.0591
.95000	1.5641	1.4916	-.0725
.99130	1.3751	1.2856	-.0895
1.00000	1.3233	1.2747	-.0486

TABLE III.- Continued

(c) Right semispan, upper-surface location

x/c	z, in. (nominal)	z, in. (measured)	Δz, in.
0	0.6691	0.6694	.0003
.00125	.8222	.7285	-.0937
.00250	.8869	.8058	-.0811
.00500	.9673	.9187	-.0486
.00750	1.0251	.9822	-.0429
.01000	1.0713	1.0390	-.0323
.01500	1.1436	1.1232	-.0204
.02000	1.2029	1.1883	-.0146
.02500	1.2544	1.2442	-.0102
.05000	1.4458	1.4414	-.0044
.10000	1.6815	1.6885	.0076
.15000	1.8438	1.8515	.0077
.20000	1.9600	1.9661	.0061
.25000	2.0474	2.0585	.0111
.30000	2.1187	2.1258	.0071
.35000	2.1752	2.1816	.0064
.40000	2.2165	2.2217	.0052
.45000	2.2441	2.2532	.0091
.50000	2.2662	2.2737	.0075
.55000	2.2803	2.2821	.0018
.60000	2.2858	2.2846	-.0012
.65000	2.2817	2.2772	-.0045
.70000	2.2663	2.2563	-.0100
.75000	2.2329	2.2203	-.0126
.80000	2.1842	2.1648	-.0194
.85000	2.1137	2.0874	-.0263
.90000	2.0042	1.9744	-.0298
.95000	1.8417	1.8180	-.0237
.99130	1.6990	1.6242	-.0748
1.00000	1.3233	1.3159	-.0074

TABLE III.- Concluded

(d) Right semispan, lower-surface location

x/c	z, in. (nominal)	z, in. (measured)	Δz, in.
0	0.6691	0.6793	0.0102
.00125	.5166	.6489	.1323
.00250	.4529	.5207	.0678
.00500	.3711	.4000	.0289
.00750	.3128	.3364	.0236
.01000	.2591	.2906	.0315
.01500	.2037	.2156	.0119
.02000	.1538	.1600	.0062
.02500	.1126	.1156	.0030
.05000	-.0296	-.0315	-.0019
.10000	-.1819	-.1761	.0058
.15000	-.2468	-.2406	.0062
.20000	-.2655	-.2638	.0017
.25000	-.2586	-.2639	-.0053
.30000	-.2254	-.2348	-.0094
.35000	-.1759	-.1893	-.0134
.40000	-.1079	-.1247	-.0168
.45000	-.0260	-.0407	-.0147
.50000	.0790	.0641	-.0149
.55000	.2099	.1961	-.0138
.60000	.3764	.3661	-.0103
.65000	.5867	.5718	-.0149
.70000	.8393	.8183	-.0210
.75000	1.1115	1.0842	-.0273
.80000	1.3673	1.3332	-.0341
.85000	1.5493	1.5110	-.0383
.90000	1.6245	1.5796	-.0449
.95000	1.5641	1.5125	-.0516
.99130	1.3751	1.3043	-.0708
1.00000	1.3233	1.2496	-.0737

TABLE IV.- SURFACE PRESSURE ORIFICE LOCATIONS ON RIGHT WING PANEL

Row 1 (Y_F = 29.50) location on -		Row 2 (Y_F = 55.83) location on -		Row 3 (Y_F = 69.17) location on -		Row 4 (Y_F = 78.23) location on -	
Upper x/c	Lower x/c	Upper x/c	Lower x/c	Upper x/c	Lower x/c	Upper x/c	Lower x/c
0.01		0.01		0.01		0.01	
.03	0.03	.03	0.03	.03	0.03*	.03	0.03
.10	.10	.10	.10	.10	.10*	.10	.10
.15	.15	.15	.15	.15	.15	.15	.15
.20	.20		.20				
.30*	.30	.30	.30	.30	.30*		
.40	.40	.40	.40	.40	.40	.40	.40
.45				.45		.45	
.50	.50	.50	.50	.50	.50	.50	.50
.55		.55		.55		.55	
.61	.61	.61					.61*
.65							
.70	.70		.70				
.80	.80	.80	.80				
.90	.90	.90	.90				
	.95		.95				
.98		.98					

*Not functioning on flight 11.

TABLE V.- DATA FOR PRIMARY FLIGHT-TEST CONDITIONS

Flight	Selected Mach no. conditions	Data samples	Mach number		Dynamic pressure, psf		R
			$\bar{M}$	σ	$\bar{q}_\infty$	σ	
10	0.75 ± 0.01	180	0.7547	0.0040	319.8	5.49	5.7×10^6
10	.80 ± .01	203	.8030	.0041	359.9	3.94	6.1
10	.85 ± .005	358	.8521	.0019	405.2	2.18	6.5
10	.875 ± .005	247	.8750	.0024	429.4	3.13	6.7
10	.90 ± .005	203	.9018	.0021	455.6	2.07	6.9
11	.70 ± .01	206	.6982	.0046	411.4	5.81	7.3
11	.75 ± .01	234	.7451	.0035	466.3	6.48	7.8
11	.80 ± .01	256	.7964	.0041	532.8	7.08	8.4

TABLE VI.- PRESSURE COEFFICIENT DATA ARRAY FOR FLIGHT 10 AT A MACH NUMBER OF 0.75

(a) Row 1, upper surface

x/c	Pressure coefficient for angle of attack, deg, of -					
	1.5	2.0	2.5	3.0	3.5	4.0
.01	+.0522	-.0269	-.1120	-.2032	-.3004	-.4038
.03	-.2853	-.3558	-.4370	-.5288	-.6313	-.7443
.10	-.2535	-.3079	-.3637	-.4208	-.4792	-.5389
.15	-.3360	-.3793	-.4259	-.4759	-.5292	-.5858
.20	-.3026	-.3393	-.3758	-.4123	-.4486	-.4849
.30	-.3145	-.3413	-.3686	-.3963	-.4245	-.4531
.40	-.1876	-.2101	-.2320	-.2533	-.2741	-.2944
.45	-.2369	-.2550	-.2736	-.2925	-.3118	-.3315
.50	-.1481	-.1666	-.1846	-.2019	-.2186	-.2347
.55	-.1885	-.2038	-.2191	-.2345	-.2500	-.2655
.61	-.1631	-.1767	-.1904	-.2042	-.2181	-.2321
.65	-.1666	-.1792	-.1914	-.2031	-.2144	-.2252
.70	-.1494	-.1610	-.1721	-.1824	-.1922	-.2013
.80	-.2227	-.2340	-.2440	-.2528	-.2602	-.2664
.90	-.1684	-.1750	-.1802	-.1842	-.1869	-.1883
.98	-.0937	-.0945	-.0954	-.0963	-.0972	-.0982

(b) Row 1, lower surface

x/c	Pressure coefficient for angle of attack, deg, of -					
	1.5	2.0	2.5	3.0	3.5	4.0
.03	-.2436	-.1710	-.1016	-.0355	+.0275	+.0873
.10	-.1281	-.0863	-.0438	-.0006	+.0434	+.0881
.15	-.2771	-.2415	-.2058	-.1702	-.1347	-.0992
.20	-.2234	-.1979	-.1711	-.1432	-.1141	-.0837
.30	-.1244	-.1067	-.0883	-.0694	-.0499	-.0297
.40	-.2028	-.1881	-.1717	-.1537	-.1339	-.1125
.50	-.1772	-.1659	-.1536	-.1403	-.1259	-.1105
.61	-.0884	-.0820	-.0745	-.0659	-.0562	-.0455
.70	+.0313	+.0343	+.0379	+.0423	+.0473	+.0529
.80	+.2305	+.2364	+.2426	+.2491	+.2558	+.2627
.90	+.3385	+.3442	+.3501	+.3563	+.3626	+.3692
.95	+.2938	+.2988	+.3036	+.3082	+.3125	+.3166

(c) Row 2, upper surface

x/c	Pressure coefficient for angle of attack, deg, of -					
	1.5	2.0	2.5	3.0	3.5	4.0
.01	+.0008	-.0997	-.2173	-.3521	-.5041	-.6732
.03	-.1943	-.2781	-.3747	-.4841	-.6064	-.7414
.10	-.1479	-.2031	-.2590	-.3156	-.3730	-.4312
.15	-.1616	-.2080	-.2503	-.2885	-.3226	-.3526
.30	-.1620	-.1853	-.2107	-.2384	-.2682	-.3003
.40	-.1394	-.1509	-.1684	-.1920	-.2217	-.2575
.50	-.1687	-.1785	-.1925	-.2107	-.2332	-.2599
.55	-.1729	-.1848	-.1992	-.2161	-.2357	-.2578
.61	-.1515	-.1730	-.1926	-.2105	-.2266	-.2409
.80	-.2294	-.2395	-.2493	-.2590	-.2684	-.2777
.90	-.3037	-.3063	-.3089	-.3115	-.3142	-.3169
.98	-.0636	-.0590	-.0557	-.0535	-.0526	-.0528

(d) Row 2, lower surface

x/c	Pressure coefficient for angle of attack, deg, of -					
	1.5	2.0	2.5	3.0	3.5	4.0
.03	-.6468	-.5422	-.4419	-.3459	-.2542	-.1669
.10	-.3296	-.2810	-.2317	-.1816	-.1308	-.0792
.15	-.2792	-.2437	-.2078	-.1716	-.1352	-.0984
.20	-.2158	-.2036	-.1825	-.1525	-.1136	-.0659
.30	-.1428	-.1210	-.0982	-.0745	-.0499	-.0244
.40	-.1365	-.1215	-.1062	-.0908	-.0751	-.0592
.50	-.1136	-.1038	-.0932	-.0819	-.0697	-.0568
.70	+.1588	+.1598	+.1617	+.1646	+.1683	+.1730
.80	+.2373	+.2471	+.2563	+.2650	+.2731	+.2806
.90	+.3143	+.3273	+.3399	+.3521	+.3638	+.3751
.95	+.2990	+.3060	+.3139	+.3227	+.3323	+.3429

(e) Row 3, upper surface

x/c	Pressure coefficient for angle of attack, deg, of -					
	1.5	2.0	2.5	3.0	3.5	4.0
.01	+.1192	+.0330	-.0704	-.1910	-.3289	-.4841
.03	-.0959	-.1687	-.2549	-.3544	-.4673	-.5935
.10	-.2236	-.2657	-.3137	-.3676	-.4273	-.4928
.15	-.1031	-.1422	-.1826	-.2240	-.2667	-.3104
.30	-.0916	-.1057	-.1157	-.1214	-.1228	-.1201
.40	-.1177	-.1317	-.1472	-.1642	-.1826	-.2026
.45	-.1128	-.1265	-.1423	-.1602	-.1801	-.2020
.50	-.1648	-.1787	-.1932	-.2083	-.2241	-.2404
.55	-.1309	-.1440	-.1574	-.1712	-.1853	-.1998

TABLE VI.- Concluded

(f) Row 3, lower surface

x/c	Pressure coefficient for angle of attack, deg, of -					
	1.5	2.0	2.5	3.0	3.5	4.0
.03	-.6606	-.5522	-.4470	-.3451	-.2465	-.1511
.10	-.4105	-.3562	-.3022	-.2483	-.1948	-.1414
.15	-.2613	-.2480	-.2247	-.1912	-.1476	-.0939
.30	-.1698	-.1410	-.1212	-.1103	-.1084	-.1154
.40	-.1184	-.1077	-.0938	-.0769	-.0570	-.0340
.50	-.1244	-.1192	-.1115	-.1012	-.0884	-.0731

(g) Row 4, upper surface

x/c	Pressure coefficient for angle of attack, deg, of -					
	1.5	2.0	2.5	3.0	3.5	4.0
.01	+.2132	+.1330	+.0344	-.0823	-.2173	-.3706
.03	-.0605	-.1346	-.2226	-.3245	-.4402	-.5699
.10	-.0697	-.1116	-.1591	-.2120	-.2704	-.3344
.15	-.1242	-.1593	-.1973	-.2383	-.2823	-.3292
.40	-.0599	-.0760	-.0911	-.1052	-.1184	-.1306
.45	-.1414	-.1530	-.1642	-.1748	-.1848	-.1943
.50	-.1278	-.1398	-.1524	-.1656	-.1794	-.1938
.55	-.1513	-.1635	-.1764	-.1899	-.2041	-.2190

(h) Row 4, lower surface

x/c	Pressure coefficient for angle of attack, deg, of -					
	1.5	2.0	2.5	3.0	3.5	4.0
.03	-.7092	-.5907	-.4747	-.3613	-.2505	-.1423
.10	-.3813	-.3302	-.2781	-.2248	-.1703	-.1148
.15	-.3676	-.3520	-.3279	-.2954	-.2545	-.2051
.40	-.1325	-.1225	-.1107	-.0971	-.0816	-.0644
.50	-.0776	-.0733	-.0675	-.0603	-.0517	-.0416
.61	-.0557	-.0507	-.0454	-.0399	-.0341	-.0281

TABLE VII.- PRESSURE COEFFICIENT DATA ARRAY FOR FLIGHT 10 AT A MACH NUMBER OF 0.80

(a) Row 1, upper surface

x/c	Pressure coefficient for angle of attack, deg, of -		
	2.0	2.5	3.0
.01	-.0069	-.0881	-.1749
.03	-.3383	-.4237	-.5193
.10	-.3203	-.3734	-.4249
.15	-.4093	-.4659	-.5197
.20	-.3549	-.3914	-.4233
.30	-.3487	-.3759	-.4003
.40	-.2298	-.2514	-.2699
.45	-.2616	-.2797	-.2952
.50	-.1827	-.2009	-.2146
.55	-.2065	-.2229	-.2389
.61	-.1801	-.1936	-.2073
.65	-.1810	-.1928	-.2045
.70	-.1664	-.1780	-.1881
.80	-.2508	-.2591	-.2649
.90	-.1855	-.1901	-.1924
.98	-.0840	-.0860	-.0874

(b) Row 1, lower surface

x/c	Pressure coefficient for angle of attack, deg, of -		
	2.0	2.5	3.0
.03	-.1851	-.1153	-.0504
.10	-.1311	-.0834	-.0343
.15	-.2678	-.2286	-.1879
.20	-.2236	-.1930	-.1608
.30	-.1292	-.1083	-.0848
.40	-.2206	-.1994	-.1738
.50	-.1841	-.1696	-.1532
.61	-.0979	-.0898	-.0798
.70	+.0338	+.0370	+.0421
.80	+.2303	+.2377	+.2471
.90	+.3374	+.3440	+.3514
.95	+.3011	+.3055	+.3105

TABLE VII.- Continued

(c) Row 2, upper surface

x/c	Pressure coefficient for angle of attack, deg, of -		
	2.0	2.5	3.0
.01	-.0798	-.1952	-.3246
.03	-.2660	-.3648	-.4732
.10	-.2043	-.2592	-.3159
.15	-.2036	-.2469	-.2914
.30	-.1806	-.2052	-.2307
.40	-.1619	-.1734	-.1924
.50	-.1802	-.1931	-.2123
.55	-.1781	-.1942	-.2136
.61	-.1700	-.1933	-.2180
.80	-.2575	-.2660	-.2725
.90	-.3251	-.3246	-.3186
.98	-.0537	-.0518	-.0476

(d) Row 2, lower surface

x/c	Pressure coefficient for angle of attack, deg, of -		
	2.0	2.5	3.0
.03	-.5673	-.4624	-.3637
.10	-.3268	-.2695	-.2106
.15	-.2752	-.2329	-.1896
.20	-.2410	-.2111	-.1690
.30	-.1405	-.1161	-.0923
.40	-.1462	-.1282	-.1059
.50	-.1217	-.1097	-.0944
.70	+.1550	+.1570	+.1609
.80	+.2364	+.2474	+.2582
.90	+.3167	+.3304	+.3429
.95	+.3026	+.3085	+.3141

(e) Row 3, upper surface

x/c	Pressure coefficient for angle of attack, deg, of -		
	2.0	2.5	3.0
.01	+.0627	-.0382	-.1559
.03	-.1396	-.2283	-.3296
.10	-.2414	-.2938	-.3521
.15	-.1366	-.1771	-.2196
.30	-.0973	-.1322	-.1481
.40	-.1389	-.1622	-.1682
.45	-.1434	-.1671	-.1701
.50	-.1954	-.2169	-.2150
.55	-.1660	-.1868	-.1793

TABLE VII.- Concluded

(f) Row 3, lower surface

x/c	Pressure coefficient for angle of attack, deg, of -		
	2.0	2.5	3.0
.03	-.6246	-.5006	-.3816
.10	-.4022	-.3399	-.2773
.15	-.2936	-.2631	-.2187
.30	-.1709	-.1461	-.1180
.40	-.1282	-.1128	-.0958
.50	-.1294	-.1209	-.1131

(g) Row 4, upper surface

x/c	Pressure coefficient for angle of attack, deg, of -		
	2.0	2.5	3.0
.01	+.1704	+.0756	-.0375
.03	-.0986	-.1886	-.2912
.10	-.1040	-.1531	-.2026
.15	-.1483	-.1873	-.2283
.40	-.0914	-.1131	-.1222
.45	-.1640	-.1852	-.1867
.50	-.1545	-.1684	-.1715
.55	-.1682	-.1806	-.1912

(h) Row 4, lower surface

x/c	Pressure coefficient for angle of attack, deg, of -		
	2.0	2.5	3.0
.03	-.6980	-.5585	-.4210
.10	-.3820	-.3337	-.2539
.15	-.3651	-.3448	-.3375
.40	-.1402	-.1281	-.1137
.50	-.0809	-.0745	-.0678
.61	-.0426	-.0379	-.0322

TABLE VIII.- PRESSURE COEFFICIENT DATA ARRAY FOR FLIGHT 10 AT A MACH NUMBER OF 0.85

(a) Row 1, upper surface

x/c	Pressure coefficient for angle of attack, deg, of -		
	2.0	2.5	3.0
.01	+.0112	-.0628	-.1020
.03	-.3303	-.4193	-.4461
.10	-.3141	-.3523	-.3677
.15	-.4306	-.4616	-.4738
.20	-.5100	-.5406	-.5523
.30	-.3500	-.3150	-.3937
.40	-.2675	-.2850	-.2708
.45	-.2680	-.2884	-.2982
.50	-.1985	-.2160	-.2224
.55	-.2119	-.2280	-.2362
.61	-.1801	-.1951	-.2026
.65	-.1808	-.1928	-.1976
.70	-.1745	-.1829	-.1861
.80	-.2746	-.2838	-.2877
.90	-.1994	-.2016	-.2015
.98	-.0711	-.0759	-.0769

(b) Row 1, lower surface

x/c	Pressure coefficient for angle of attack, deg, of -		
	2.0	2.5	3.0
.03	-.1977	-.1261	-.0910
.10	-.1801	-.1271	-.0998
.15	-.3064	-.2588	-.2383
.20	-.2537	-.2219	-.2056
.30	-.1520	-.1321	-.1207
.40	-.2687	-.2408	-.2268
.50	-.2080	-.1895	-.1795
.61	-.1197	-.1083	-.1018
.70	+.0345	+.0396	+.0444
.80	+.2220	+.2318	+.2389
.90	+.3264	+.3373	+.3448
.95	+.3007	+.3074	+.3122

TABLE VIII.- Continued

(c) Row 2, upper surface

x/c	Pressure coefficient for angle of attack, deg, of -		
	2.0	2.5	3.0
.01	-.0605	-.1738	-.2419
.03	-.2520	-.3577	-.4178
.10	-.2043	-.2658	-.3010
.15	-.2032	-.2504	-.2783
.30	-.1780	-.1964	-.1997
.40	-.1771	-.1820	-.2026
.50	-.1914	-.1940	-.2079
.55	-.1741	-.1881	-.2009
.61	-.1599	-.1870	-.2035
.80	-.2957	-.2937	-.3039
.90	-.3550	-.3449	-.3405
.98	-.0423	-.0414	-.0403

(d) Row 2, lower surface

x/c	Pressure coefficient for angle of attack, deg, of -		
	2.0	2.5	3.0
.03	-.6033	-.4907	-.4391
.10	-.3894	-.3171	-.2808
.15	-.3127	-.2607	-.2405
.20	-.2811	-.2364	-.2169
.30	-.1716	-.1390	-.1232
.40	-.1735	-.1512	-.1372
.50	-.1439	-.1295	-.1235
.70	+.1482	+.1514	+.1549
.80	+.2210	+.2343	+.2428
.90	+.2996	+.3157	+.3277
.95	+.2911	+.3001	+.3052

(e) Row 3, upper surface

x/c	Pressure coefficient for angle of attack, deg, of -		
	2.0	2.5	3.0
.01	+.1003	-.0014	-.0588
.03	-.1029	-.1984	-.2547
.10	-.2147	-.2742	-.3072
.15	-.1271	-.1730	-.1967
.30	-.0451	-.0972	-.1367
.40	-.1080	-.1302	-.1499
.45	-.1196	-.1389	-.1538
.50	-.1684	-.1863	-.1985
.55	-.1412	-.1545	-.1627

TABLE VIII.- Concluded

(f) Row 3, lower surface

x/c	Pressure coefficient for angle of attack, deg, of -		
	2.0	2.5	3.0
.03	-.7301	-.5762	-.5113
.10	-.4740	-.3904	-.3547
.15	-.3013	-.3038	-.2771
.30	-.2004	-.1692	-.1520
.40	-.1573	-.1358	-.1227
.50	-.1487	-.1358	-.1292

(g) Row 4, upper surface

x/c	Pressure coefficient for angle of attack, deg, of -		
	2.0	2.5	3.0
.01	+.2223	+.1270	+.0728
.03	-.0484	-.1466	-.2026
.10	-.0762	-.1331	-.1592
.15	-.1228	-.1684	-.1899
.40	-.0832	-.1184	-.1300
.45	-.1399	-.1676	-.1778
.50	-.1491	-.1640	-.1713
.55	-.1714	-.1816	-.1840

(h) Row 4, lower surface

x/c	Pressure coefficient for angle of attack, deg, of -		
	2.0	2.5	3.0
.03	-.8558	-.6620	-.5722
.10	-.5306	-.4130	-.3579
.15	-.4251	-.3829	-.3574
.40	-.1599	-.1478	-.1389
.50	-.0896	-.0829	-.0772
.61	-.0308	-.0260	-.0171

TABLE IX.- PRESSURE COEFFICIENT DATA ARRAY FOR FLIGHT 10 AT A MACH NUMBER OF 0.875

(a) Row 1, upper surface

x/c	Pressure coefficient for angle of attack, deg, of -		
	2.0	2.5	3.0
.01	+.0169	-.0472	-.1006
.03	-.3367	-.3968	-.5084
.10	-.2987	-.3287	-.3468
.15	-.4131	-.4346	-.4590
.20	-.4956	-.5181	-.5364
.30	-.5200	-.5500	-.5434
.40	-.2200	-.1850	-.3167
.45	-.2900	-.2500	-.2264
.50	-.2118	-.2087	-.1717
.55	-.2148	-.2240	-.2136
.61	-.1813	-.1930	-.1941
.65	-.1799	-.1899	-.1963
.70	-.1731	-.1807	-.1848
.80	-.2907	-.3023	-.3055
.90	-.2016	-.2055	-.2075
.98	-.0668	-.0670	-.0689

(b) Row 1, lower surface

x/c	Pressure coefficient for angle of attack, deg, of -		
	2.0	2.5	3.0
.03	-.1931	-.1261	-.0747
.10	-.1924	-.1482	-.0938
.15	-.3373	-.2855	-.2419
.20	-.3290	-.2646	-.1949
.30	-.1557	-.1395	-.1190
.40	-.3250	-.2989	-.2497
.50	-.2076	-.1962	-.1798
.61	-.1246	-.1163	-.1046
.70	+.0375	+.0422	+.0485
.80	+.2206	+.2295	+.2398
.90	+.3250	+.3338	+.3440
.95	+.3017	+.3085	+.3171

TABLE IX.- Continued

(c) Row 2, upper surface

x/c	Pressure coefficient for angle of attack, deg, of -		
	2.0	2.5	3.0
.01	-.0591	-.1651	-.2790
.03	-.2563	-.3524	-.4394
.10	-.2135	-.2707	-.3197
.15	-.2095	-.2578	-.3132
.30	-.1739	-.1877	-.1781
.40	-.1858	-.2062	-.2290
.50	-.1825	-.1898	-.2125
.55	-.1637	-.1792	-.1904
.61	-.1517	-.1741	-.1972
.80	-.2479	-.2401	-.2739
.90	-.3509	-.3521	-.3410
.98	-.0346	-.0367	-.0371

(d) Row 2, lower surface

x/c	Pressure coefficient for angle of attack, deg, of -		
	2.0	2.5	3.0
.03	-.6091	-.5045	-.4157
.10	-.4104	-.3478	-.2795
.15	-.3342	-.2771	-.2306
.20	-.2846	-.2468	-.2112
.30	-.1841	-.1551	-.1242
.40	-.1875	-.1652	-.1378
.50	-.1549	-.1422	-.1218
.70	+.1454	+.1464	+.1520
.80	+.2120	+.2236	+.2396
.90	+.2890	+.3047	+.3228
.95	+.2825	+.2937	+.3046

(e) Row 3, upper surface

x/c	Pressure coefficient for angle of attack, deg, of -		
	2.0	2.5	3.0
.01	+.1053	+.0167	-.0813
.03	-.0985	-.1826	-.2763
.10	-.2132	-.2635	-.3181
.15	-.1283	-.1700	-.2133
.30	-.0404	-.0770	-.1297
.40	-.1043	-.1209	-.1331
.45	-.1158	-.1319	-.1500
.50	-.1645	-.1821	-.2022
.55	-.1411	-.1541	-.1663

TABLE IX.- Concluded

(f) Row 3, lower surface

x/c	Pressure coefficient for angle of attack, deg, of -		
	2.0	2.5	3.0
.03	-.7824	-.6204	-.4900
.10	-.5014	-.4132	-.3648
.15	-.3140	-.3210	-.2920
.30	-.2019	-.1782	-.1511
.40	-.1662	-.1512	-.1294
.50	-.1541	-.1450	-.1347

(g) Row 4, upper surface

x/c	Pressure coefficient for angle of attack, deg, of -		
	2.0	2.5	3.0
.01	+.2318	+.1537	+.0598
.03	-.0422	-.1222	-.2150
.10	-.0710	-.1132	-.1849
.15	-.1174	-.1552	-.1942
.40	-.0928	-.1185	-.1407
.45	-.1386	-.1580	-.1714
.50	-.1504	-.1644	-.1689
.55	-.1710	-.1824	-.1890

(h) Row 4, lower surface

x/c	Pressure coefficient for angle of attack, deg, of -		
	2.0	2.5	3.0
.03	-.8675	-.7238	-.5509
.10	-.6049	-.4981	-.3507
.15	-.3744	-.3328	-.3556
.40	-.1636	-.1567	-.1453
.50	-.0863	-.0834	-.0790
.61	-.0247	-.0198	-.0154

TABLE X.- PRESSURE COEFFICIENT DATA ARRAY FOR FLIGHT 10 AT A MACH NUMBER OF 0.90

(a) Row 1, upper surface

x/c	Pressure coefficient for angle of attack, deg, of -		
	2.0	2.5	3.0
.01	+.0304	-.0288	-.0990
.03	-.2996	-.3952	-.5030
.10	-.2698	-.2891	-.3196
.15	-.3813	-.4015	-.4249
.20	-.4700	-.4832	-.5089
.30	-.5200	-.5500	-.5808
.40	-.4500	-.4700	-.5058
.45	-.3300	-.4600	-.4900
.50	-.1400	-.3700	-.4200
.55	-.1500	-.2000	-.3500
.61	-.1400	-.1200	-.2000
.65	-.1500	-.1300	-.1400
.70	-.1600	-.1400	-.1250
.80	-.3244	-.2850	-.2475
.90	-.2306	-.2408	-.2231
.98	-.0538	-.0551	-.0641

(b) Row 1, lower surface

x/c	Pressure coefficient for angle of attack, deg, of -		
	2.0	2.5	3.0
.03	-.1844	-.1149	-.0691
.10	-.1790	-.1392	-.1256
.15	-.3470	-.2982	-.2567
.20	-.3486	-.3057	-.2805
.30	-.2326	-.2010	-.1710
.40	-.2500	-.2527	-.3223
.50	-.2242	-.1953	-.1784
.61	-.1270	-.1197	-.1170
.70	+.0417	+.0480	+.0482
.80	+.2152	+.2259	+.2305
.90	+.3169	+.3290	+.3353
.95	+.2997	+.3104	+.3120

TABLE X.- Continued

(c) Row 2, upper surface

x/c	Pressure coefficient for angle of attack, deg, of -		
	2.0	2.5	3.0
.01	-.0598	-.1655	-.3284
.03	-.2613	-.3496	-.5054
.10	-.2174	-.2550	-.2603
.15	-.2212	-.2690	-.2990
.30	-.1686	-.2341	-.2618
.40	-.1648	-.1758	-.1970
.50	-.2084	-.1982	-.3040
.55	-.1508	-.1635	-.2307
.61	-.1370	-.1417	-.1438
.80	-.4159	-.4131	-.4305
.90	-.2652	-.2524	-.2540
.98	-.0269	-.0255	-.0288

(d) Row 2, lower surface

x/c	Pressure coefficient for angle of attack, deg, of -		
	2.0	2.5	3.0
.03	-.6234	-.4858	-.3920
.10	-.4095	-.3640	-.3195
.15	-.3878	-.3189	-.2122
.20	-.3346	-.2708	-.1716
.30	-.1857	-.1593	-.1568
.40	-.1884	-.1723	-.1686
.50	-.1605	-.1459	-.1374
.70	+.1377	+.1425	+.1429
.80	+.1907	+.2102	+.2143
.90	+.2646	+.2881	+.2907
.95	+.2649	+.2839	+.2846

(e) Row 3, upper surface

x/c	Pressure coefficient for angle of attack, deg, of -		
	2.0	2.5	3.0
.01	+.1085	+.0203	-.0908
.03	-.0953	-.1790	-.2910
.10	-.2072	-.2541	-.3169
.15	-.1278	-.1657	-.2098
.30	-.0363	-.0695	-.1040
.40	-.0993	-.1239	-.1561
.45	-.1078	-.1231	-.1431
.50	-.1621	-.1845	-.2008
.55	-.1237	-.1536	-.1752

TABLE X.- Concluded

(f) Row 3, lower surface

x/c	Pressure coefficient for angle of attack, deg, of -		
	2.0	2.5	3.0
.03	-.8003	-.6413	-.4872
.10	-.6004	-.4356	-.3707
.15	-.2346	-.2870	-.3296
.30	-.2488	-.1980	-.1432
.40	-.1745	-.1550	-.1559
.50	-.1672	-.1567	-.1594

(g) Row 4, upper surface

x/c	Pressure coefficient for angle of attack, deg, of -		
	2.0	2.5	3.0
.01	+.2416	+.1649	+.0699
.03	-.0309	-.1103	-.2094
.10	-.0666	-.1164	-.1769
.15	-.1074	-.1447	-.1915
.40	-.1205	-.1310	-.1425
.45	-.1742	-.1994	-.2130
.50	-.1665	-.2180	-.2310
.55	-.1731	-.1663	-.1728

(h) Row 4, lower surface

x/c	Pressure coefficient for angle of attack, deg, of -		
	2.0	2.5	3.0
.03	-.8499	-.7379	-.5897
.10	-.6631	-.5487	-.4397
.15	-.2778	-.3478	-.3365
.40	-.1874	-.1858	-.1661
.50	-.0744	-.0749	-.0783
.61	-.0108	-.0099	-.0084

TABLE XI.- PRESSURE COEFFICIENT DATA ARRAY FOR FLIGHT 11 AT A MACH NUMBER OF 0.70

(a) Row 1, upper surface

x/c	Pressure coefficient for angle of attack, deg, of -		
	2.0	2.5	3.0
.01	-.0446	-.1295	-.2290
.03	-.3368	-.4137	-.5006
.10	-.3109	-.3598	-.4142
.15	-.3410	-.3804	-.4251
.20	-.3222	-.3535	-.3854
.40	-.2222	-.2412	-.2630
.45	-.2183	-.2343	-.2533
.50	-.1783	-.1932	-.2117
.55	-.1950	-.2086	-.2242
.61	-.1692	-.1808	-.1944
.65	-.1814	-.1917	-.2045
.70	-.1467	-.1567	-.1697
.80	-.2370	-.2443	-.2535
.90	-.1790	-.1829	-.1898
.98	-.1057	-.1064	-.1101

(b) Row 1, lower surface

x/c	Pressure coefficient for angle of attack, deg, of -		
	2.0	2.5	3.0
.03	-.2047	-.1371	-.0738
.10	-.2720	-.2290	-.1881
.15	-.2494	-.2140	-.1801
.20	-.2084	-.1823	-.1568
.30	-.1814	-.1600	-.1405
.40	-.1932	-.1766	-.1598
.50	-.1766	-.1636	-.1522
.61	-.1066	-.0977	-.0904
.70	+.0029	+.0084	+.0116
.80	+.1951	+.2010	+.2050
.90	+.3050	+.3103	+.3142
.95	+.2543	+.2595	+.2614

TABLE XI.- Continued

(c) Row 2, upper surface

x/c	Pressure coefficient for angle of attack, deg, of -		
	2.0	2.5	3.0
.01	-.1039	-.2087	-.3329
.03	-.2568	-.3424	-.4402
.10	-.2113	-.2574	-.3104
.15	-.2083	-.2458	-.2841
.30	-.1952	-.2183	-.2468
.40	-.1552	-.1657	-.1928
.50	-.1323	-.1463	-.1688
.55	-.1834	-.2011	-.2217
.61	-.1741	-.1919	-.2120
.80	-.2057	-.2145	-.2271
.90	-.2990	-.3013	-.3064
.98	-.1062	-.0994	-.0947

(d) Row 2, lower surface

x/c	Pressure coefficient for angle of attack, deg, of -		
	2.0	2.5	3.0
.03	-.6120	-.5195	-.4327
.10	-.3133	-.2657	-.2185
.15	-.3038	-.2672	-.2300
.20	-.2260	-.2129	-.1835
.30	-.1692	-.1808	-.1944
.40	-.1425	-.1249	-.1079
.50	-.1437	-.1315	-.1202
.70	+.1062	+.1091	+.1097
.80	+.2156	+.2240	+.2297
.90	+.2733	+.2822	+.2908
.95	+.2728	+.2778	+.2832

(e) Row 3, upper surface

x/c	Pressure coefficient for angle of attack, deg, of -		
	2.0	2.5	3.0
.01	+.0441	-.0452	-.1524
.03	-.1399	-.2177	-.3065
.10	-.1745	-.2199	-.2702
.15	-.1503	-.1844	-.2237
.30	-.1050	-.1425	-.1417
.40	-.1481	-.1694	-.1622
.45	-.1550	-.1735	-.1665
.50	-.2134	-.2302	-.2239
.55	-.1663	-.1797	-.1678

TABLE XI.- Concluded

(f) Row 3, lower surface

x/c	Pressure coefficient for angle of attack, deg, of -		
	2.0	2.5	3.0
.15	-.2606	-.2513	-.2240
.40	-.1400	-.1253	-.1119
.50	-.1172	-.1199	-.1355

(g) Row 4, upper surface

x/c	Pressure coefficient for angle of attack, deg, of -		
	2.0	2.5	3.0
.01	+.1582	+.0727	-.0289
.03	-.0709	-.1508	-.2391
.10	-.1126	-.1537	-.2001
.15	-.1301	-.1625	-.1983
.40	-.0978	-.1169	-.1339
.45	-.1307	-.1465	-.1618
.50	-.1524	-.1665	-.1797
.55	-.1568	-.1687	-.1798

(h) Row 4, lower surface

x/c	Pressure coefficient for angle of attack, deg, of -		
	2.0	2.5	3.0
.03	-.6630	-.5477	-.4417
.10	-.3466	-.3112	-.2627
.15	-.2937	-.2654	-.2595
.40	-.1456	-.1384	-.1314
.50	-.1191	-.1144	-.1117

TABLE XII.- PRESSURE COEFFICIENT DATA ARRAY FOR FLIGHT 11 AT A MACH NUMBER OF 0.75

(a) Row 1, upper surface

x/c	Pressure coefficient for angle of attack, deg, of -		
	2.0	2.5	3.0
.01	-.0305	-.1101	-.1905
.03	-.3298	-.4019	-.4750
.10	-.3255	-.3717	-.4184
.15	-.3557	-.3955	-.4359
.20	-.3254	-.3569	-.3861
.40	-.2352	-.2521	-.2668
.45	-.2231	-.2384	-.2516
.50	-.1875	-.2009	-.2146
.55	-.1936	-.2067	-.2181
.61	-.1667	-.1788	-.1886
.65	-.1787	-.1892	-.1987
.70	-.1555	-.1650	-.1718
.80	-.2479	-.2555	-.2612
.90	-.1882	-.1920	-.1950
.98	-.0989	-.1008	-.1005

(b) Row 1, lower surface

x/c	Pressure coefficient for angle of attack, deg, of -		
	2.0	2.5	3.0
.03	-.2158	-.1497	-.0931
.10	-.2915	-.2476	-.2084
.15	-.2702	-.2336	-.2011
.20	-.2282	-.2012	-.1762
.30	-.1936	-.1722	-.1545
.40	-.2150	-.1963	-.1790
.50	-.1950	-.1804	-.1667
.61	-.1217	-.1121	-.1036
.70	+.0036	+.0079	+.0133
.80	+.1925	+.1978	+.2032
.90	+.2978	+.3039	+.3091
.95	+.2581	+.2619	+.2661

TABLE XII.- Continued

(c) Row 2, upper surface

x/c	Pressure coefficient for angle of attack, deg, of -		
	2.0	2.5	3.0
.01	-.0678	-.1641	-.2665
.03	-.2317	-.3108	-.3950
.10	-.1985	-.2442	-.2902
.15	-.1982	-.2334	-.2685
.30	-.1835	-.2086	-.2307
.40	-.1437	-.1617	-.1843
.50	-.1321	-.1487	-.1679
.55	-.1803	-.1954	-.2103
.61	-.1747	-.1894	-.2051
.80	-.2246	-.2299	-.2372
.90	-.3085	-.3095	-.3110
.98	-.1010	-.0965	-.0890

(d) Row 2, lower surface

x/c	Pressure coefficient for angle of attack, deg, of -		
	2.0	2.5	3.0
.03	-.6451	-.5494	-.4671
.10	-.3583	-.3085	-.2630
.15	-.3283	-.2911	-.2582
.20	-.2221	-.2386	-.2195
.30	-.1667	-.1788	-.1886
.40	-.1639	-.1468	-.1300
.50	-.1624	-.1495	-.1359
.70	+.1005	+.1020	+.1054
.80	+.2043	+.2128	+.2197
.90	+.2627	+.2714	+.2785
.95	+.2667	+.2723	+.2777

(e) Row 3, upper surface

x/c	Pressure coefficient for angle of attack, deg, of -		
	2.0	2.5	3.0
.01	+.0993	+.0197	-.0678
.03	-.0911	-.1617	-.2387
.10	-.1473	-.1902	-.2331
.15	-.1221	-.1631	-.1925
.30	-.0507	-.0721	-.1121
.40	-.1058	-.1189	-.1332
.45	-.1204	-.1341	-.1467
.50	-.1765	-.1889	-.2010
.55	-.1337	-.1439	-.1541

TABLE XII.- Concluded

(f) Row 3, lower surface

x/c	Pressure coefficient for angle of attack, deg, of -		
	2.0	2.5	3.0
.15	-.2691	-.2572	-.2720
.40	-.1660	-.1519	-.1375
.50	-.1095	-.1084	-.1004

(g) Row 4, upper surface

x/c	Pressure coefficient for angle of attack, deg, of -		
	2.0	2.5	3.0
.01	+.2215	+.1513	+.0732
.03	-.0118	-.0813	-.1532
.10	-.0800	-.1197	-.1603
.15	-.1040	-.1343	-.1650
.40	-.0952	-.1096	-.1235
.45	-.1250	-.1405	-.1534
.50	-.1487	-.1614	-.1719
.55	-.1504	-.1621	-.1716

(h) Row 4, lower surface

x/c	Pressure coefficient for angle of attack, deg, of -		
	2.0	2.5	3.0
.03	-.8169	-.6889	-.5758
.10	-.3652	-.3755	-.3500
.15	-.3649	-.3204	-.2888
.40	-.1716	-.1611	-.1527
.50	-.1335	-.1271	-.1218

TABLE XIII.- PRESSURE COEFFICIENT DATA ARRAY FOR FLIGHT 11 AT A MACH NUMBER OF 0.80

(a) Row 1, upper surface

x/c	Pressure coefficient for angle of attack, deg, of -		
	2.0	2.5	3.0
.01	-.0060	-.0660	-.1258
.03	-.3107	-.3716	-.4324
.10	-.3297	-.3707	-.4093
.15	-.3716	-.4114	-.4515
.20	-.3344	-.3612	-.3862
.40	-.2425	-.2578	-.2707
.45	-.2214	-.2356	-.2486
.50	-.1896	-.2041	-.2178
.55	-.1866	-.1975	-.2072
.61	-.1576	-.1669	-.1745
.65	-.1705	-.1794	-.1871
.70	-.1570	-.1648	-.1703
.80	-.2569	-.2637	-.2685
.90	-.1941	-.1984	-.2013
.98	-.0891	-.0901	-.0895

(b) Row 1, lower surface

x/c	Pressure coefficient for angle of attack, deg, of -		
	2.0	2.5	3.0
.03	-.2293	-.1749	-.1260
.10	-.3211	-.2823	-.2450
.15	-.2998	-.2688	-.2380
.20	-.2540	-.2315	-.2097
.30	-.2105	-.1953	-.1812
.40	-.2473	-.2330	-.2193
.50	-.2184	-.2075	-.1964
.61	-.1396	-.1333	-.1257
.70	+.0032	+.0064	+.0116
.80	+.1884	+.1935	+.2006
.90	+.2911	+.2957	+.3017
.95	+.2610	+.2640	+.2687

TABLE XIII.- Continued

(c) Row 2, upper surface

x/c	Pressure coefficient for angle of attack, deg, of -		
	2.0	2.5	3.0
.01	-.0127	-.0859	-.1643
.03	-.1855	-.2494	-.3158
.10	-.1722	-.2096	-.2461
.15	-.1725	-.2038	-.2271
.30	-.1662	-.1817	-.1944
.40	-.1317	-.1447	-.1558
.50	-.1267	-.1396	-.1529
.55	-.1660	-.1778	-.1901
.61	-.1660	-.1753	-.1844
.80	-.2294	-.2386	-.2433
.90	-.3063	-.3137	-.3135
.98	-.0856	-.0899	-.0856

(d) Row 2, lower surface

x/c	Pressure coefficient for angle of attack, deg, of -		
	2.0	2.5	3.0
.03	-.7078	-.6249	-.5208
.10	-.4209	-.3818	-.3219
.15	-.3587	-.3343	-.2900
.20	-.2810	-.2557	-.2480
.30	-.1576	-.1669	-.1745
.40	-.1935	-.1807	-.1667
.50	-.1867	-.1768	-.1654
.70	+.0922	+.0958	+.0998
.80	+.1839	+.1920	+.1977
.90	+.2406	+.2495	+.2548
.95	+.2520	+.2589	+.2624

(e) Row 3, upper surface

x/c	Pressure coefficient for angle of attack, deg, of -		
	2.0	2.5	3.0
.01	+.1767	+.1198	+.0586
.03	-.0179	-.0703	-.1265
.10	-.0995	-.1338	-.1688
.15	-.0646	-.0995	-.1454
.30	-.0269	-.0422	-.0537
.40	-.0792	-.0938	-.1078
.45	-.0975	-.1122	-.1260
.50	-.1518	-.1650	-.1782
.55	-.1180	-.1303	-.1418

TABLE XIII.- Concluded

(f) Row 3, lower surface

x/c	Pressure coefficient for angle of attack, deg, of -		
	2.0	2.5	3.0
.15	-.3587	-.3200	-.2718
.40	-.2040	-.1905	-.1755
.50	-.1548	-.1567	-.1504

(g) Row 4, upper surface

x/c	Pressure coefficient for angle of attack, deg, of -		
	2.0	2.5	3.0
.01	+.3063	+.2613	+.2099
.03	+.0752	+.0289	-.0199
.10	-.0260	-.0576	-.0822
.15	-.0559	-.0828	-.1080
.40	-.0796	-.0913	-.1008
.45	-.1105	-.1207	-.1281
.50	-.1360	-.1448	-.1503
.55	-.1398	-.1477	-.1518

(h) Row 4, lower surface

x/c	Pressure coefficient for angle of attack, deg, of -		
	2.0	2.5	3.0
.10	-.4643	-.4242	-.3180
.15	-.4384	-.4170	-.3528
.40	-.1970	-.1927	-.1855
.50	-.1472	-.1440	-.1387

TABLE XIV.- SECTION NORMAL-FORCE COEFFICIENTS FOR ARW-1

Orifice row	α, deg	c_n for flight 10	c_n for flight 11	c'_n for flight 10	c'_n for flight 11
*M = 0.75					
1	2.0 2.5 3.0	0.206 .247 .289	0.151 .189 .224		
2	2.0 2.5 3.0	0.173 .217 .263	0.088 .145 .182		
3	2.0 2.5 3.0			-0.032 0 .033	-0.075 -.046 -.020
4	2.0 2.5 3.0			-0.066 -.033 -.004	-0.112 -.082 -.053
**M = 0.80					
1	2.0 2.5 3.0	0.198 .241 .285	0.137 .169 .200		
2	2.0 2.5 3.0	0.157 .203 .252	0.075 .106 .136		
3	2.0 2.5 3.0			-0.055 -.015 .022	-0.129 -.097 -.062
4	2.0 2.5 3.0			-0.080 -.045 -.012	-0.148 -.123 -.088

*$\bar{q}_\infty$ = 320 psf for flight 10 and 466 psf for flight 11.

**$\bar{q}_\infty$ = 360 psf for flight 10 and 533 psf for flight 11.

(a) Upper view. L-85-129

Figure 1.- DAST BQM-34F drone aircraft with ARW-1 wing during flight testing.

(b) Lower view. L-85-130

Figure 1.- Concluded.

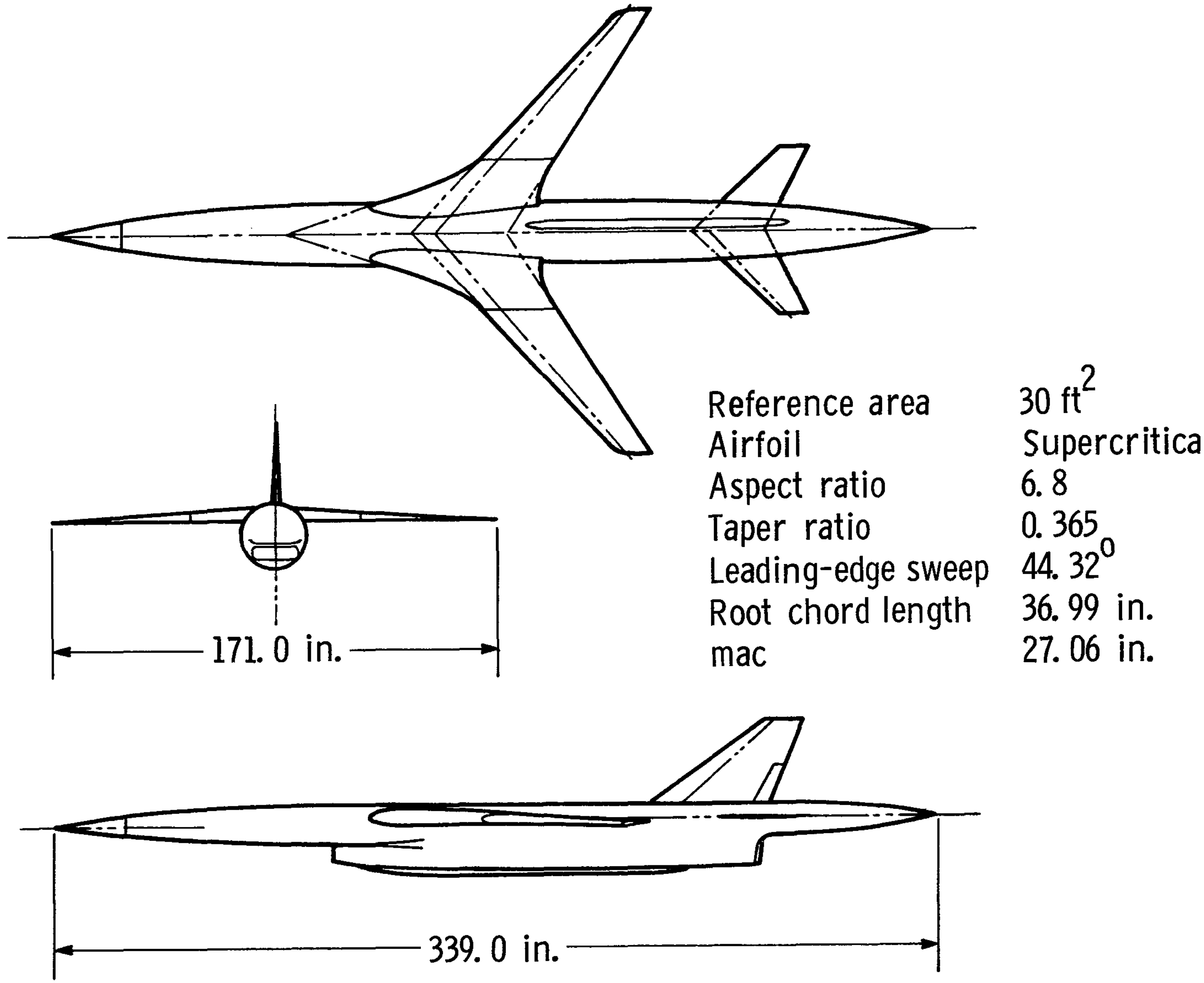

Figure 2.- General arrangement of DAST BQM-34F drone aircraft with ARW-1 wing.

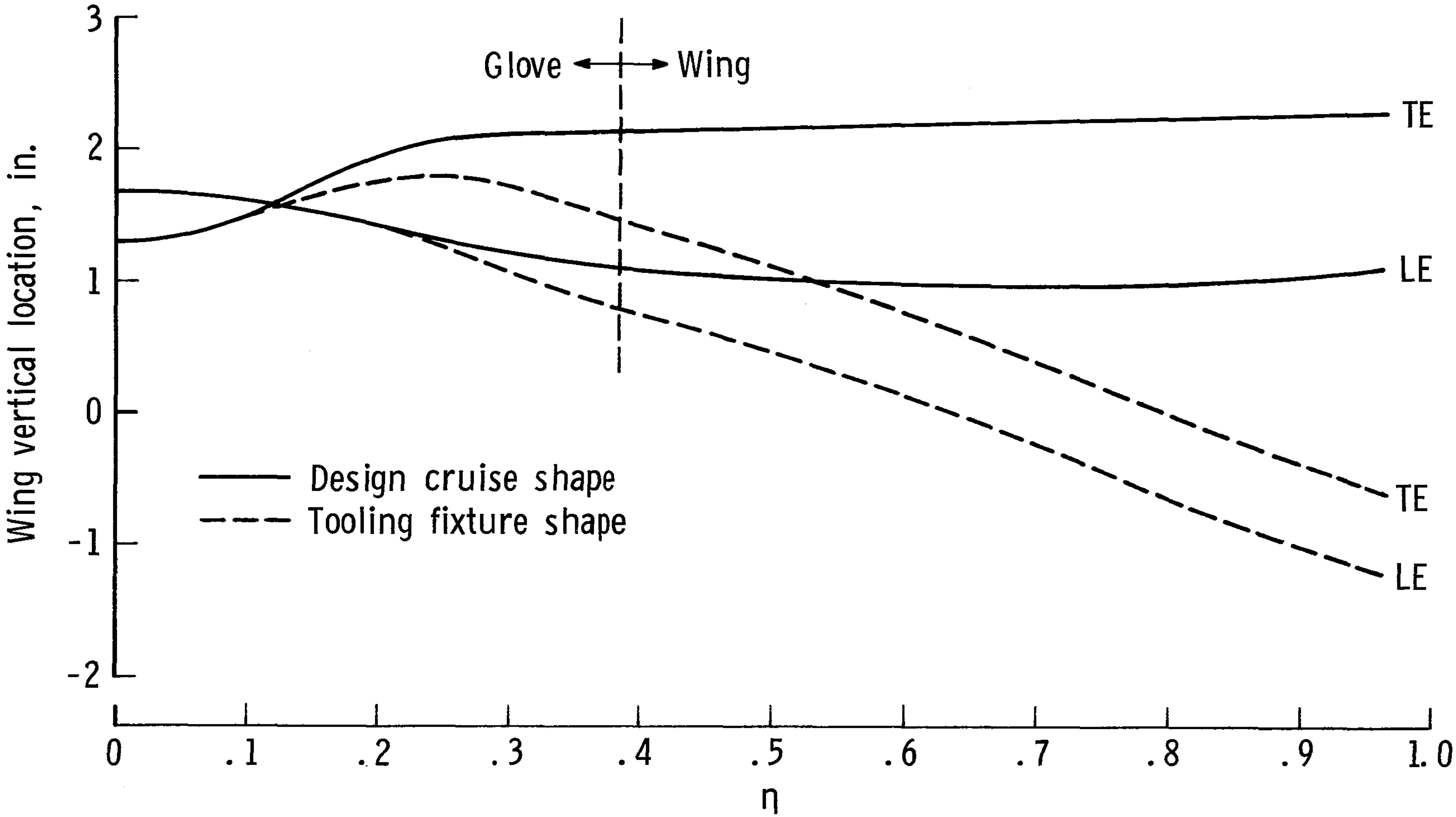

Figure 3.- Wing leading- and trailing-edge vertical locations for design cruise and tooling fixture shapes.

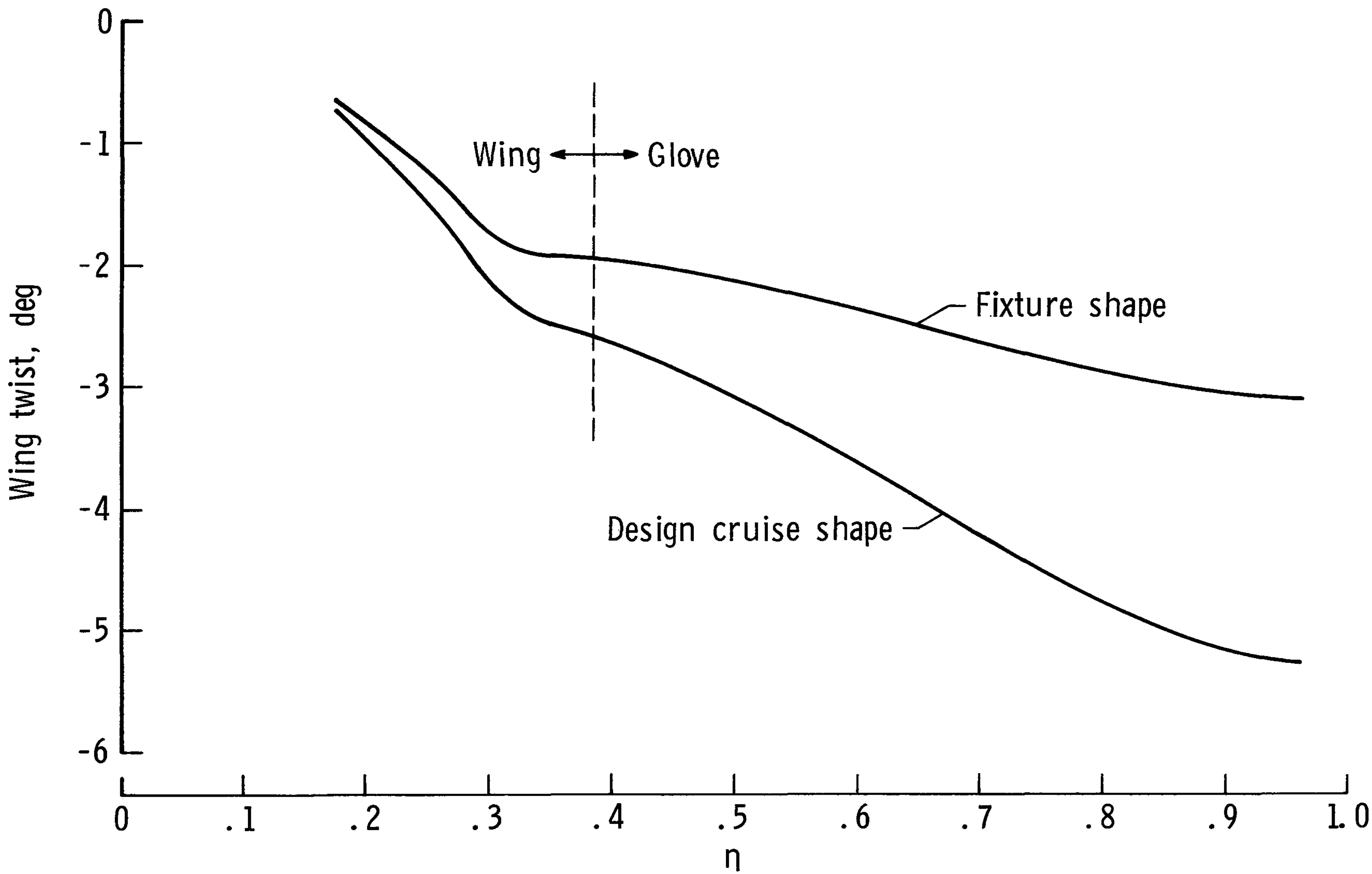

Figure 4.- Wing twist for design cruise and tooling fixture shapes.

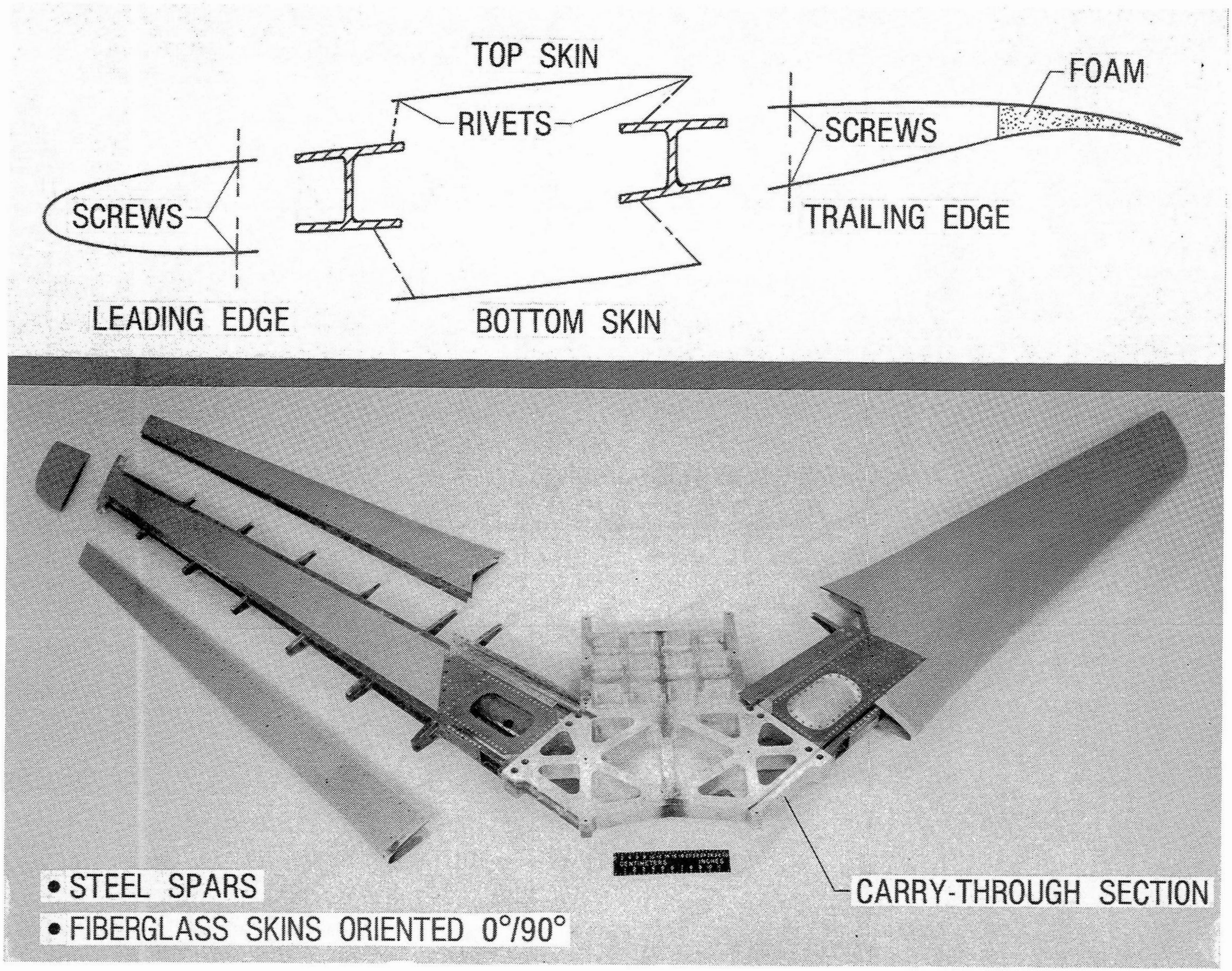

L-81-7306

Figure 5.- Wing structural arrangement.

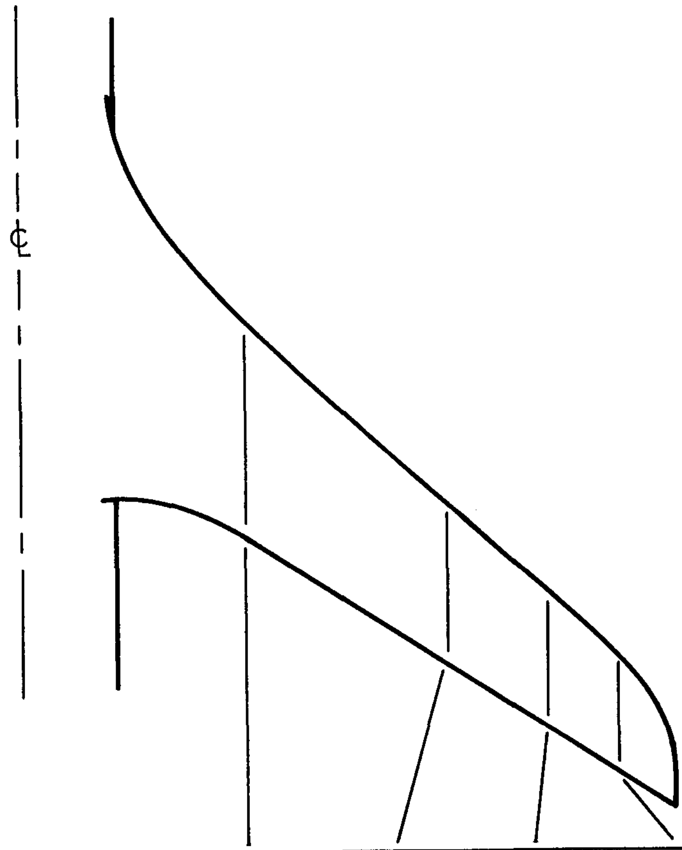

Row	1	2	3	4
η =	0.345	0.653	0.809	0.915
Y_F =	29.50	55.83	69.17	78.23

Figure 6.- Semispan locations of wing surface pressure measurements.

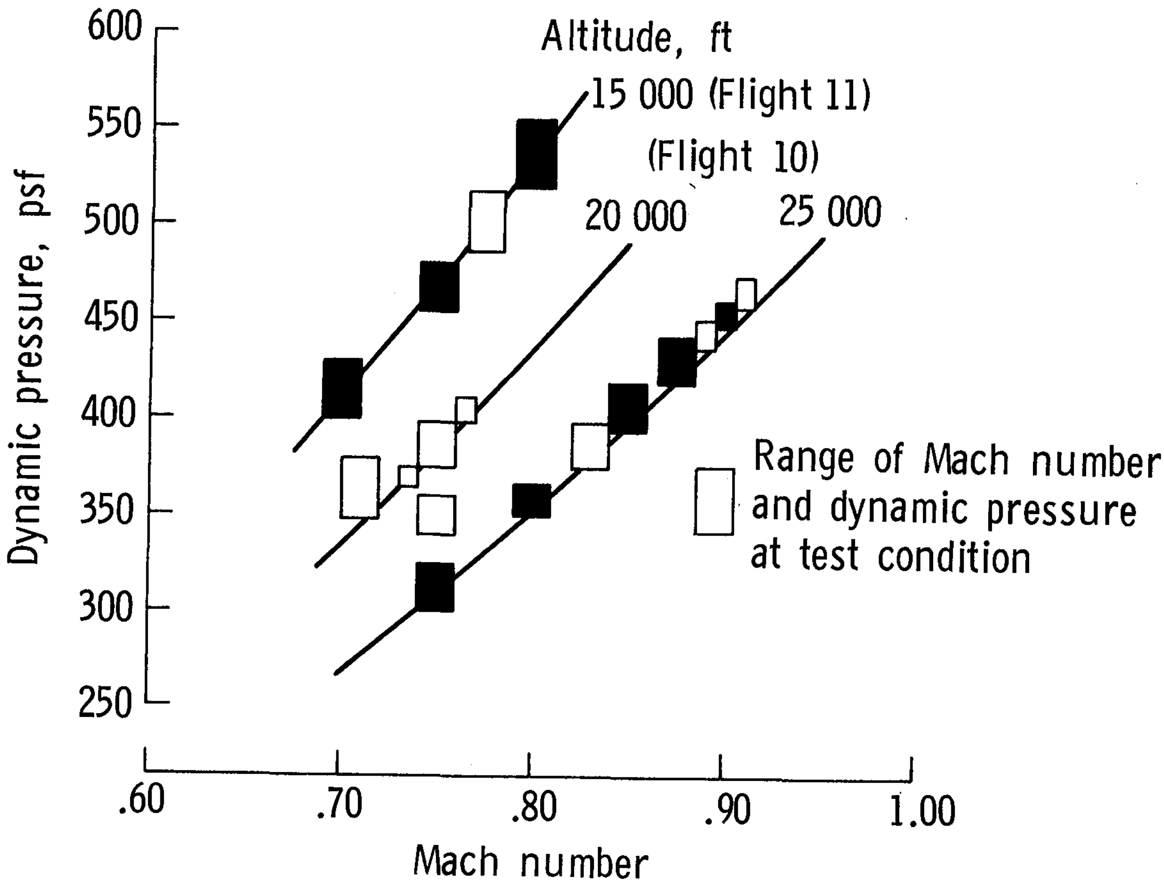

Figure 7.- Flight-test conditions. Closed symbols represent primary test conditions for data analysis.

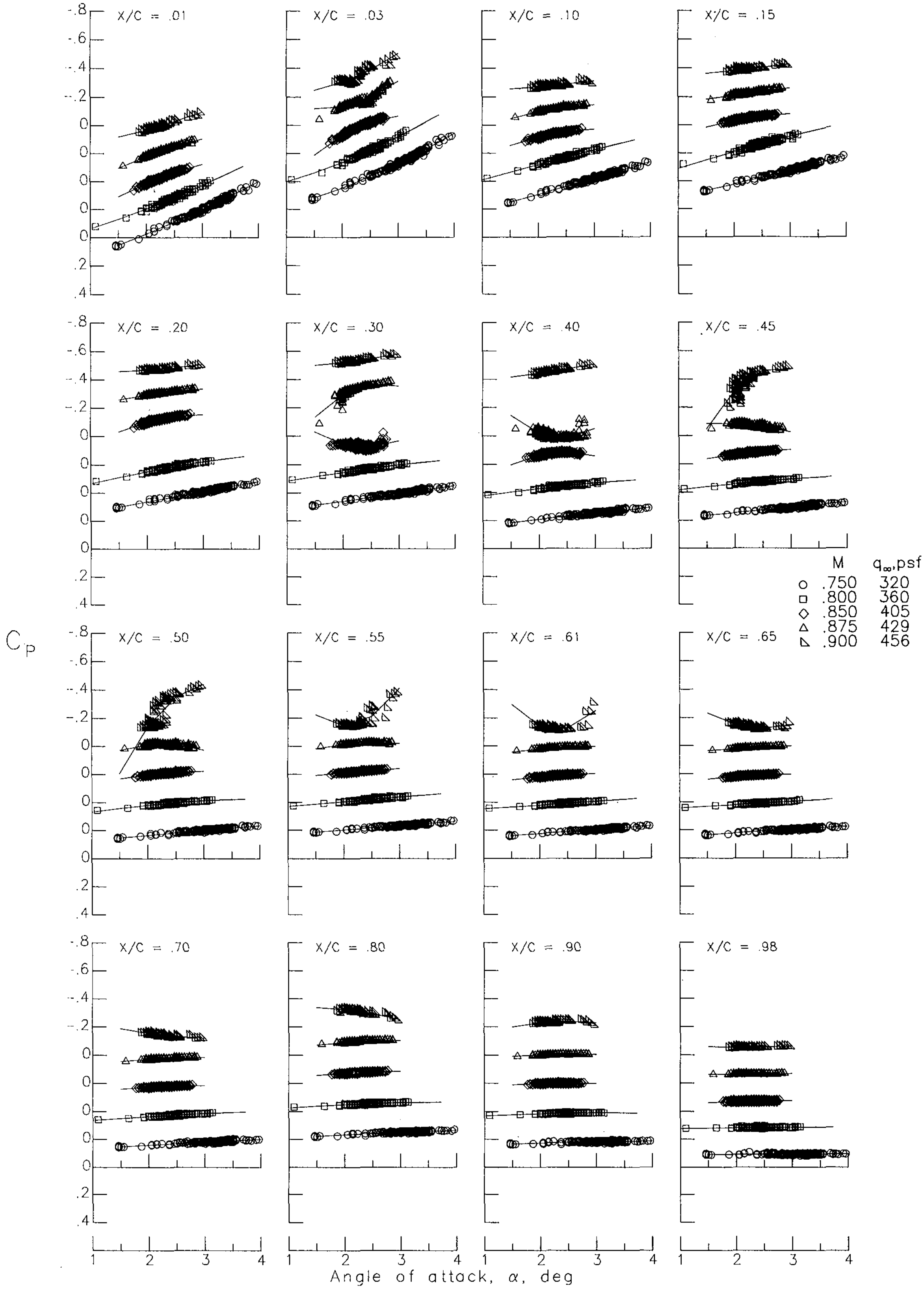

(a) Row 1, upper surface.

Figure 8.- Variations of wing surface pressure coefficients with angle of attack for flight 10.

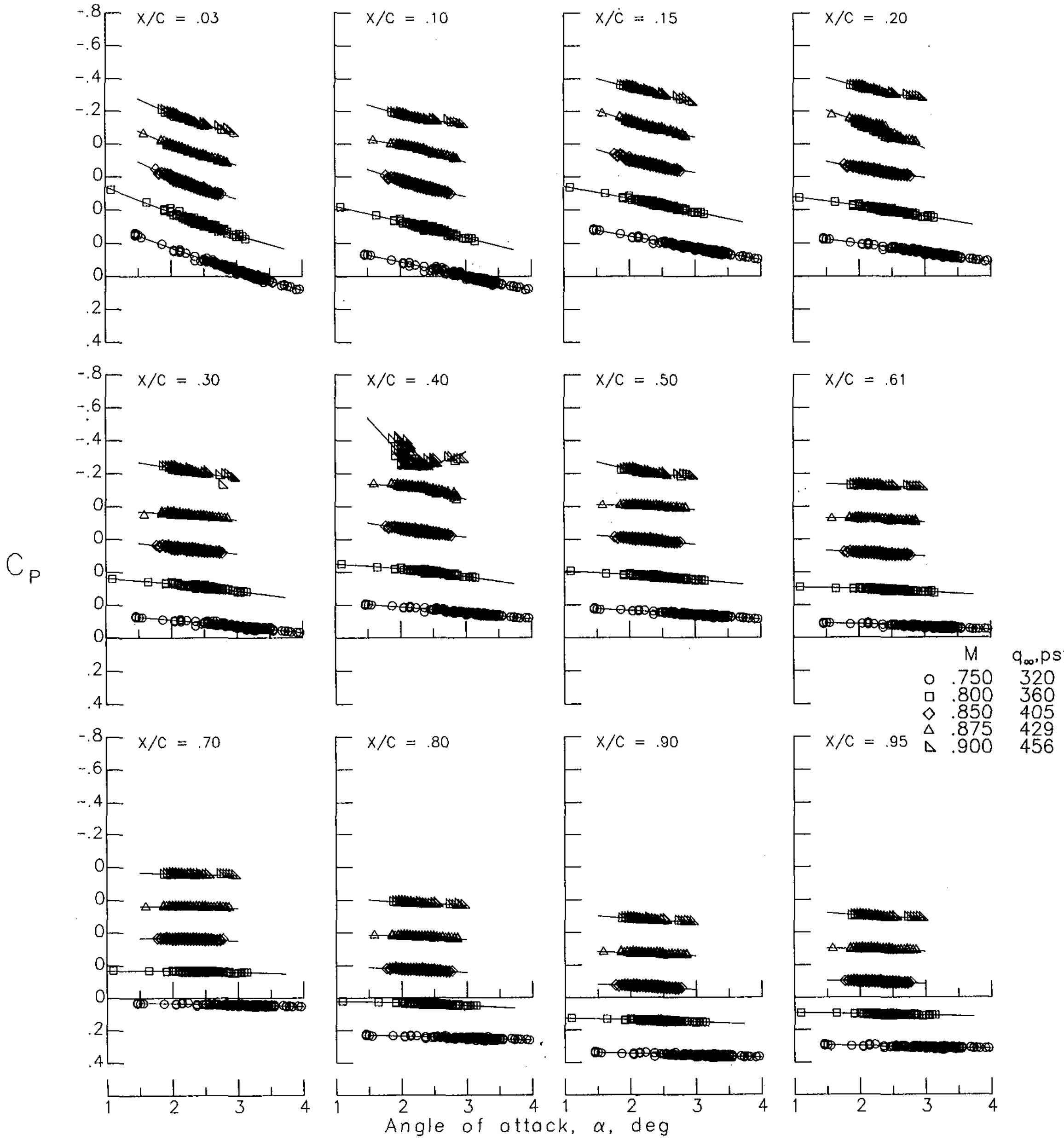

(b) Row 1, lower surface.

Figure 8.- Continued.

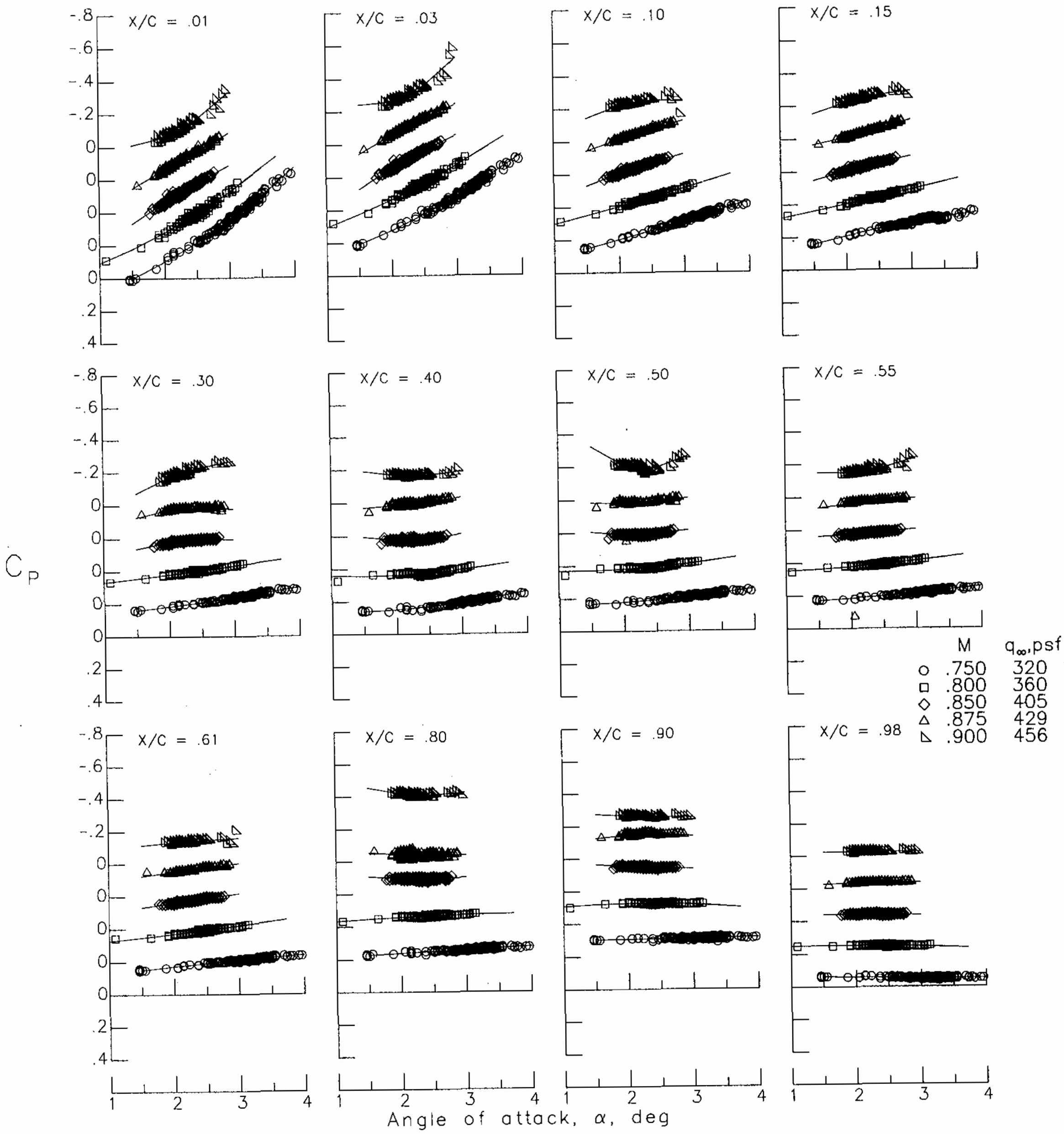

(c) Row 2, upper surface.

Figure 8.- Continued.

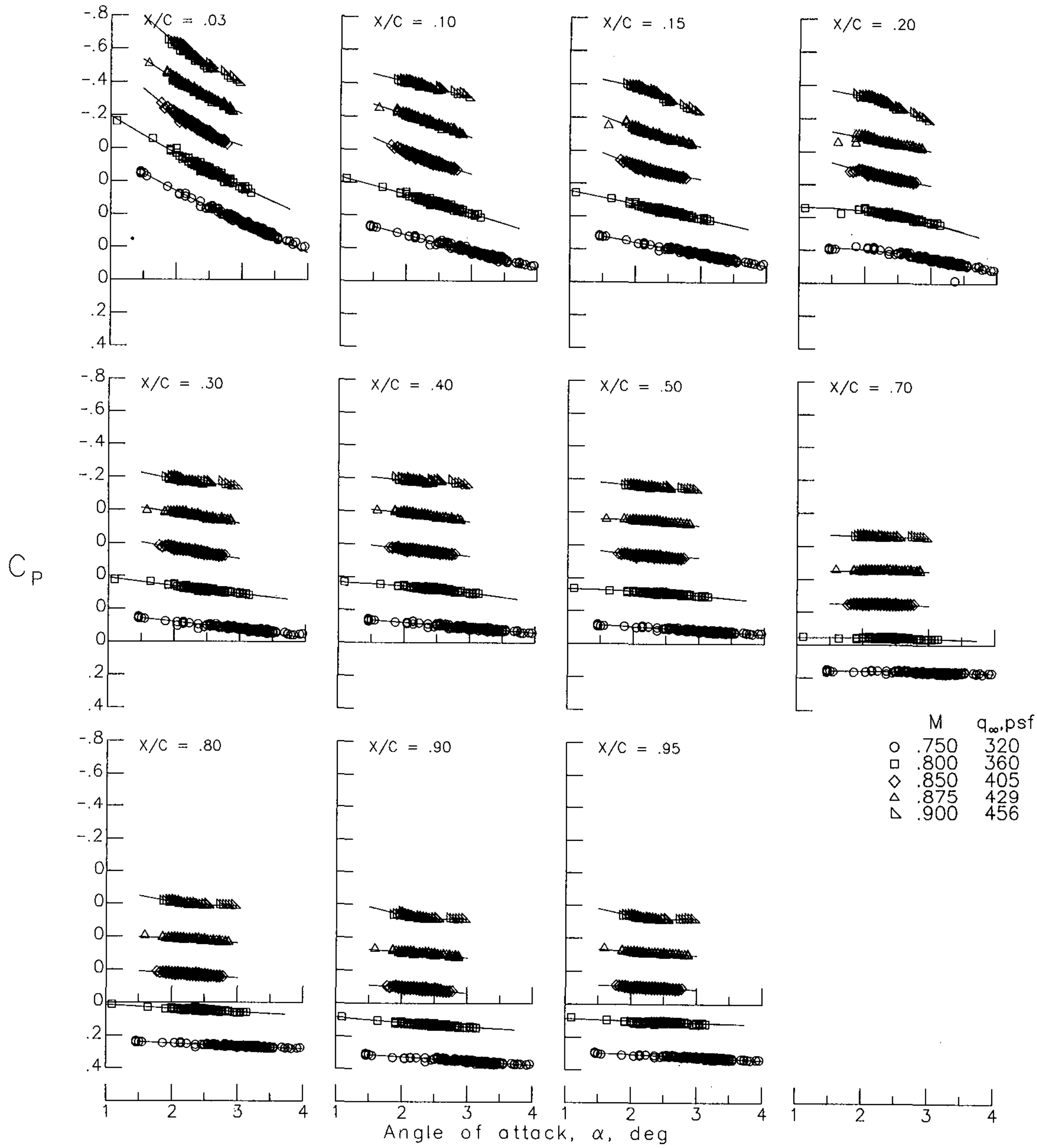

(d) Row 2, lower surface.

Figure 8.- Continued.

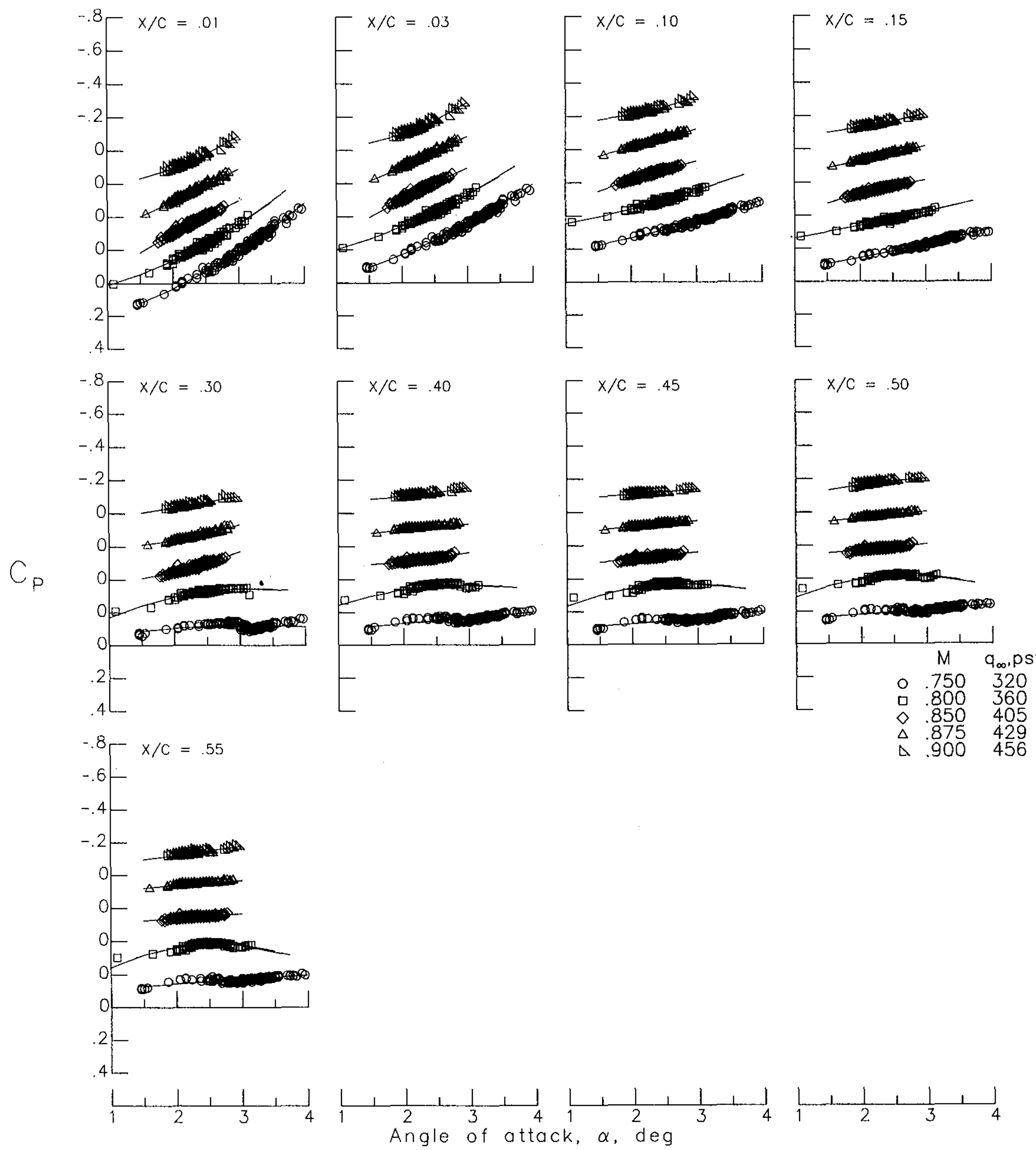

(e) Row 3, upper surface.

Figure 8.- Continued.

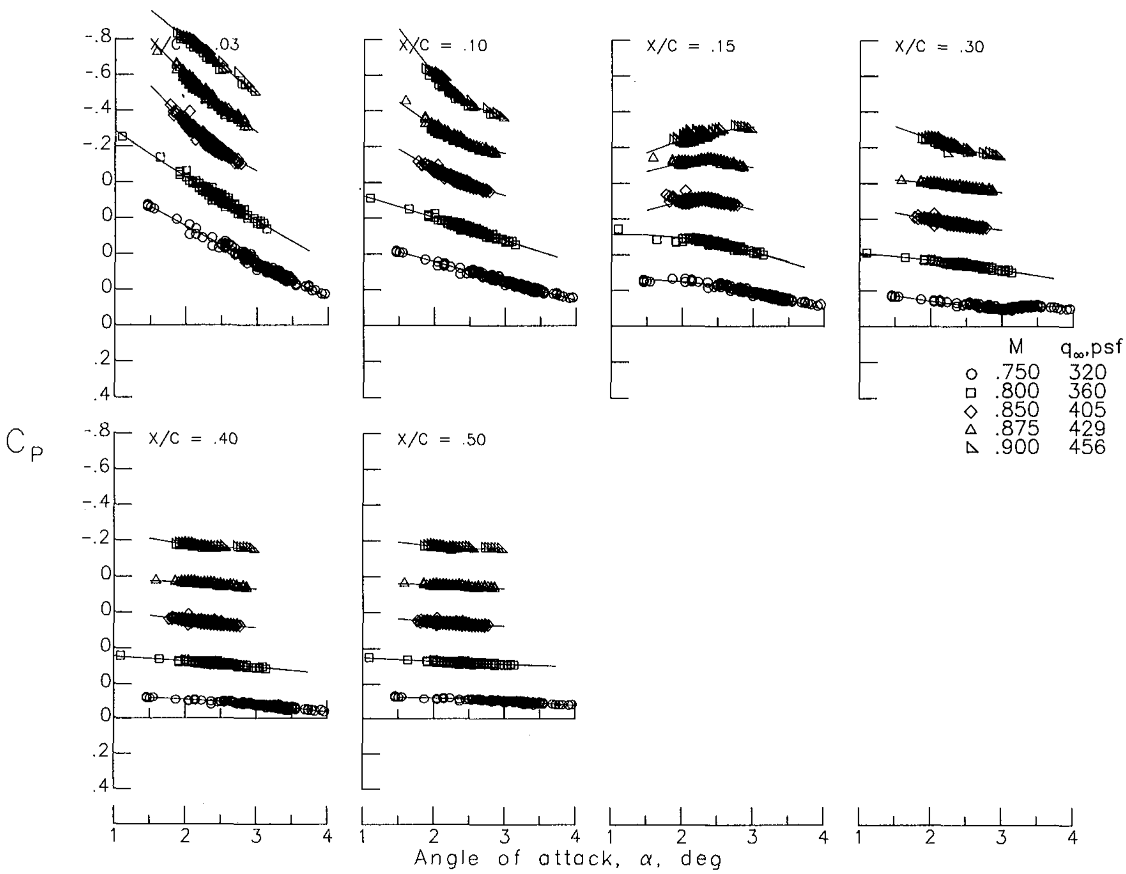

(f) Row 3, lower surface.

Figure 8.- Continued.

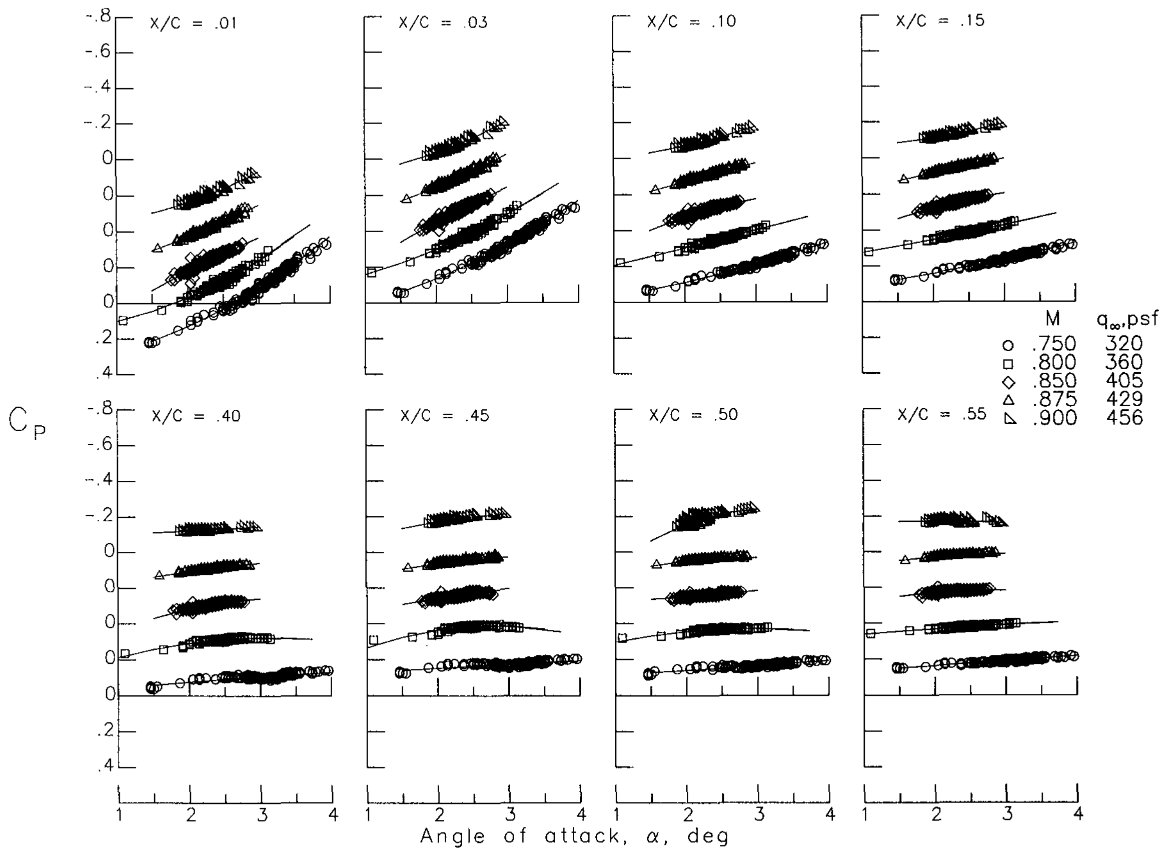

(g) Row 4, upper surface.

Figure 8.- Continued.

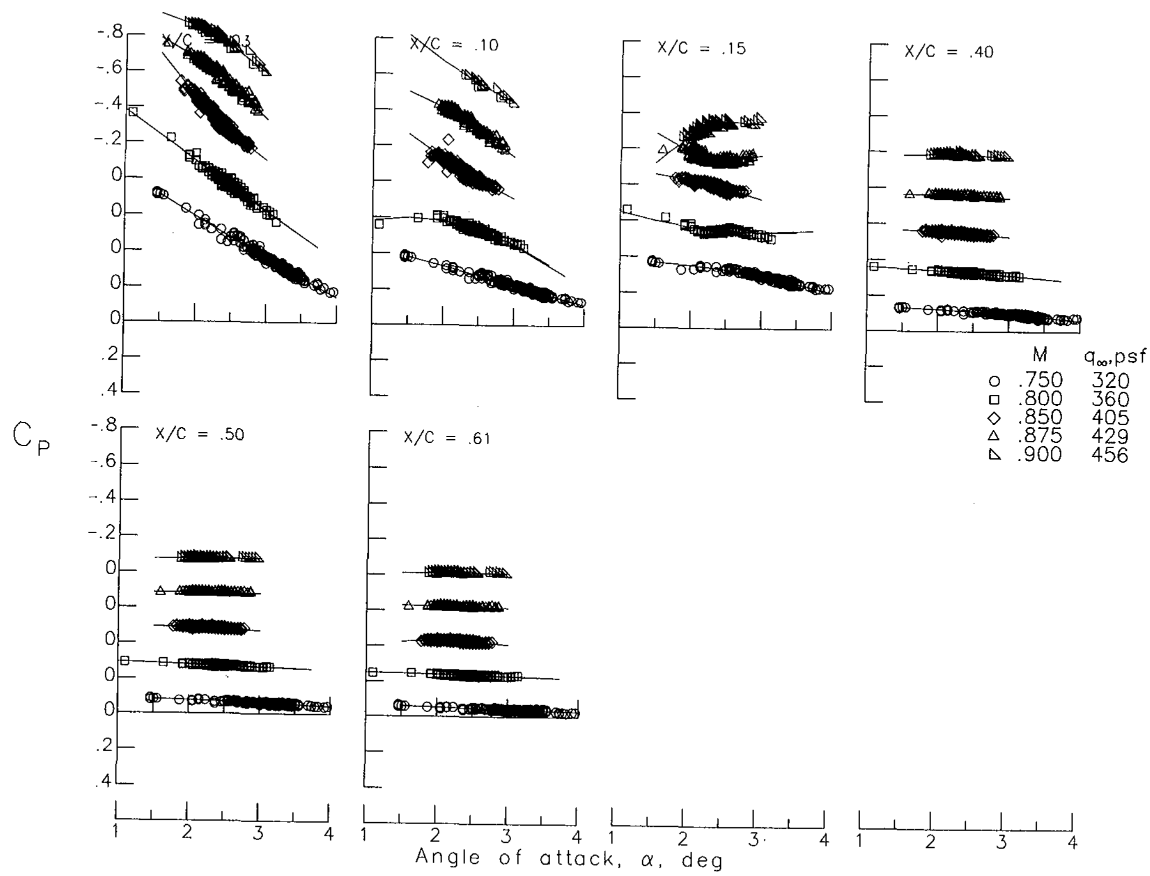

(h) Row 4, lower surface.

Figure 8.- Concluded.

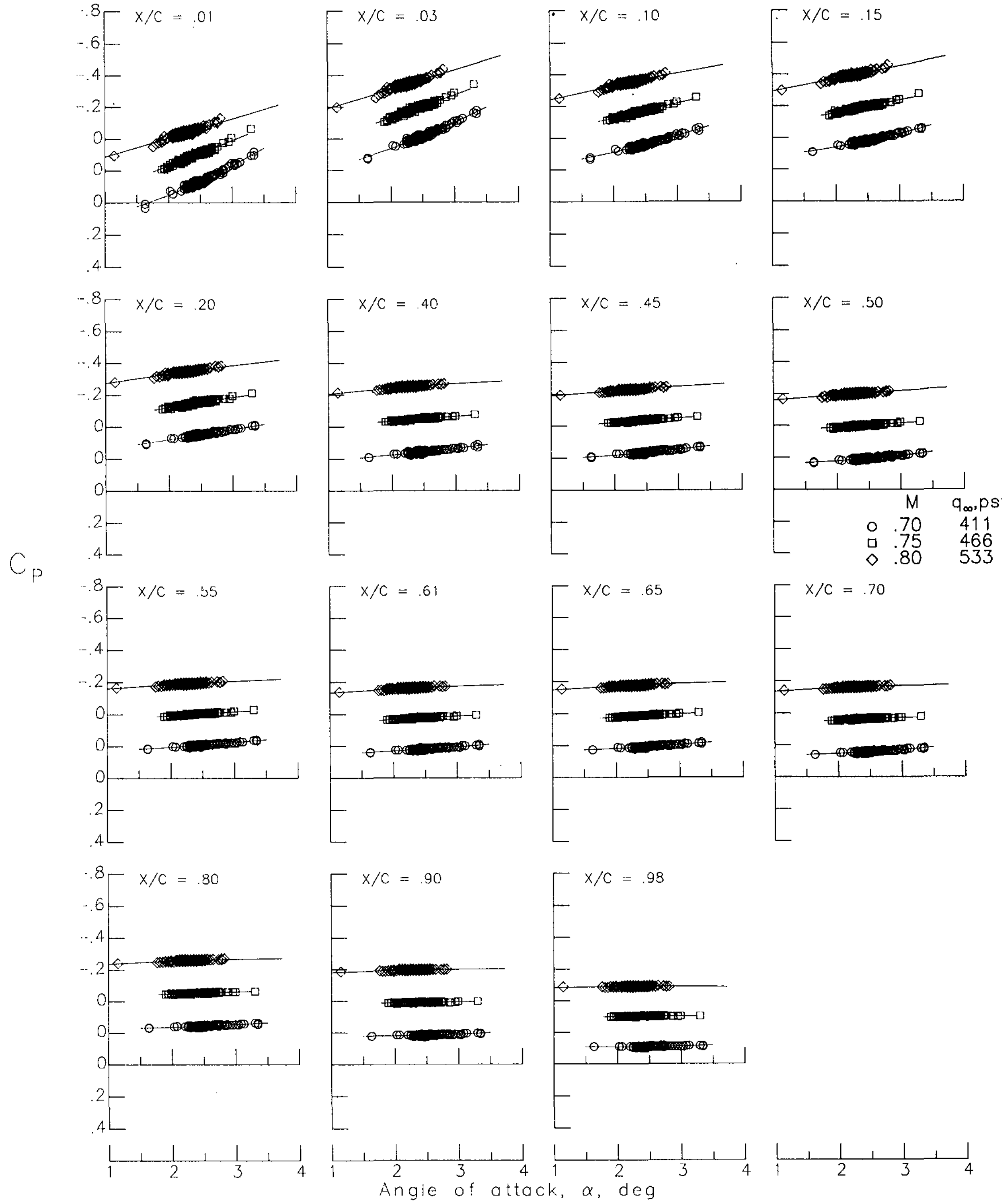

(a) Row 1, upper surface.

Figure 9.- Variations of wing surface pressure coefficients with angle of attack for flight 11.

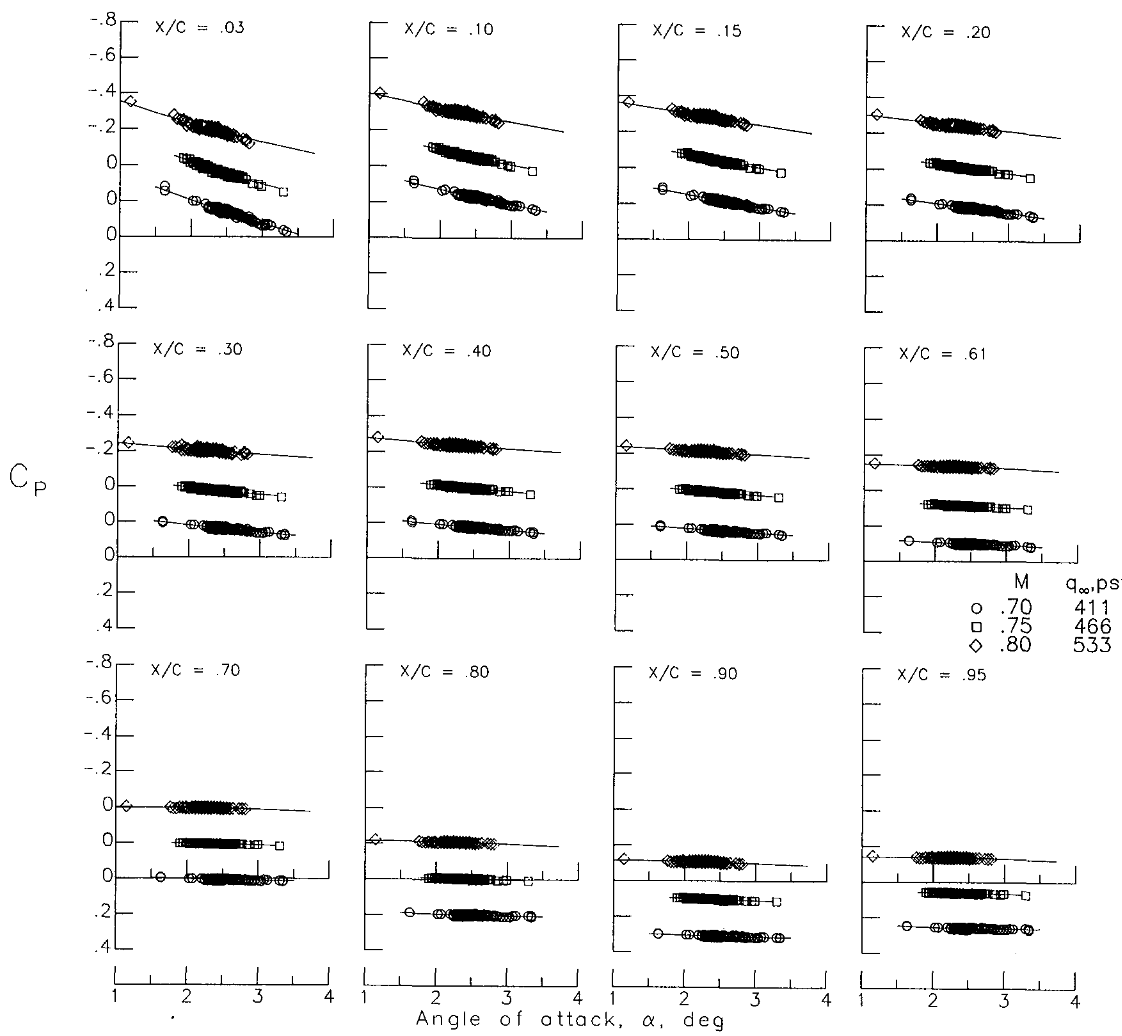

(b) Row 1, lower surface.

Figure 9.- Continued.

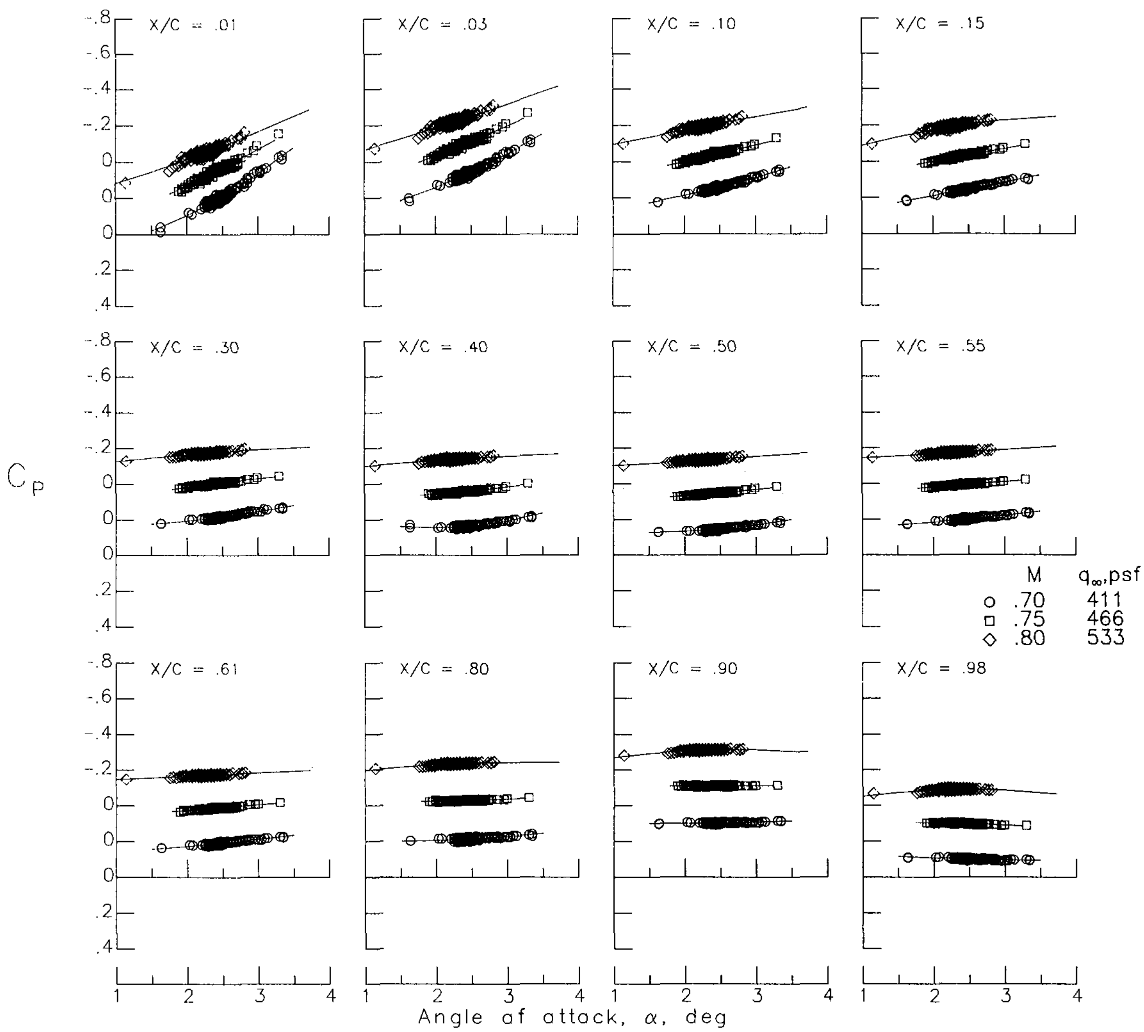

(c) Row 2, upper surface.

Figure 9.- Continued.

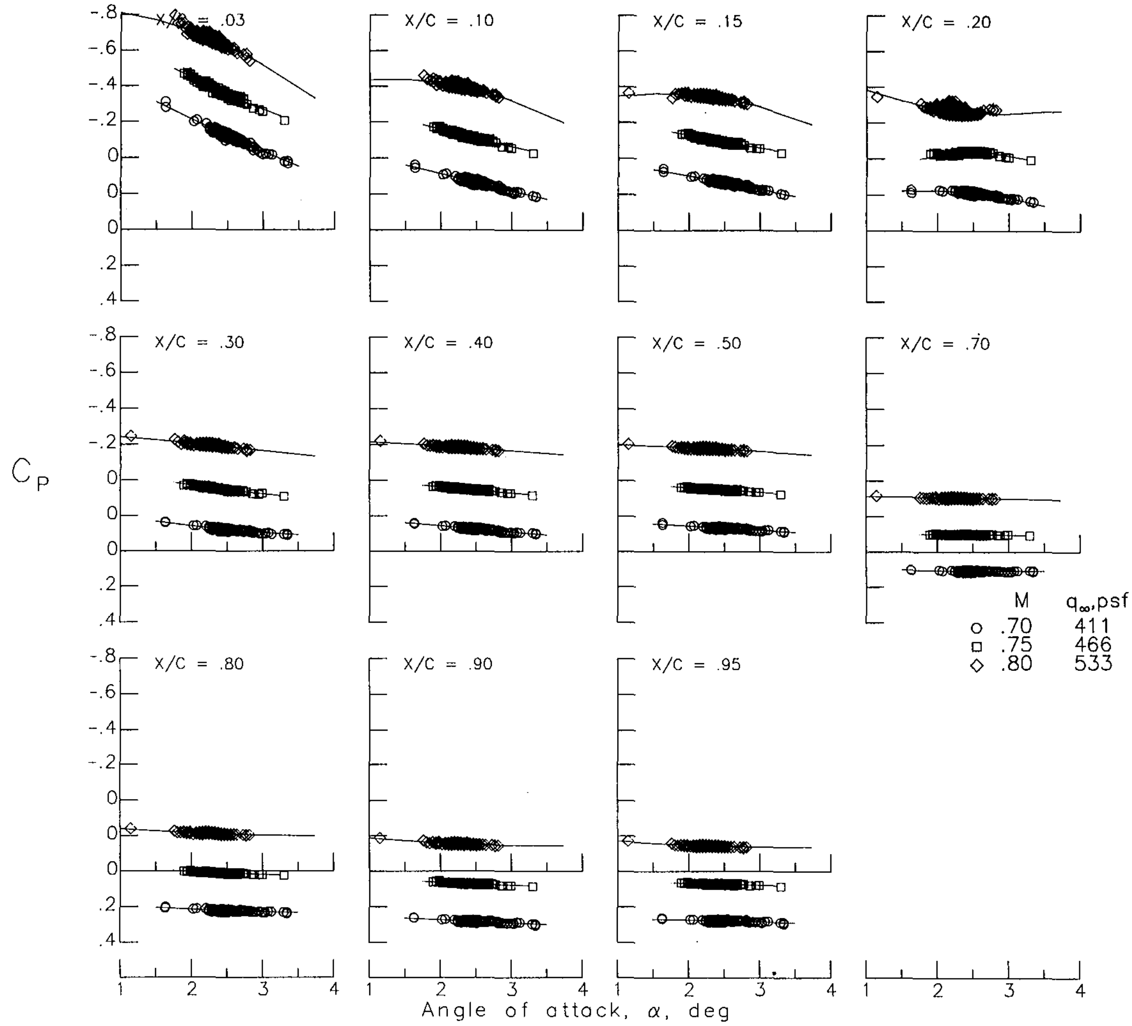

(d) Row 2, lower surface.

Figure 9.- Continued.

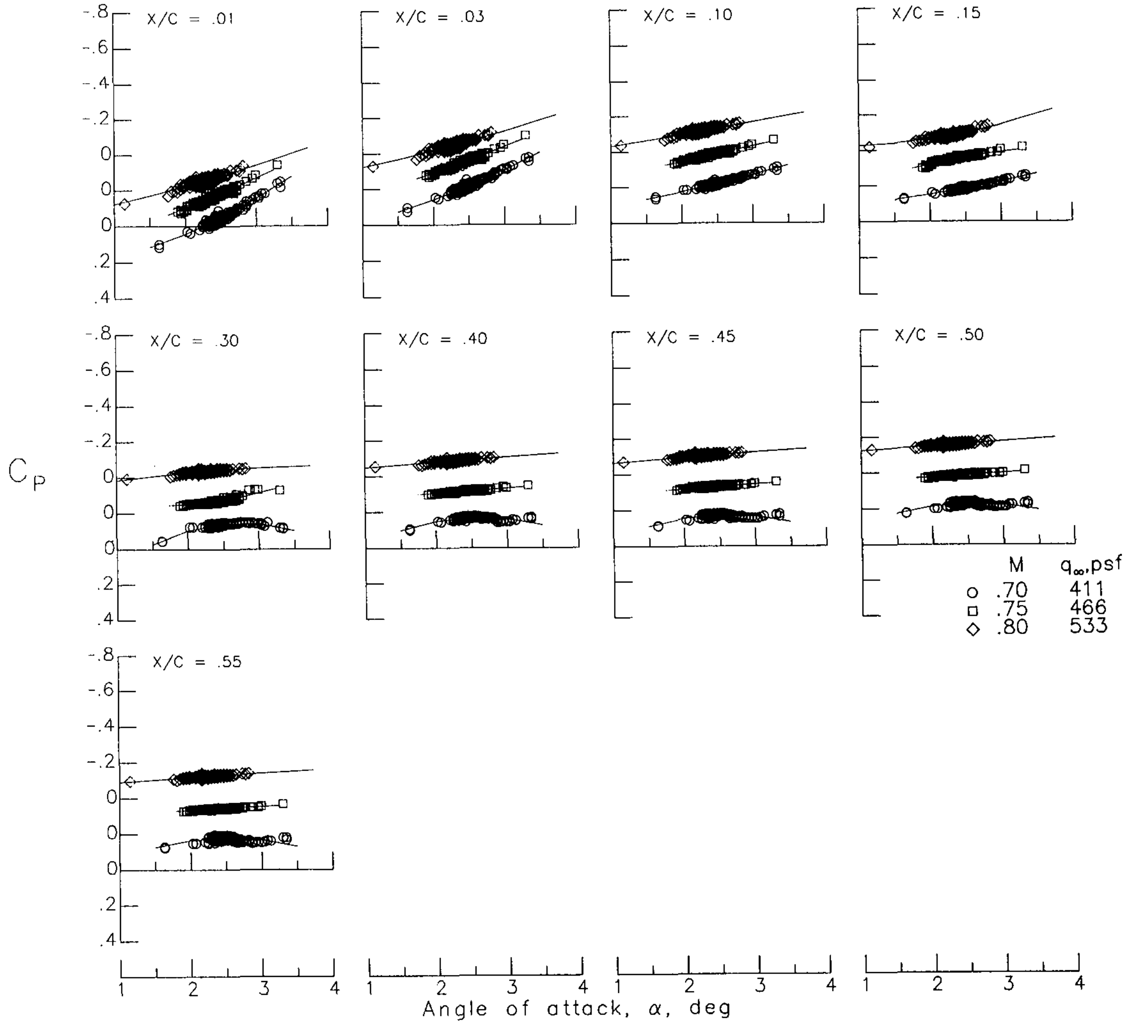

(e) Row 3, upper surface.

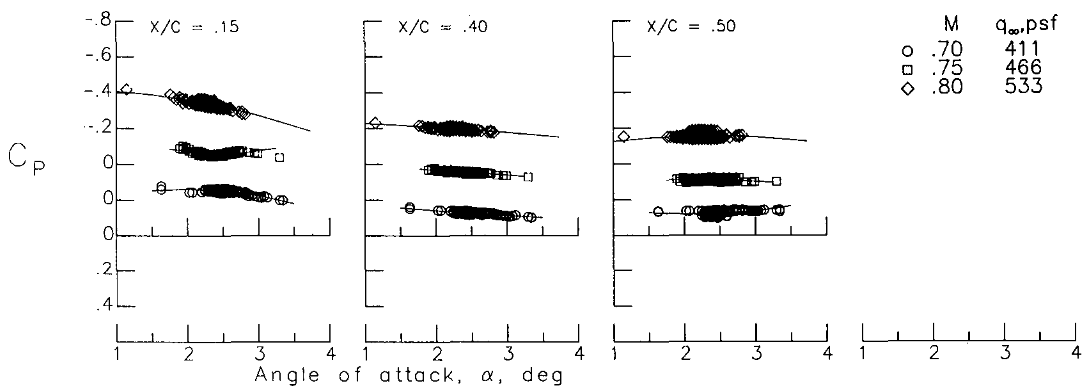

(f) Row 3, lower surface.

Figure 9.- Continued.

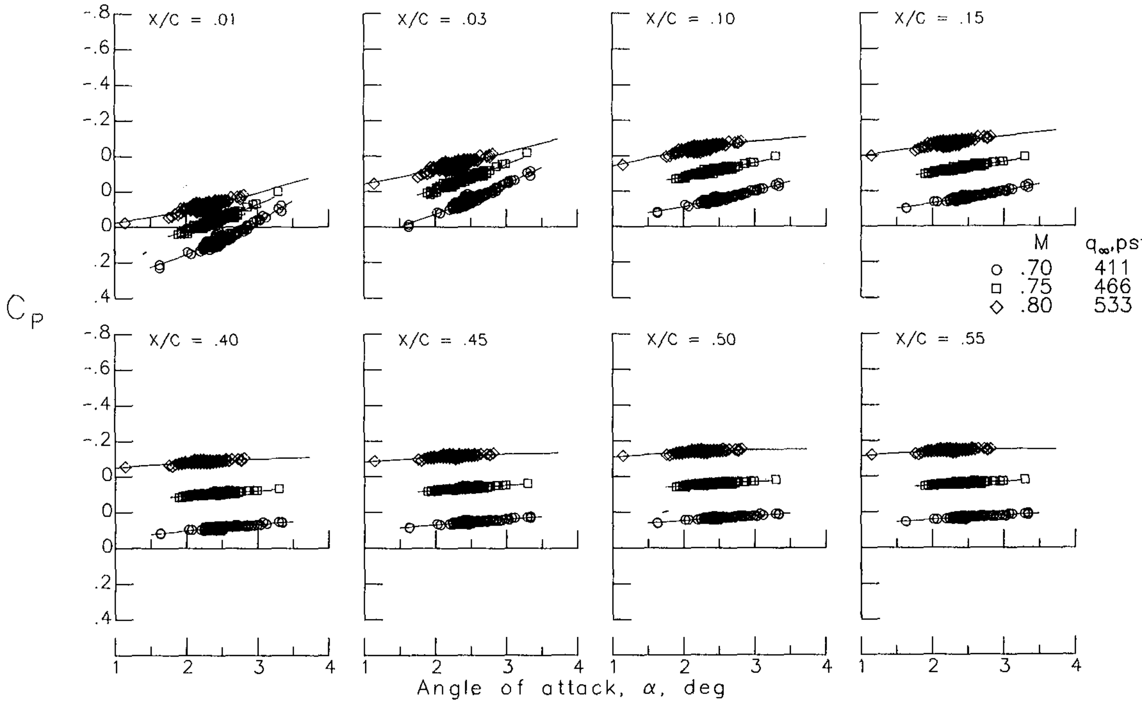

(g) Row 4, upper surface.

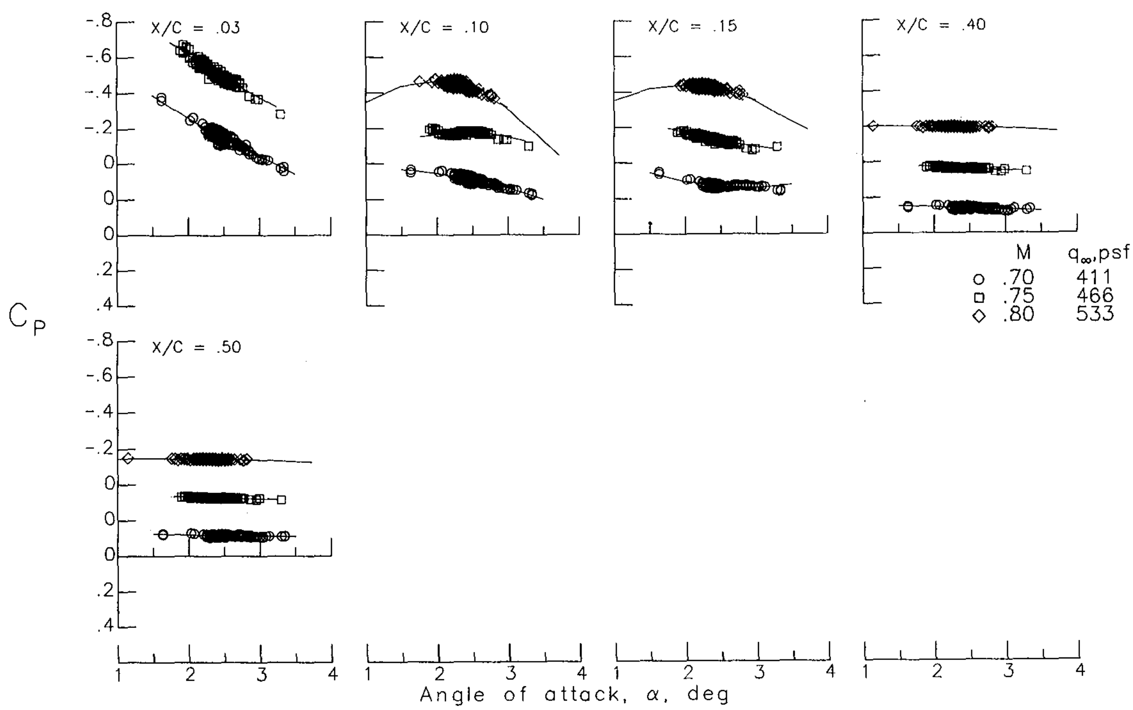

(h) Row 4, lower surface.

Figure 9.- Concluded.

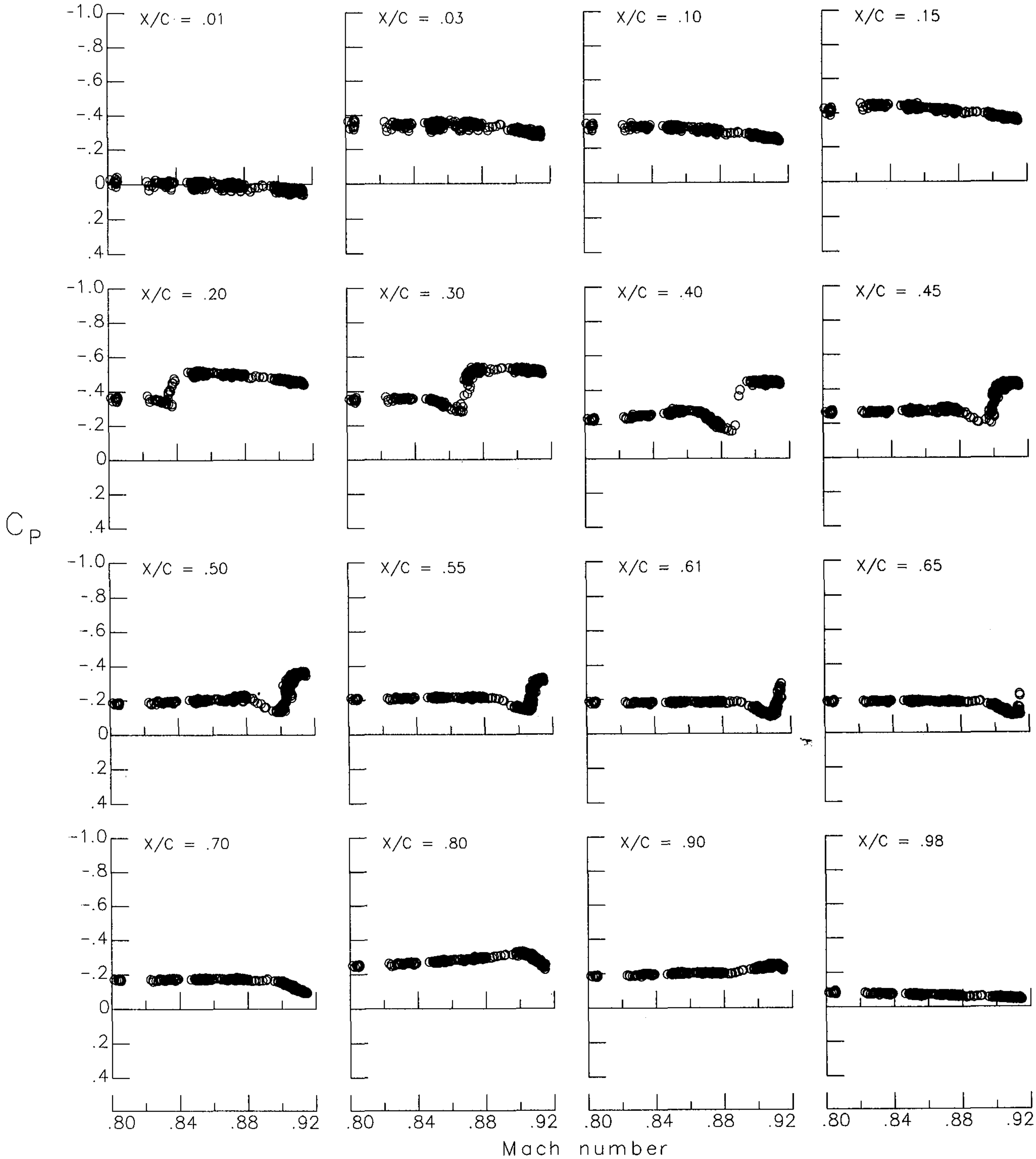

(a) Row 1, upper surface.

Figure 10.- Variations of wing surface pressure coefficients with Mach for flight 10. α = 2.0°.

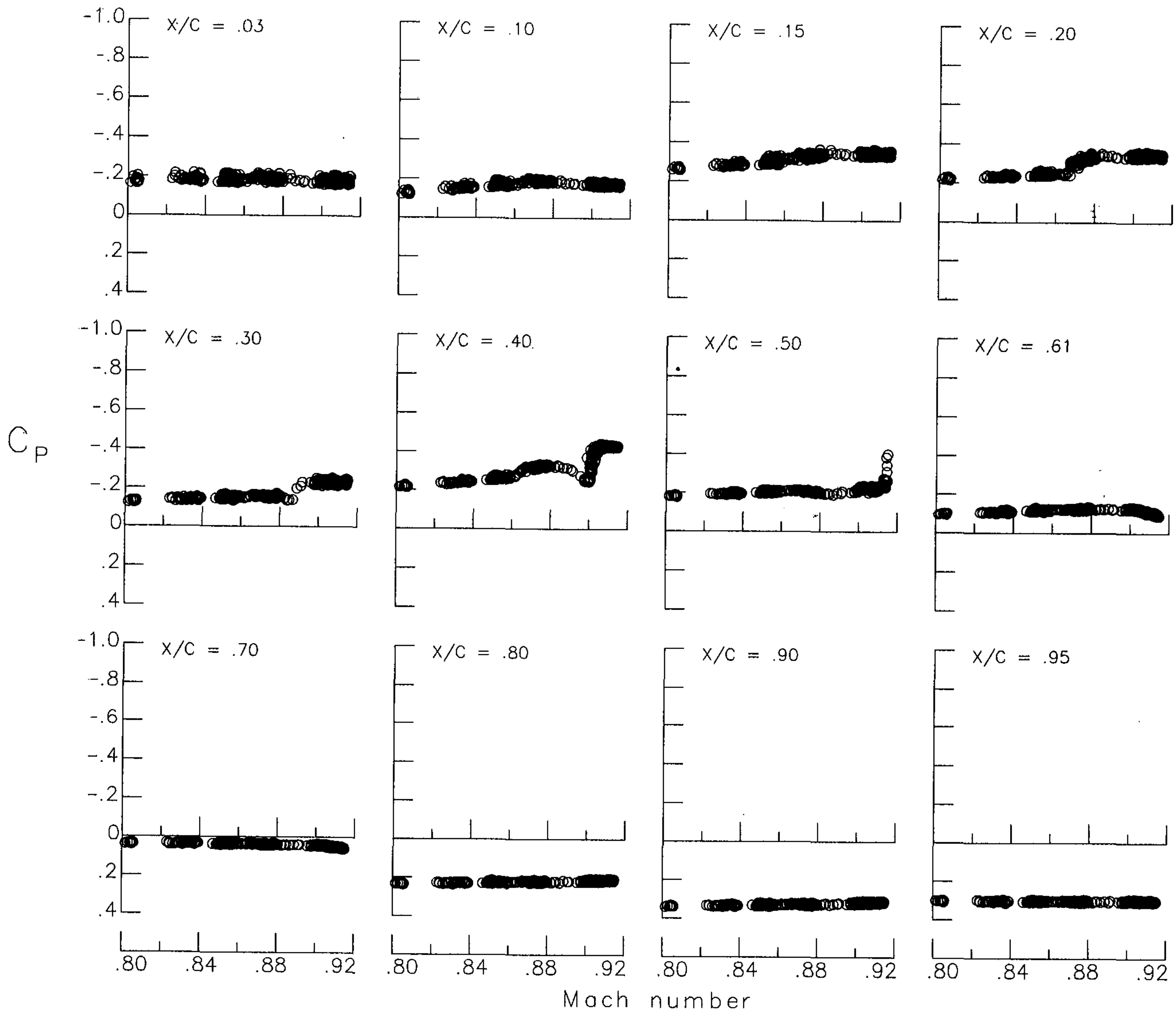

(b) Row 1, lower surface.

Figure 10.- Continued.

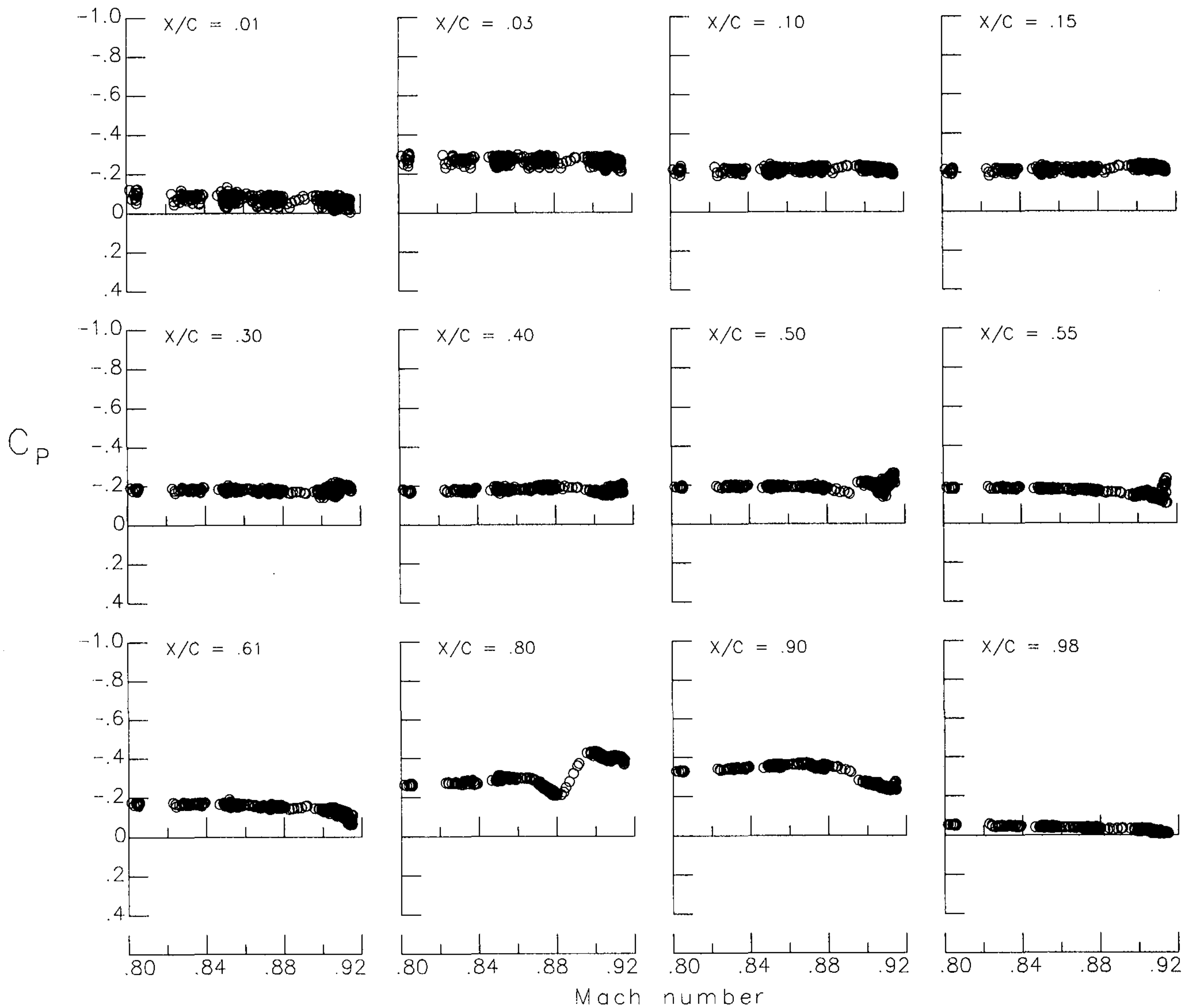

(c) Row 2, upper surface.

Figure 10.- Continued.

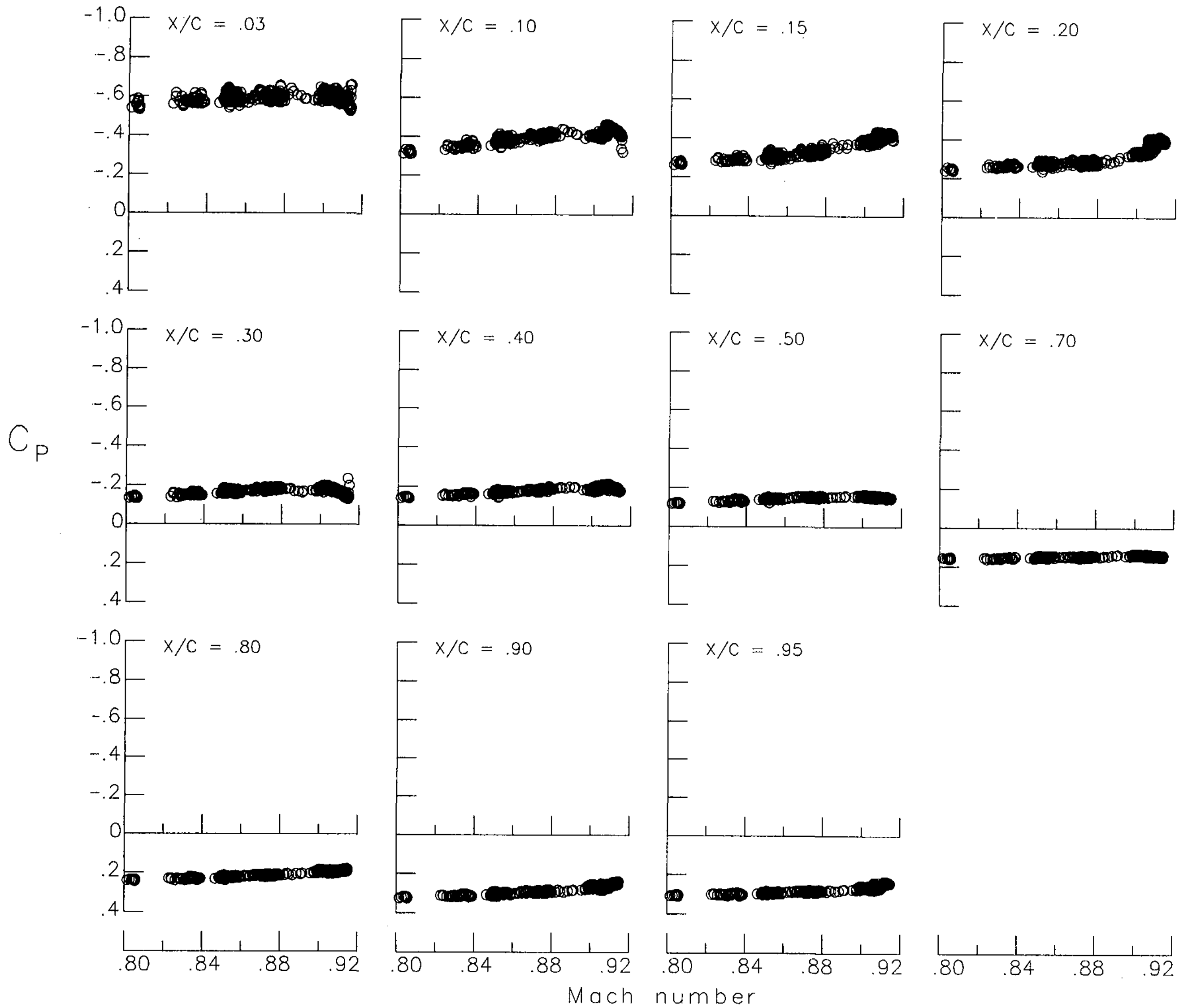

(d) Row 2, lower surface.

Figure 10.- Continued.

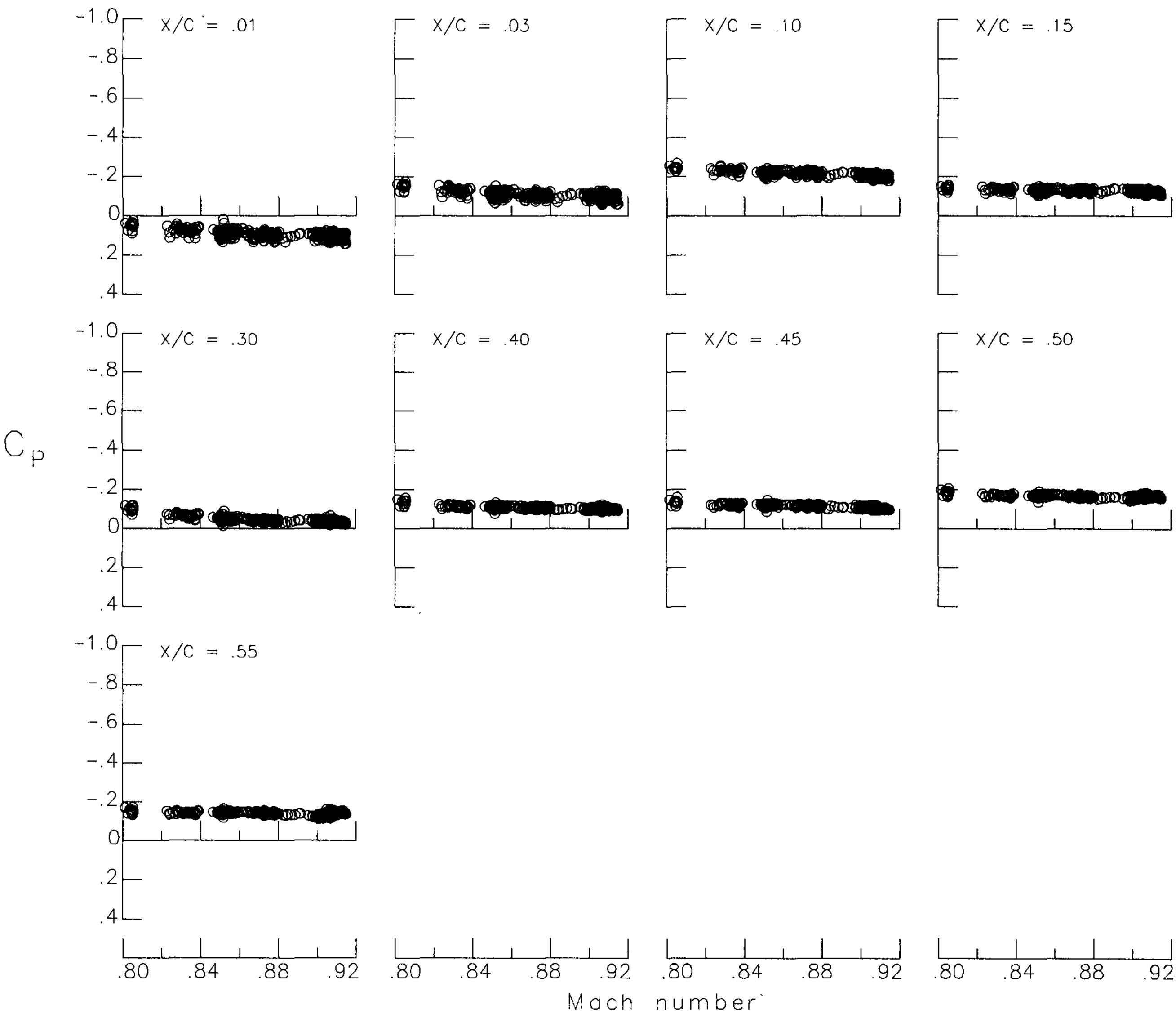

(e) Row 3, upper surface.

Figure 10.- Continued.

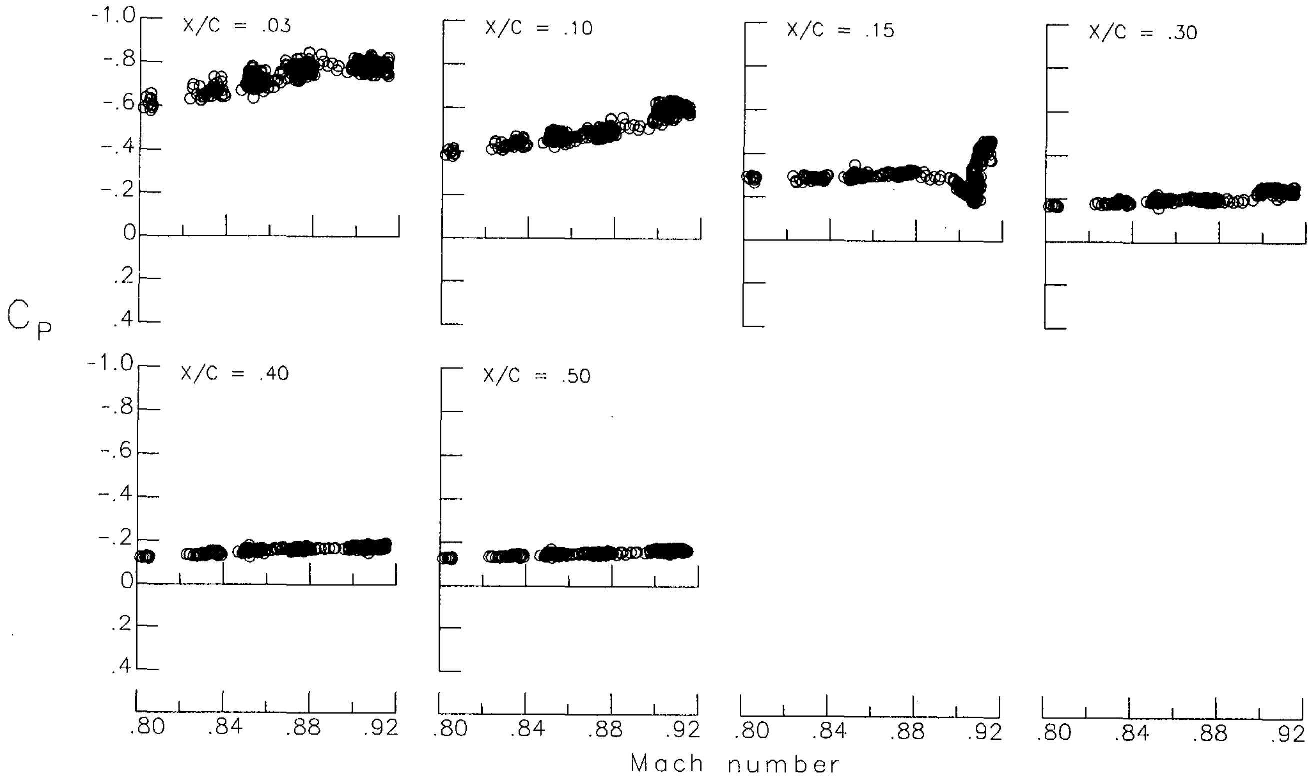

(f) Row 3, lower surface.

Figure 10.- Continued.

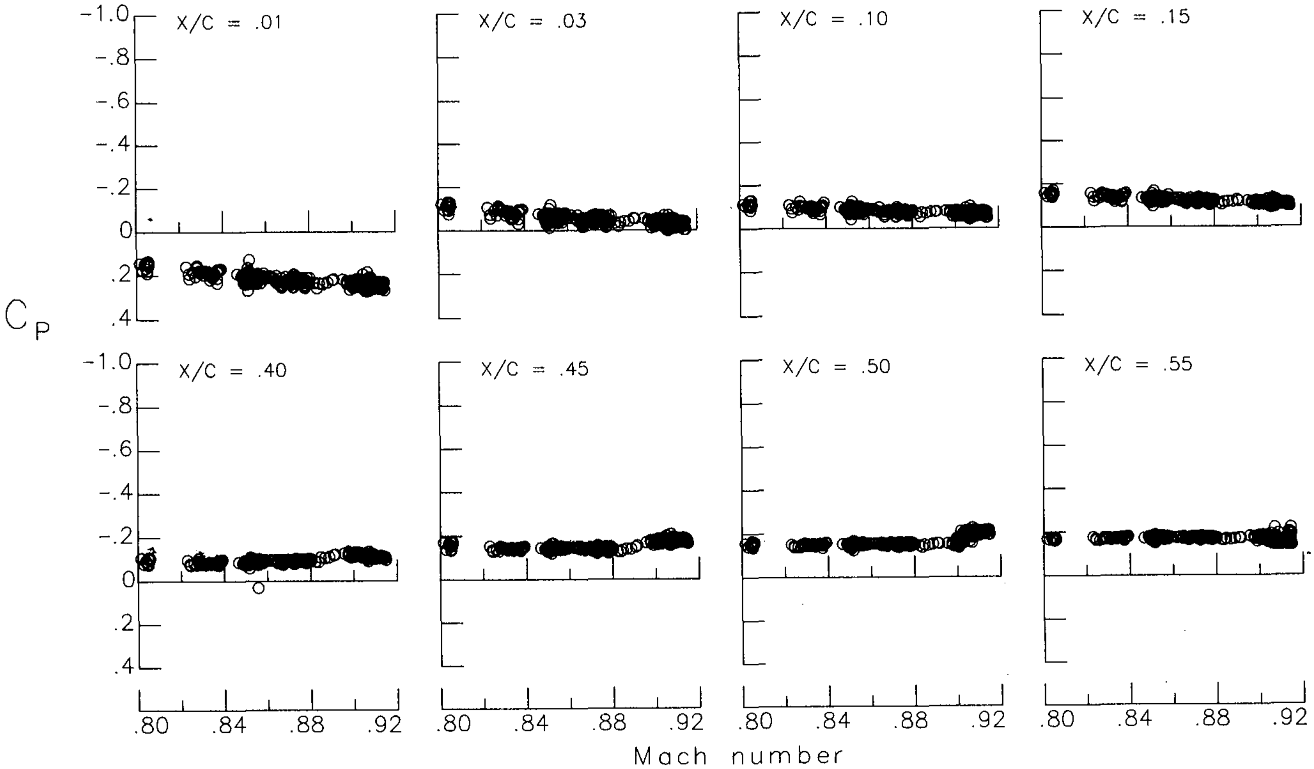

(g) Row 4, upper surface.

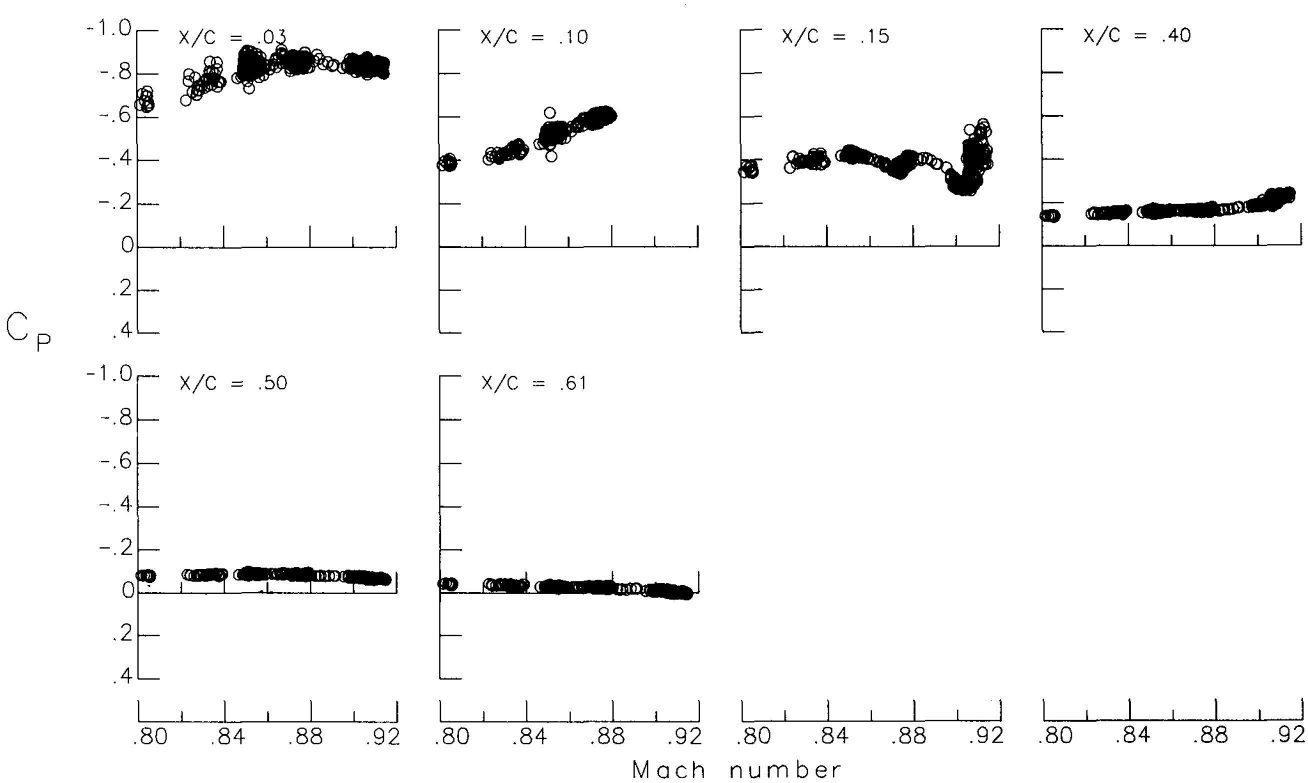

(h) Row 4, lower surface.

Figure 10.- Concluded.

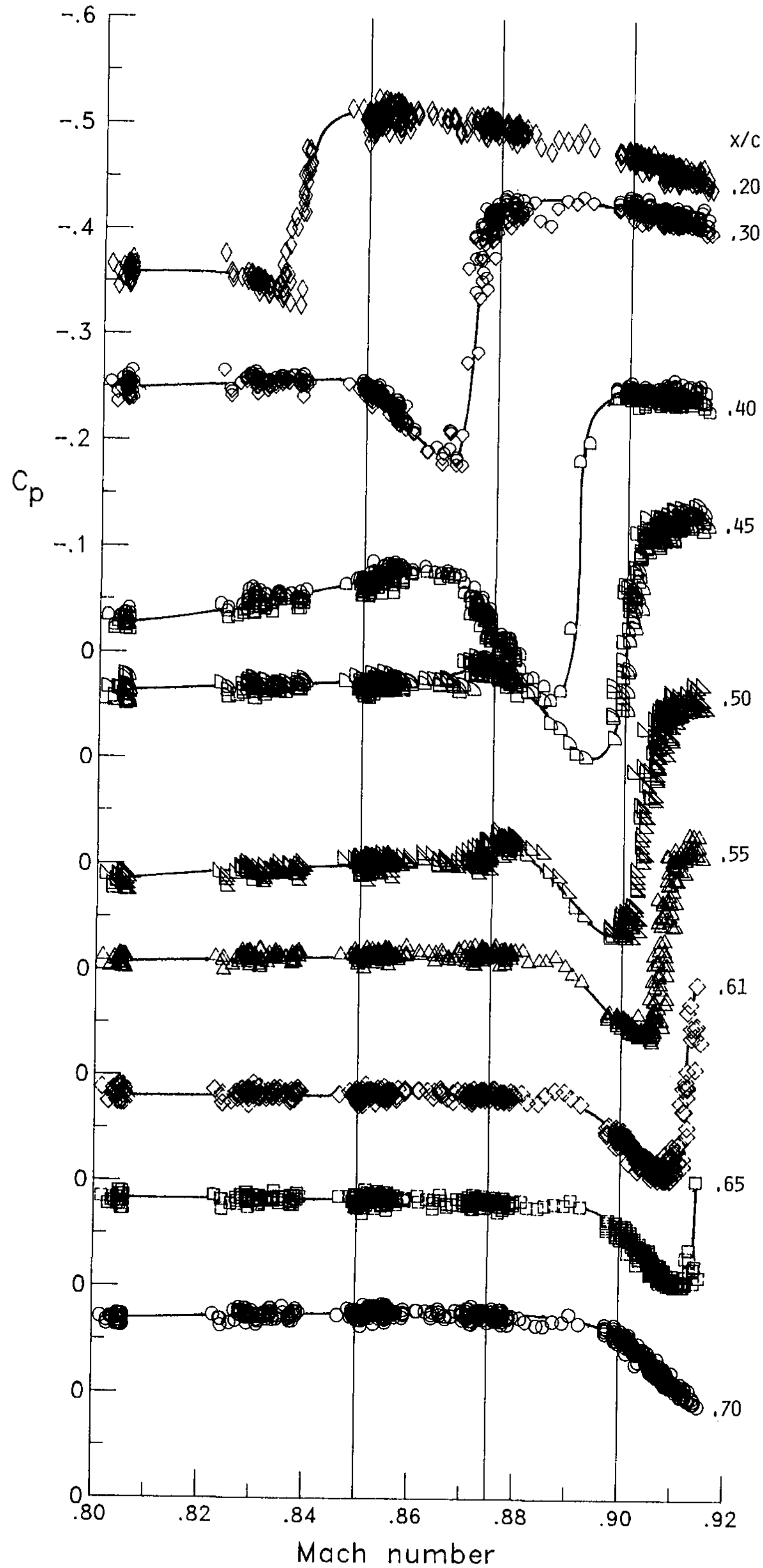

(a) α = 2.0°.

Figure 11.- Variations of wing surface pressure coefficients with Mach number for selected orifice locations on row 1 of the wing upper surface.

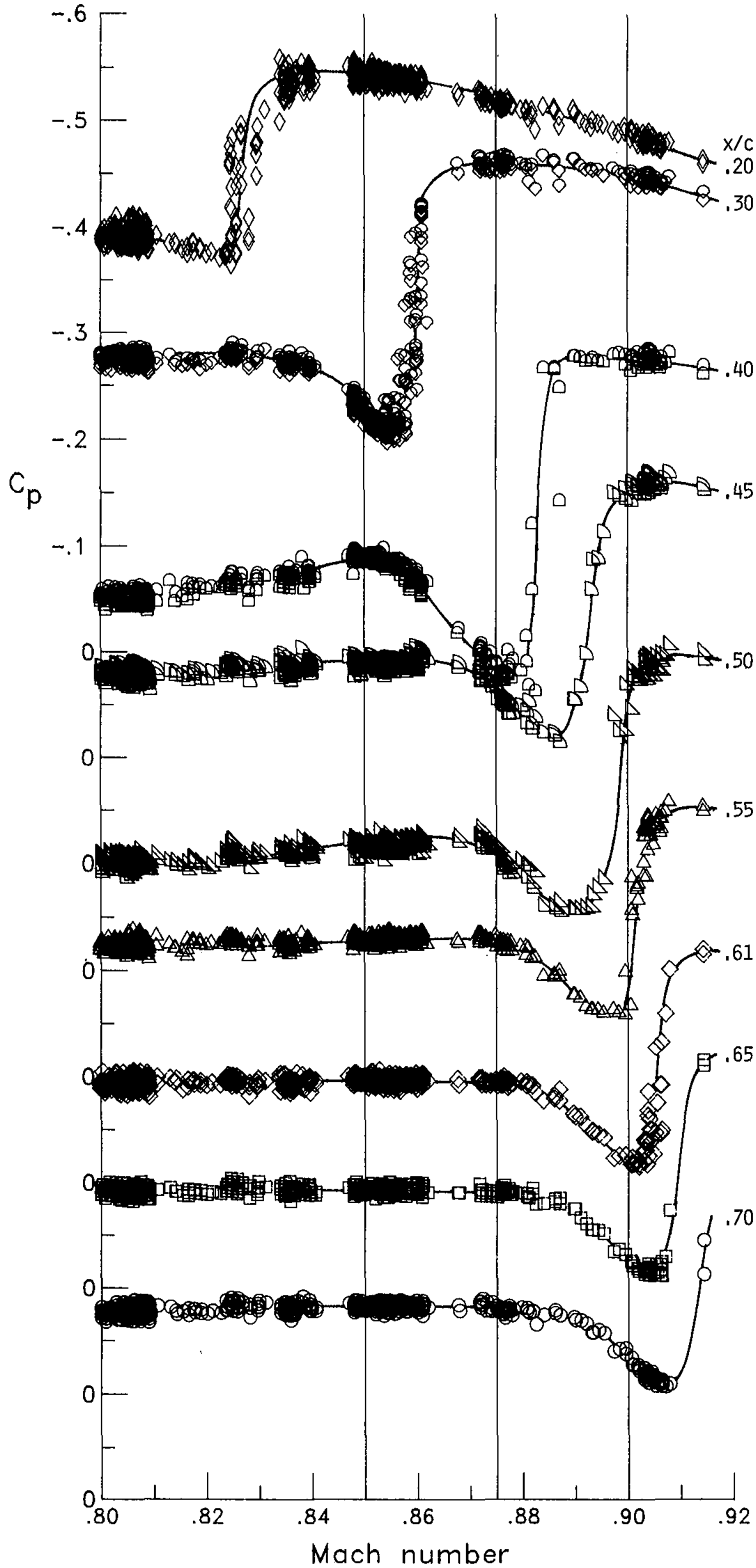

(b) α = 2.5°.

Figure 11.- Concluded.

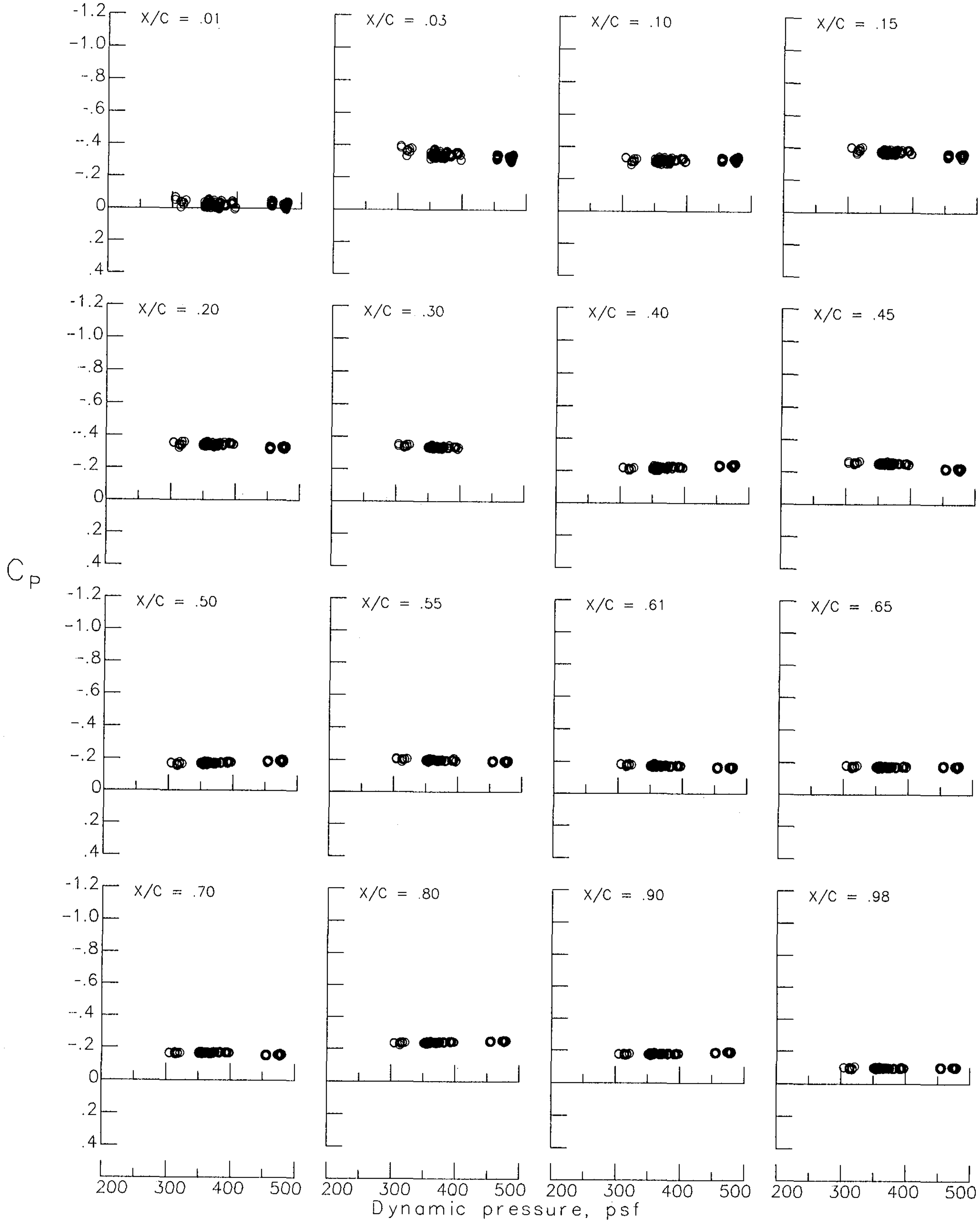

(a) Row 1, upper surface.

Figure 12.- Variations of wing surface pressure coefficients with dynamic pressure. $M = 0.75 \pm 0.01$, $\alpha = 2.0°$.

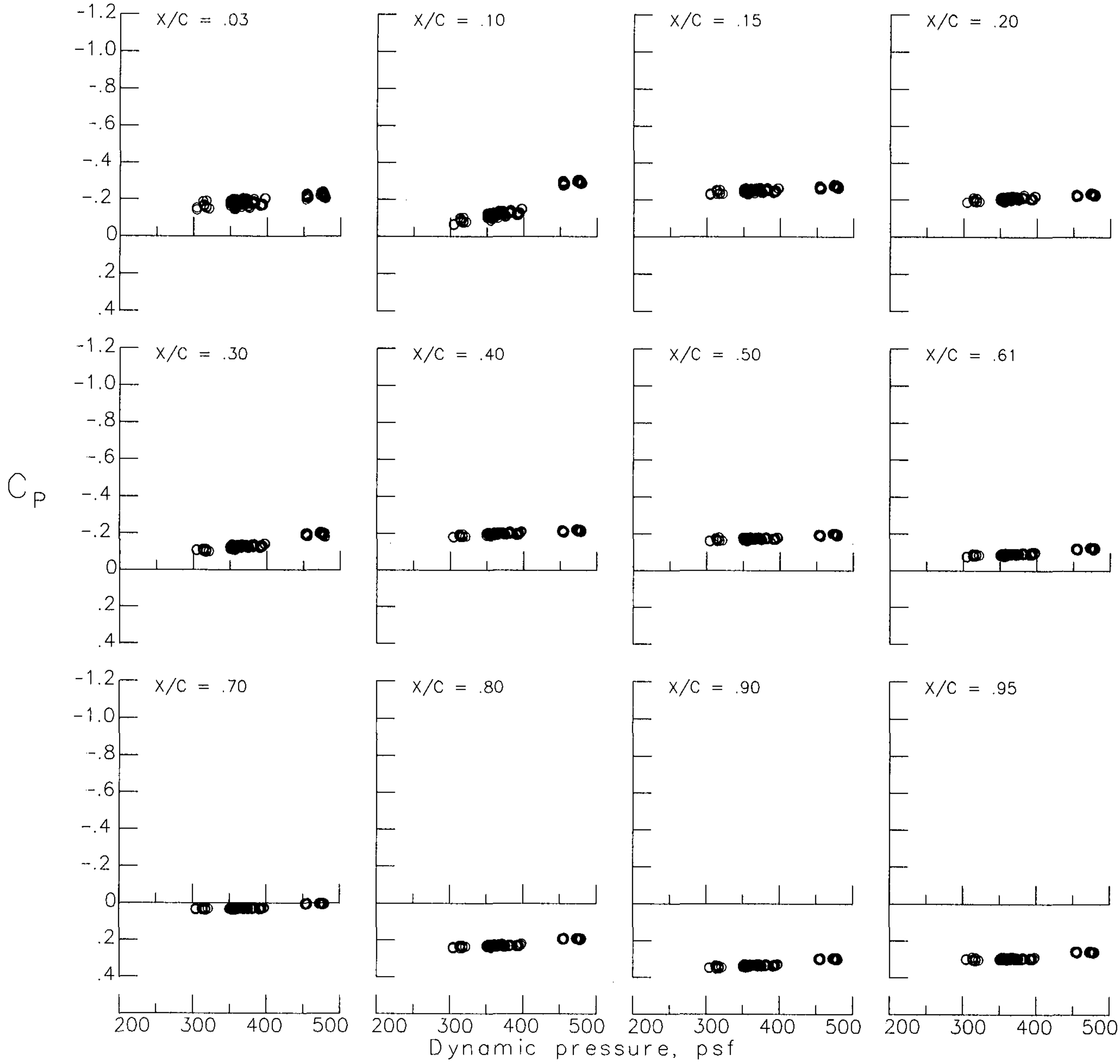

(b) Row 1, lower surface.

Figure 12.- Continued.

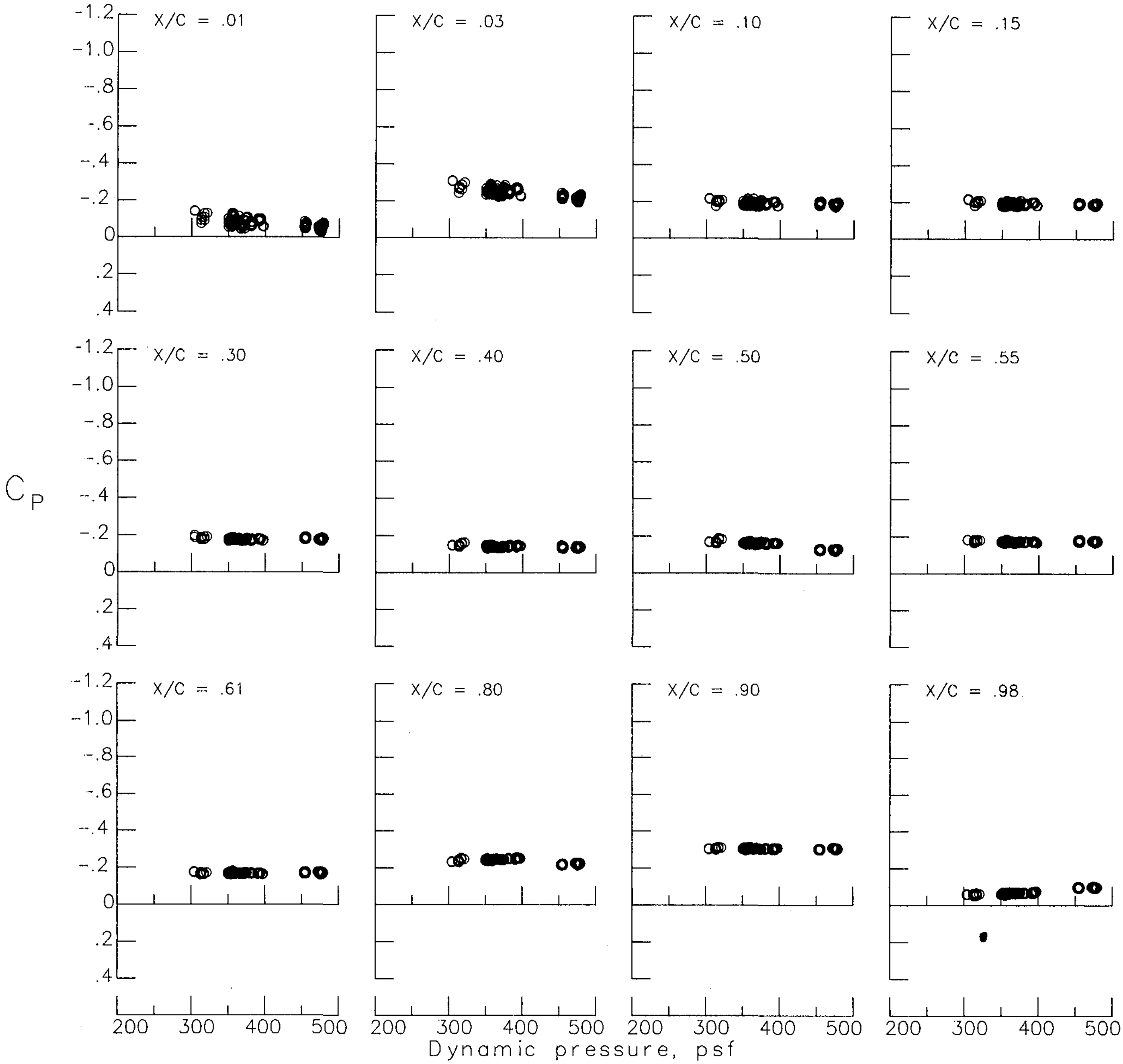

(c) Row 2, upper surface.

Figure 12.- Continued.

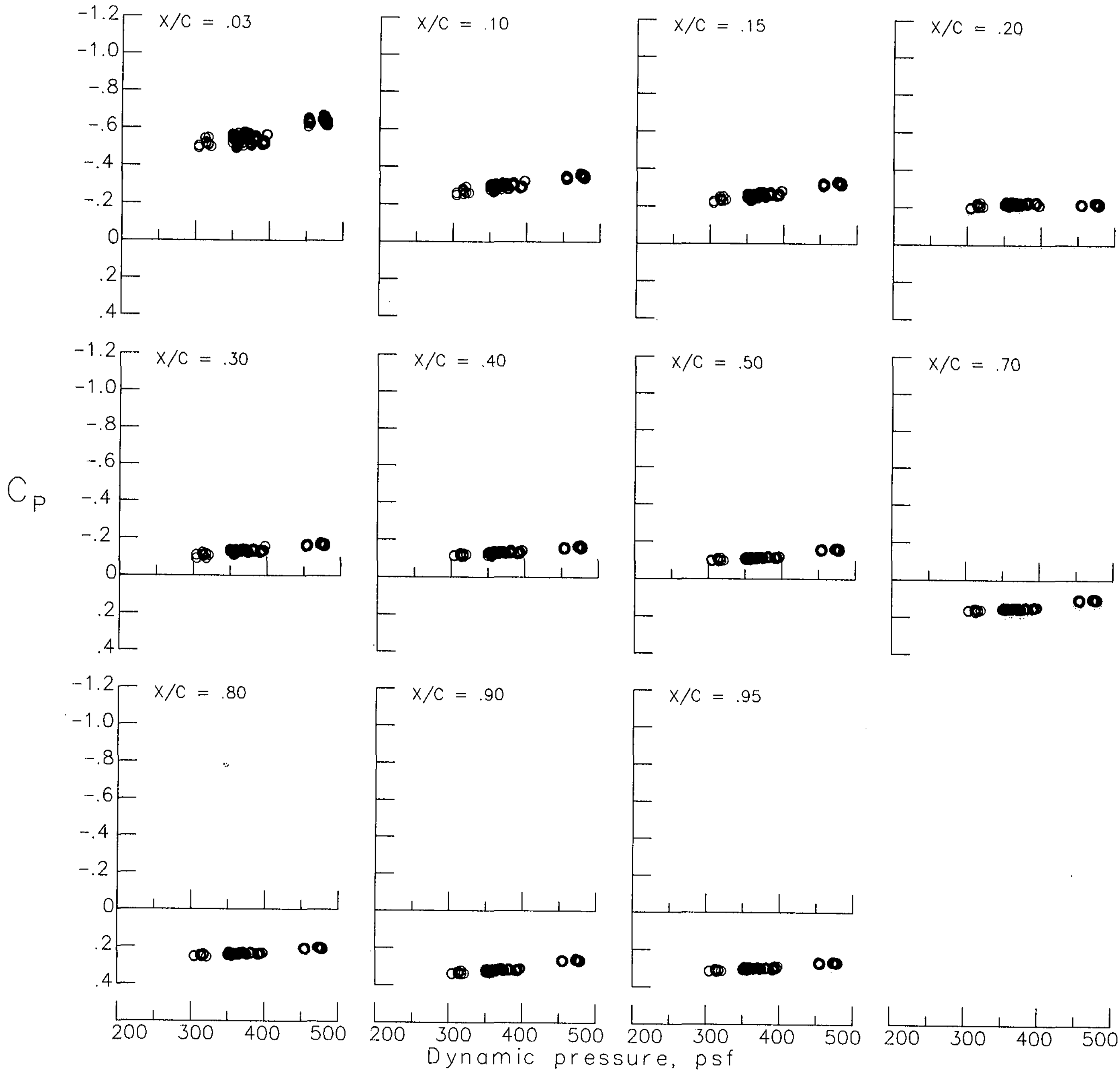

(d) Row 2, lower surface.

Figure 12.- Continued.

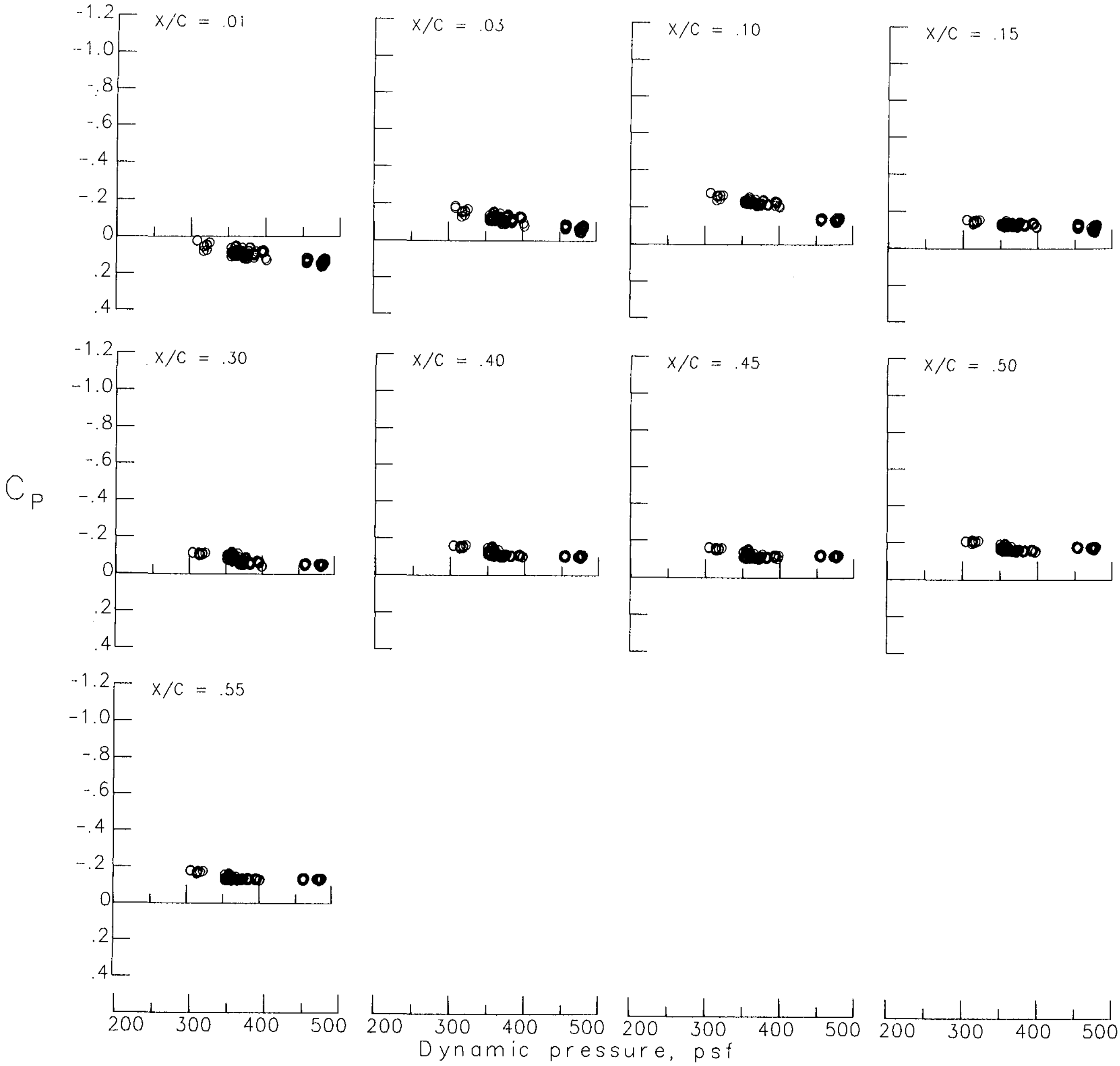

(e) Row 3, upper surface.

Figure 12.- Continued.

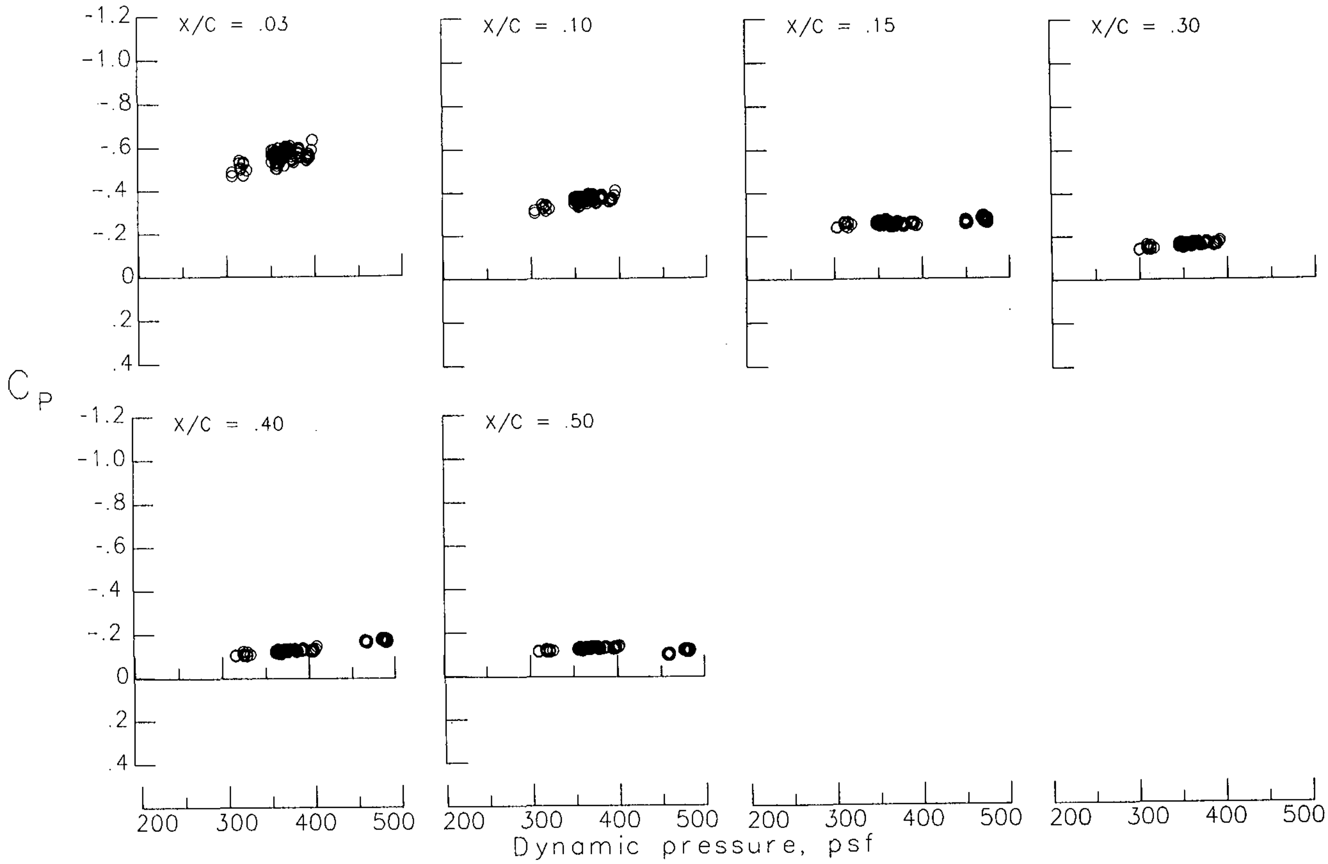

(f) Row 3, lower surface.

Figure 12.- Continued.

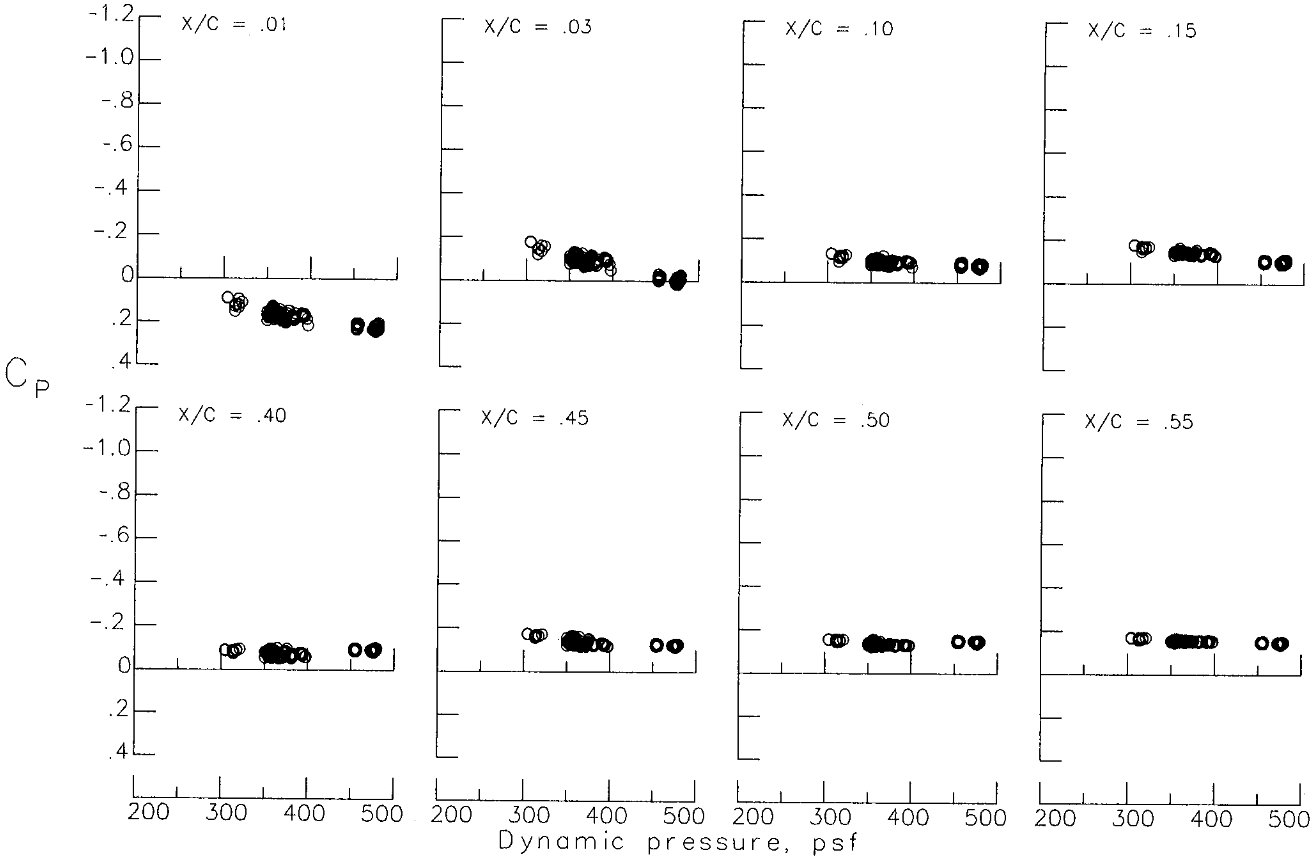

(g) Row 4, upper surface.

Figure 12.- Continued.

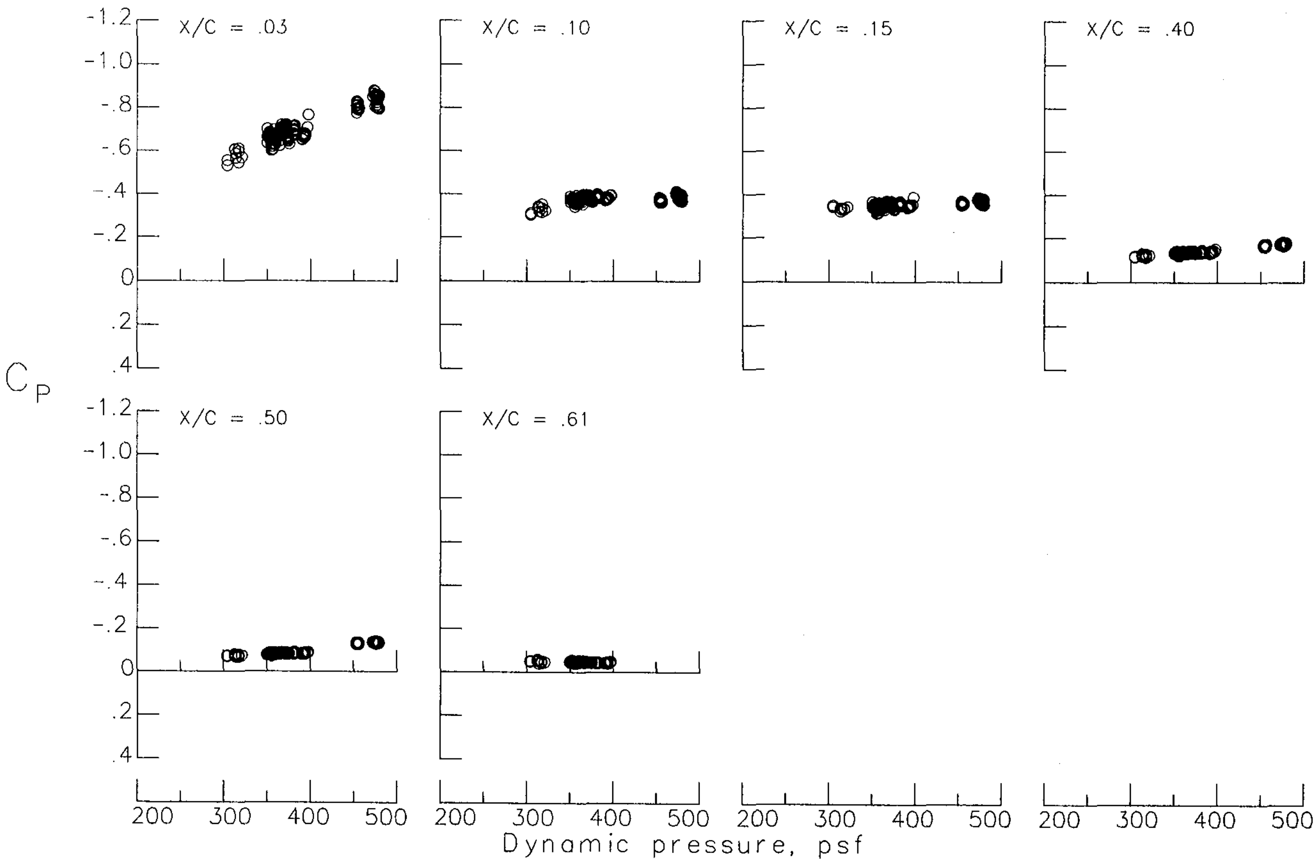

(h) Row 4, lower surface.

Figure 12.- Concluded.

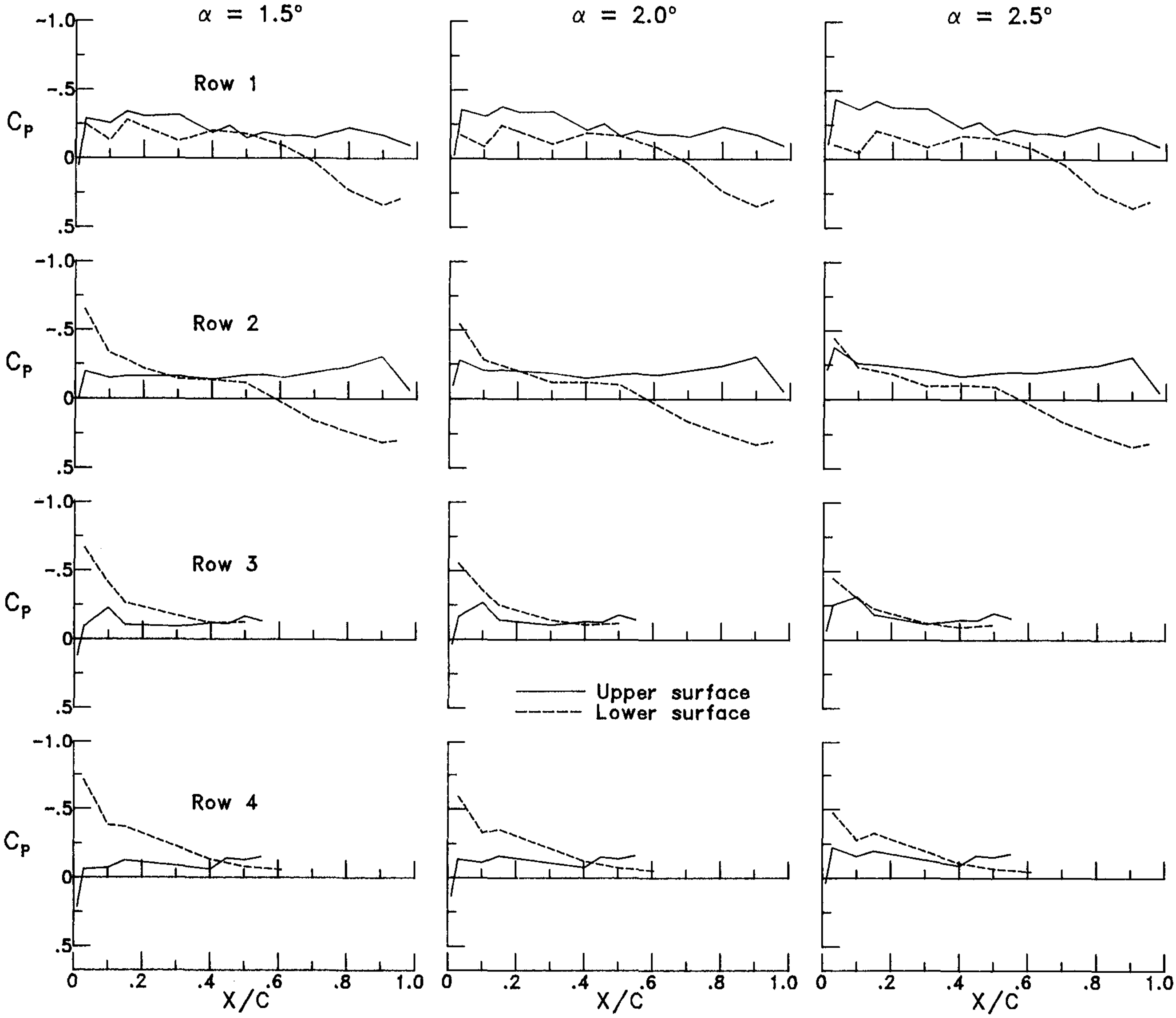

(a) M = 0.75; q_∞ = 320 psf.

Figure 13.- Chordwise pressure distributions for flight 10.

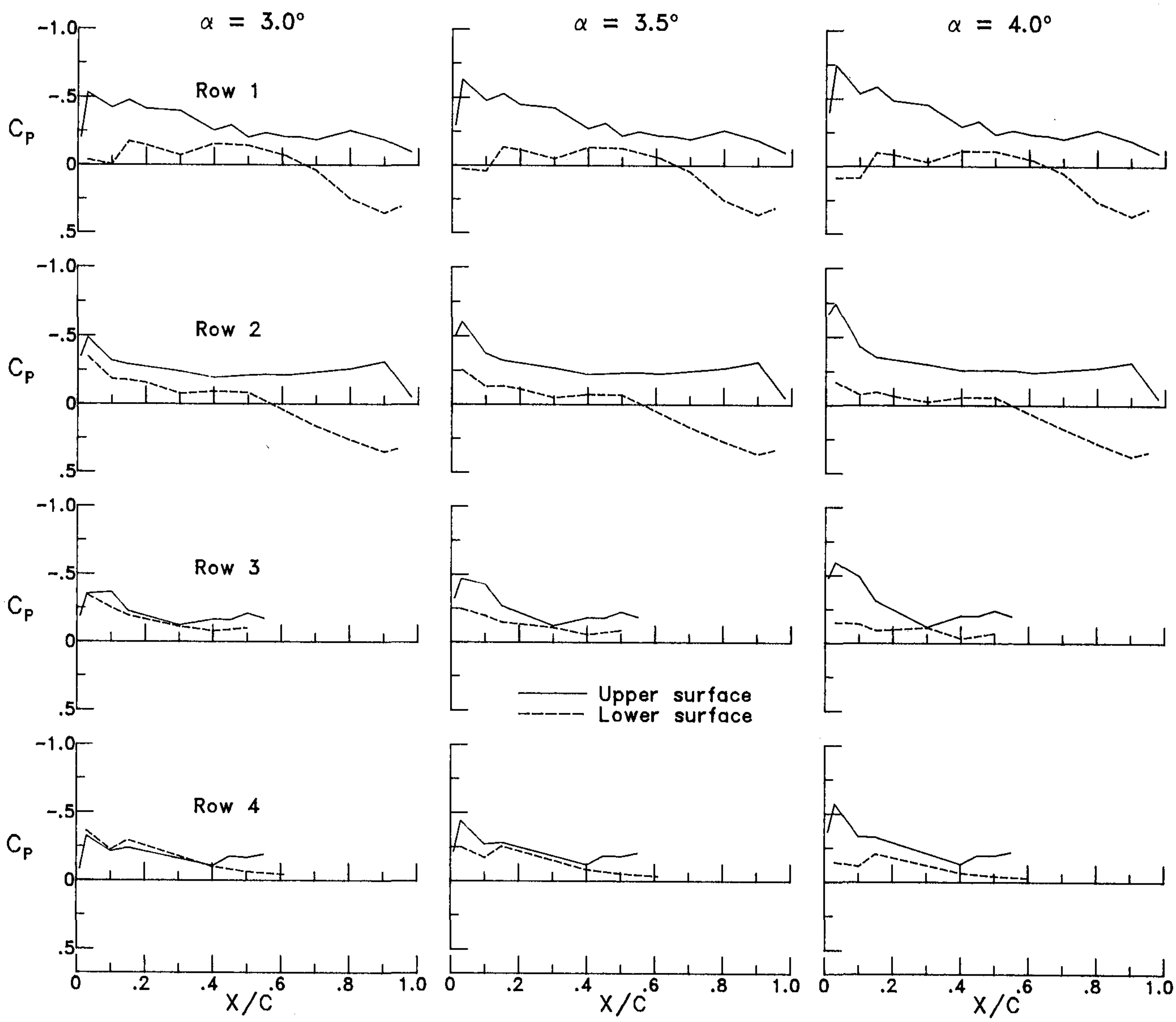

(a) Concluded.

Figure 13.- Continued.

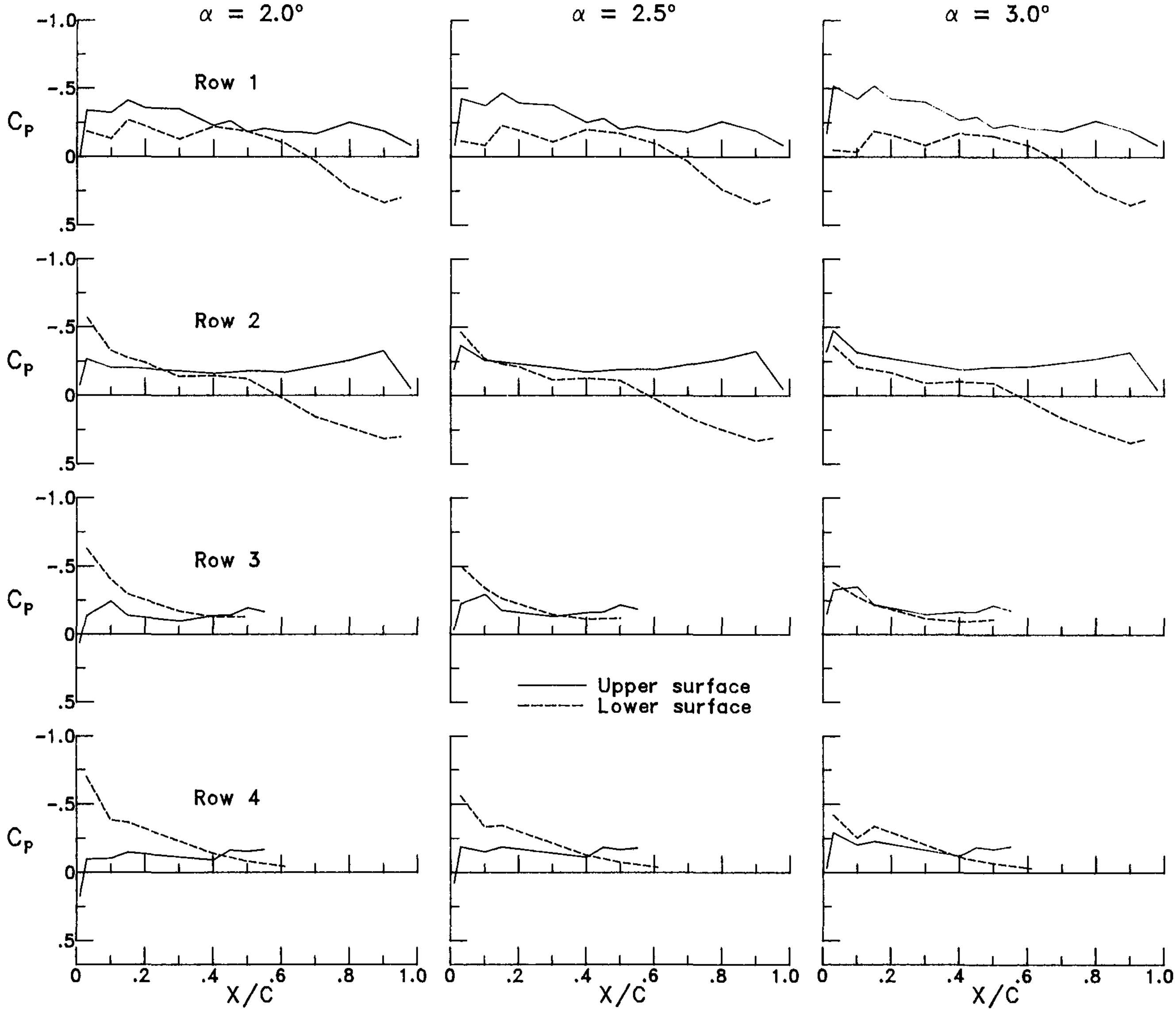

(b) M = 0.80; q_∞ = 359 psf.

Figure 13.- Continued.

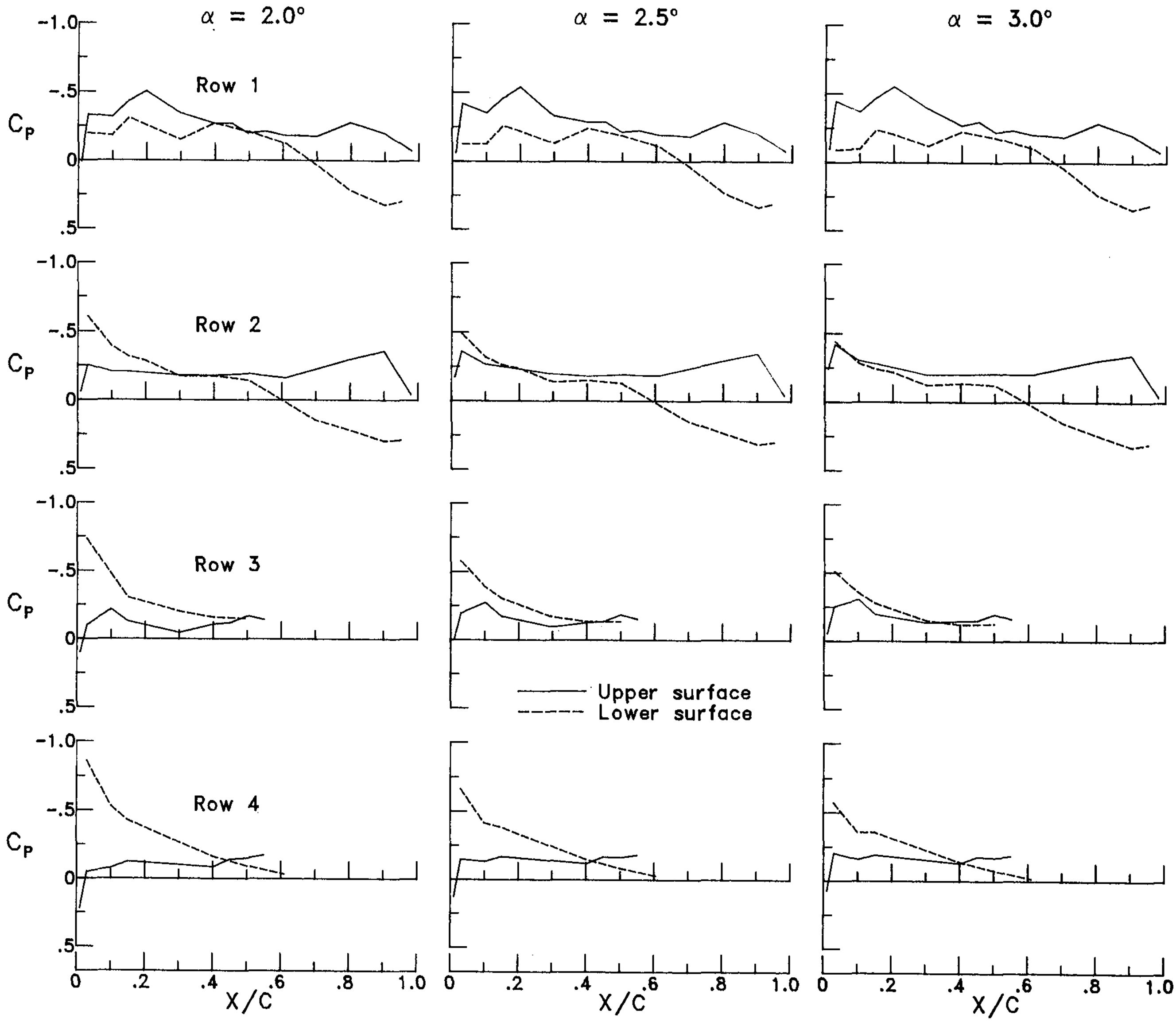

(c) M = 0.85; q_∞ = 406 psf.

Figure 13.- Continued.

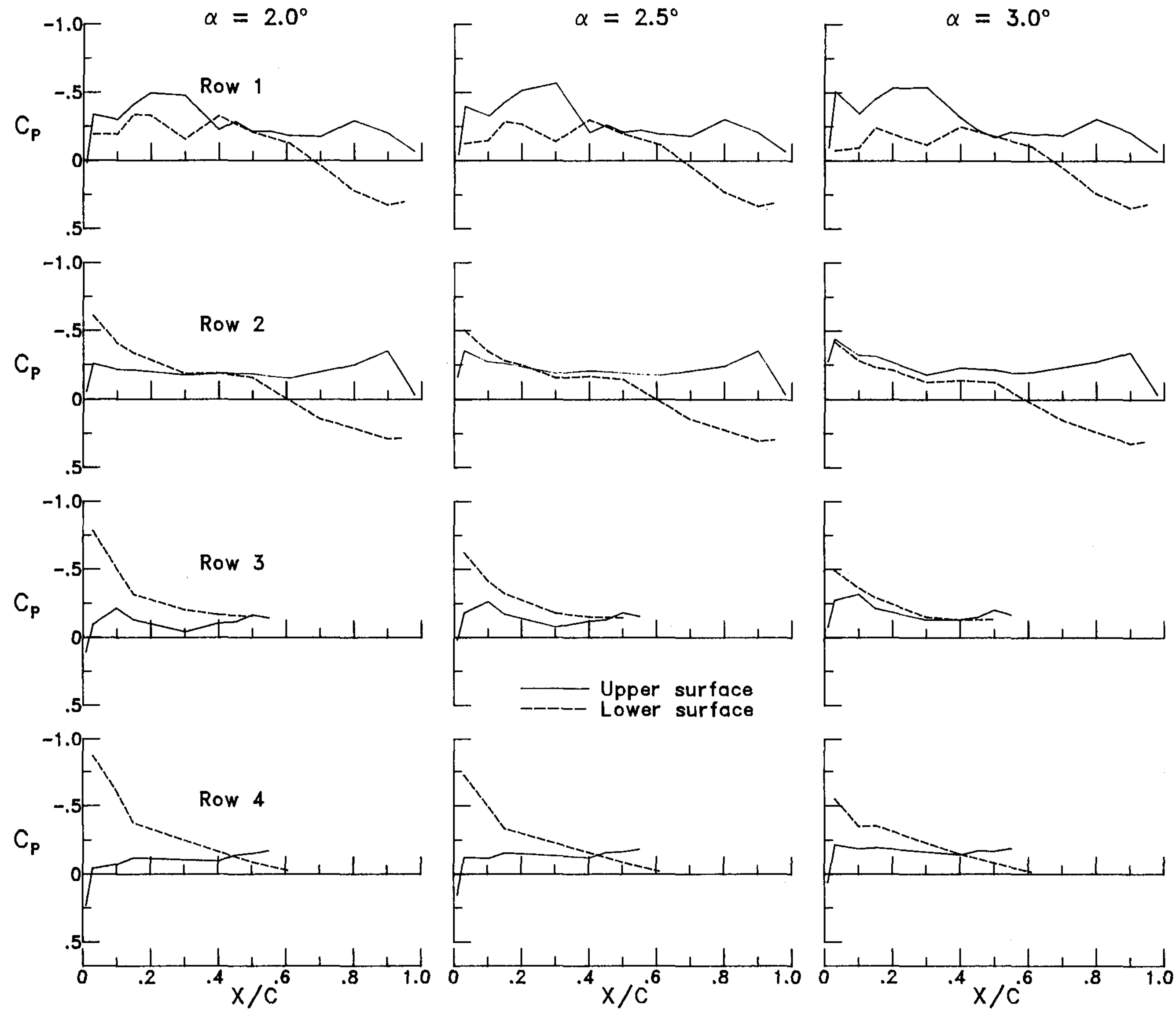

(d) M = 0.875; q_∞ = 430 psf.

Figure 13.- Continued.

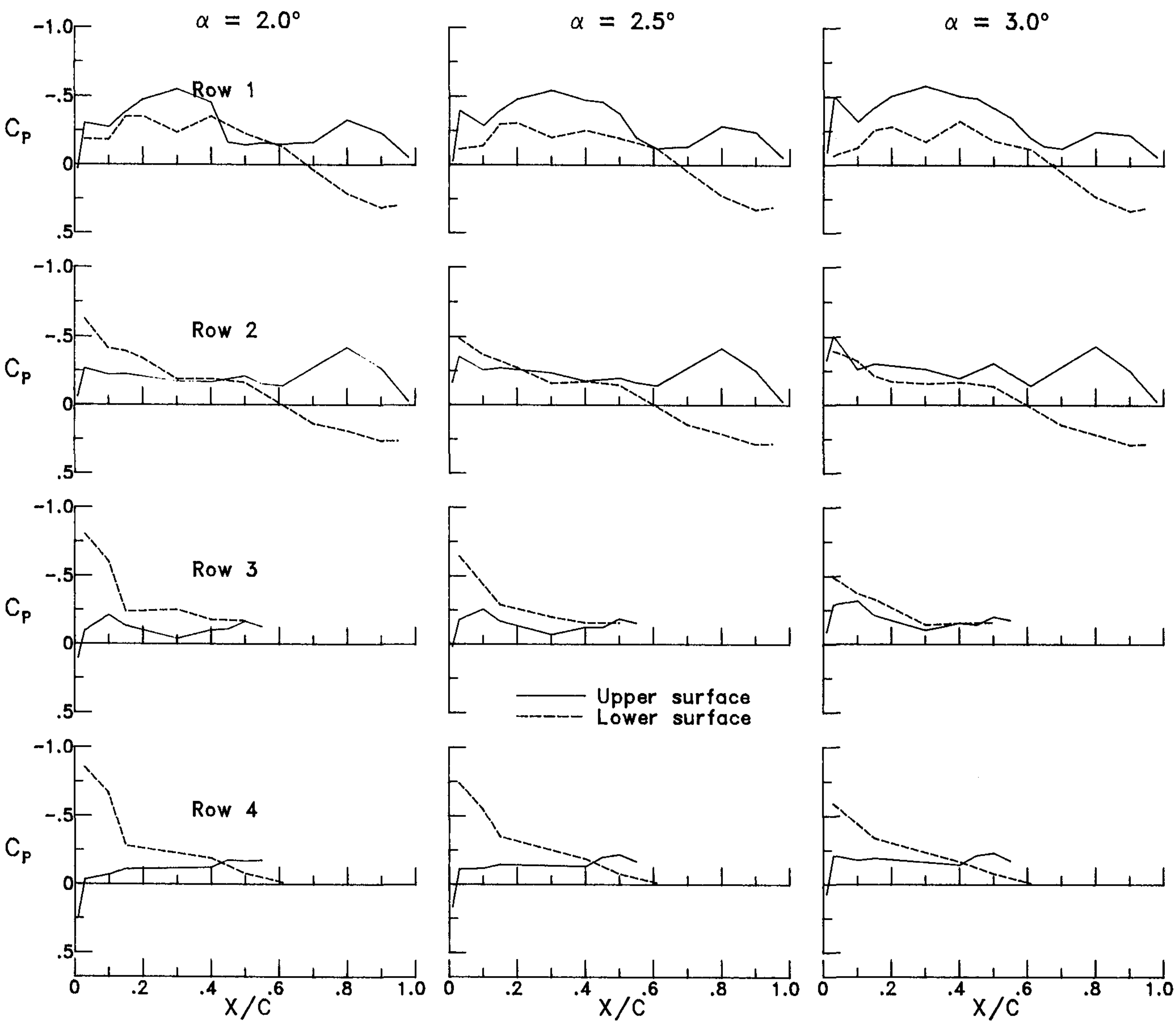

(e) M = 0.90; q_∞ = 455 psf.

Figure 13.- Concluded.

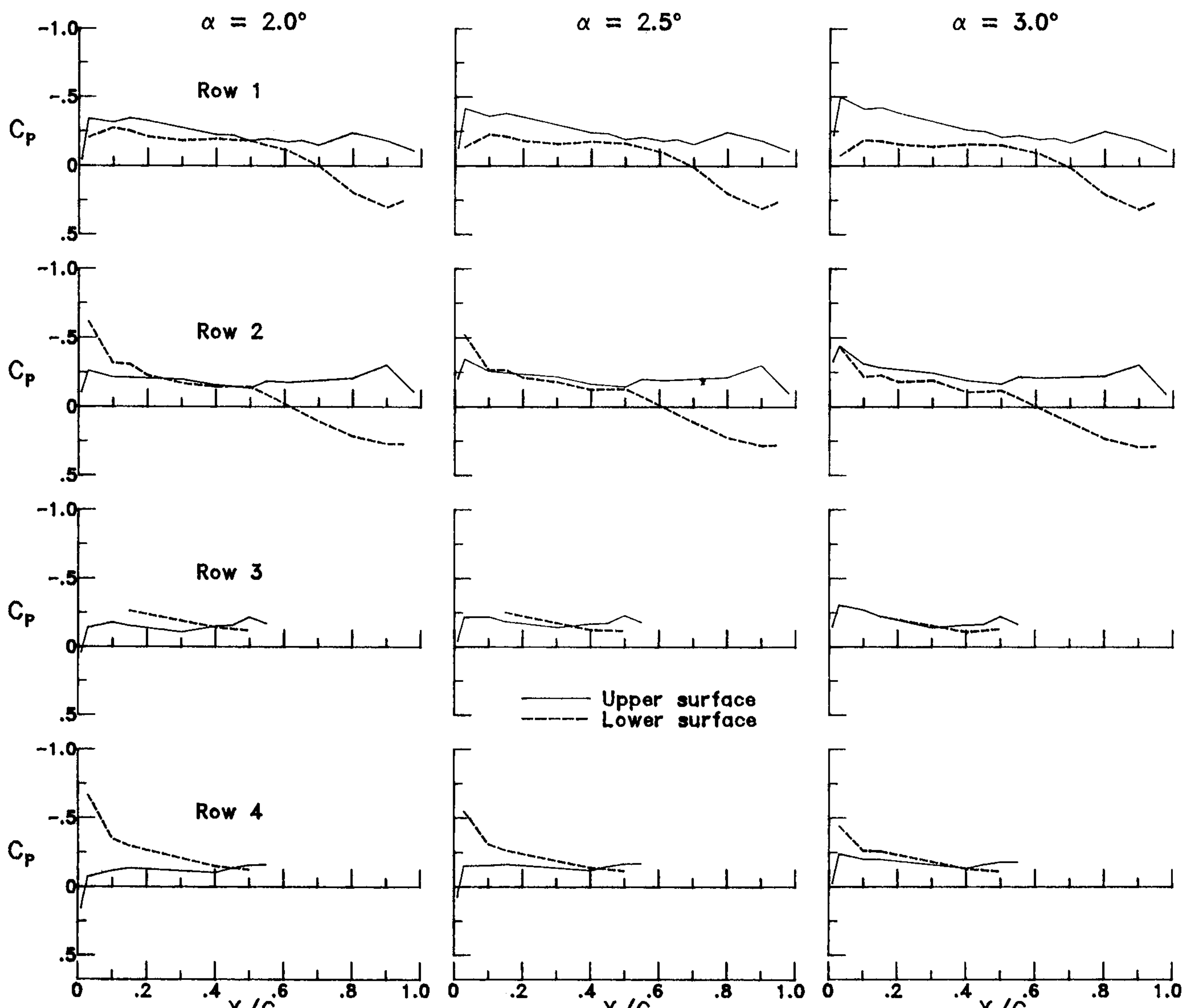

(a) M = 0.70; q_∞ = 415 psf.

Figure 14.- Chordwise pressure distributions for flight 11.

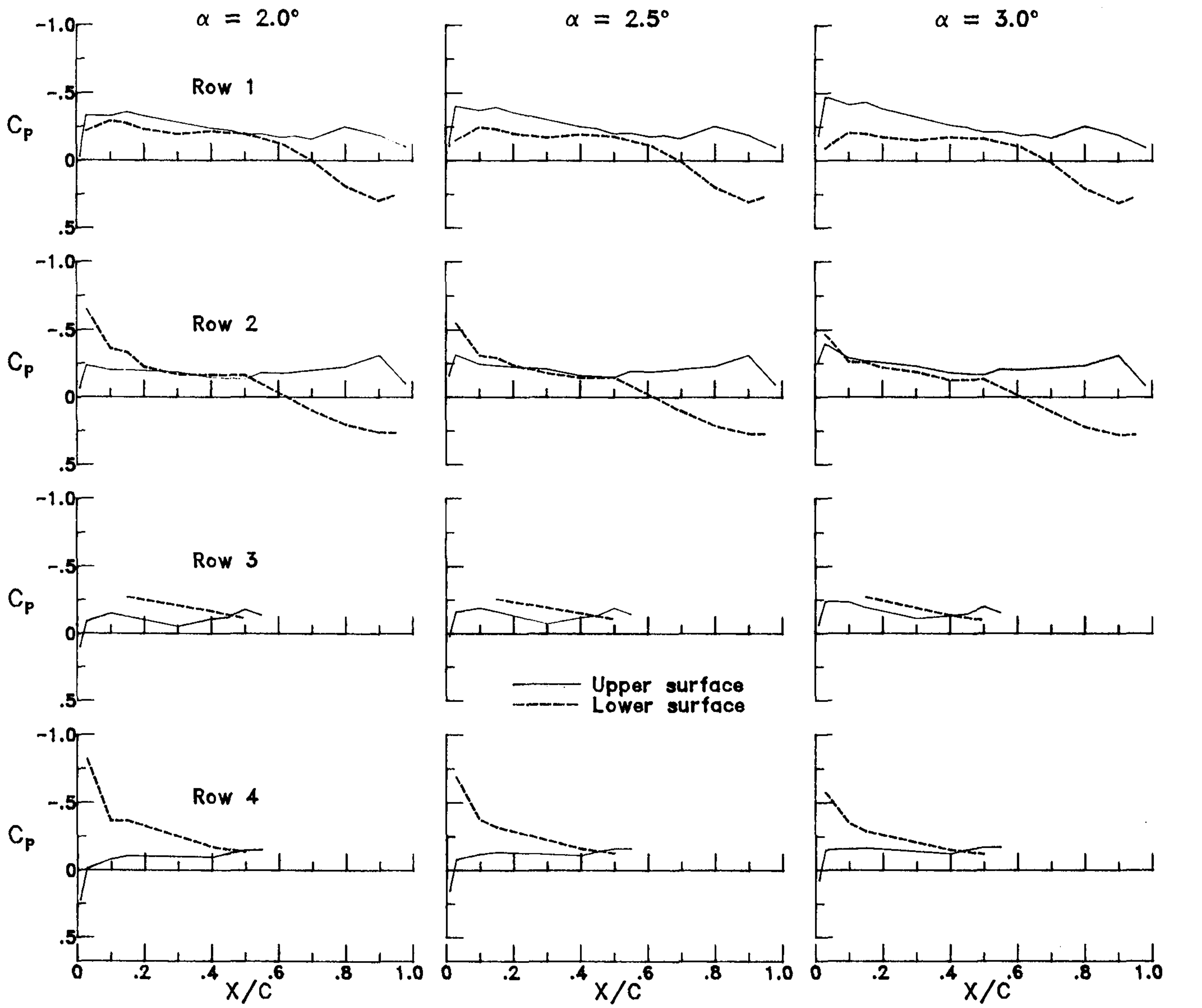

(b) M = 0.75; q_∞ = 467 psf.

Figure 14.- Continued.

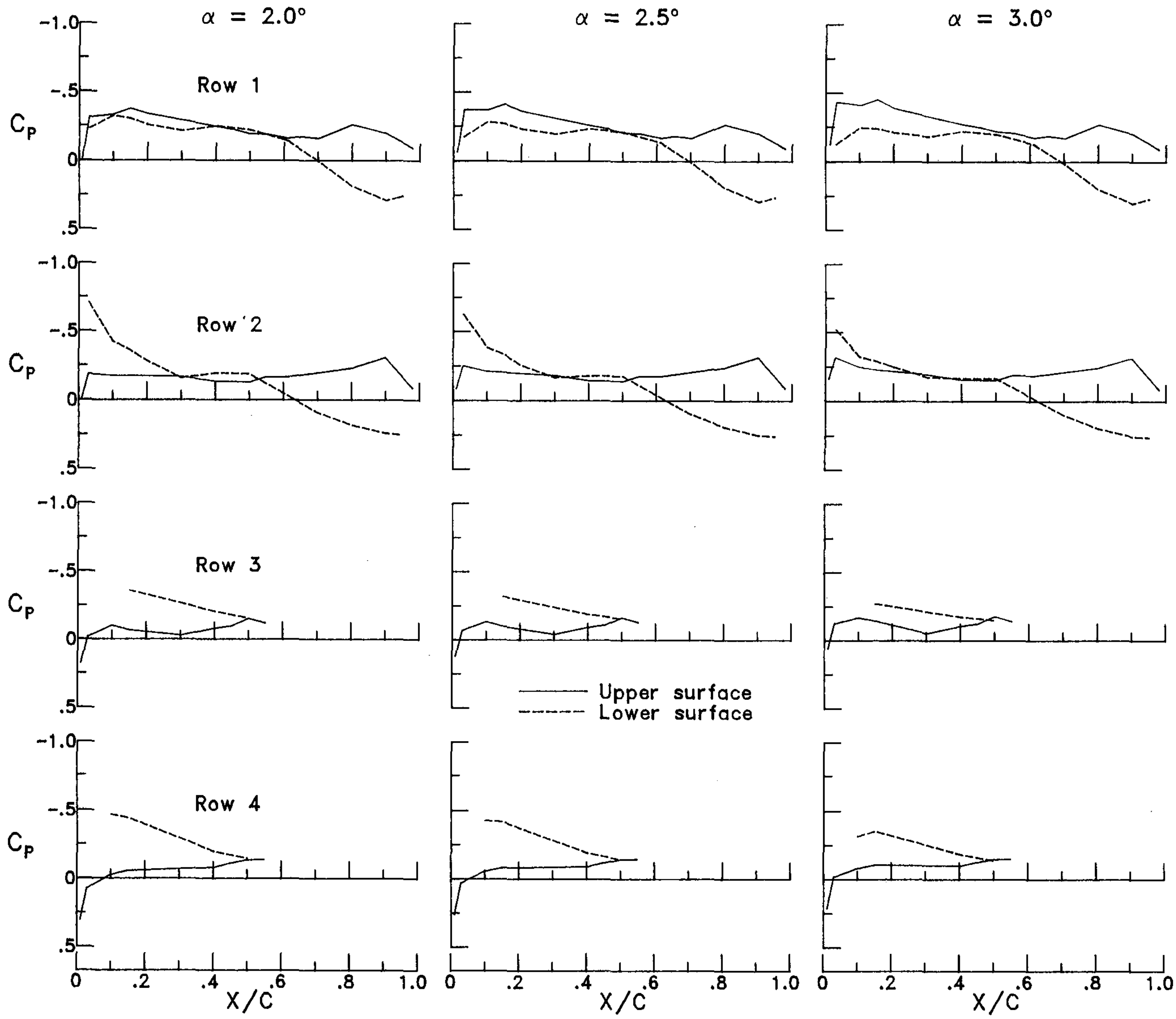

(c) M = 0.80; q_∞ = 538 psf.

Figure 14.- Concluded.

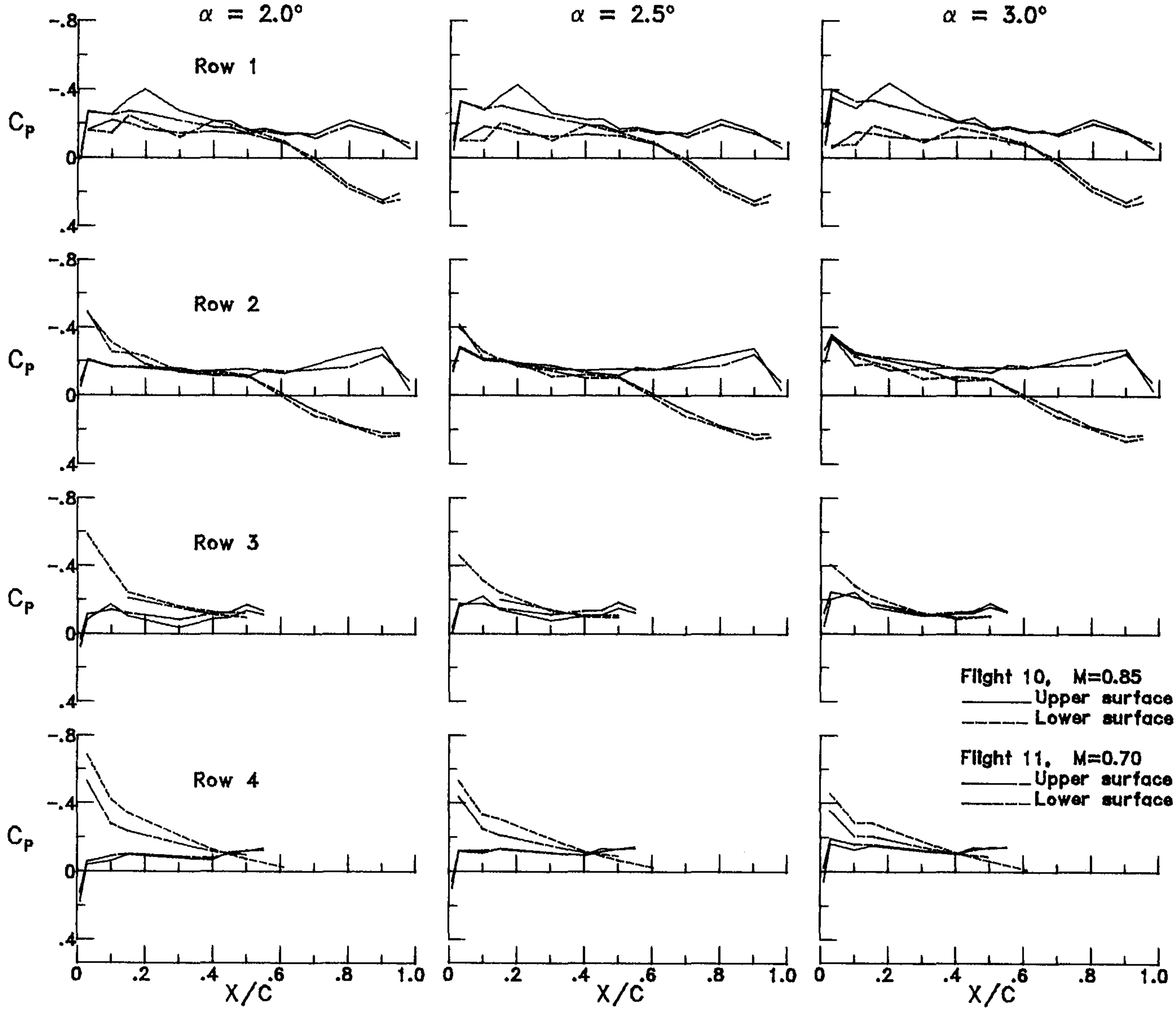

(a) M = 0.70; ($\bar{q}_\infty$ = 410 psf) and 0.85 ($\bar{q}_\infty$ = 406 psf).

Figure 15.- Variations of chordwise pressure distributions for different Mach numbers but approximately equal dynamic pressures.

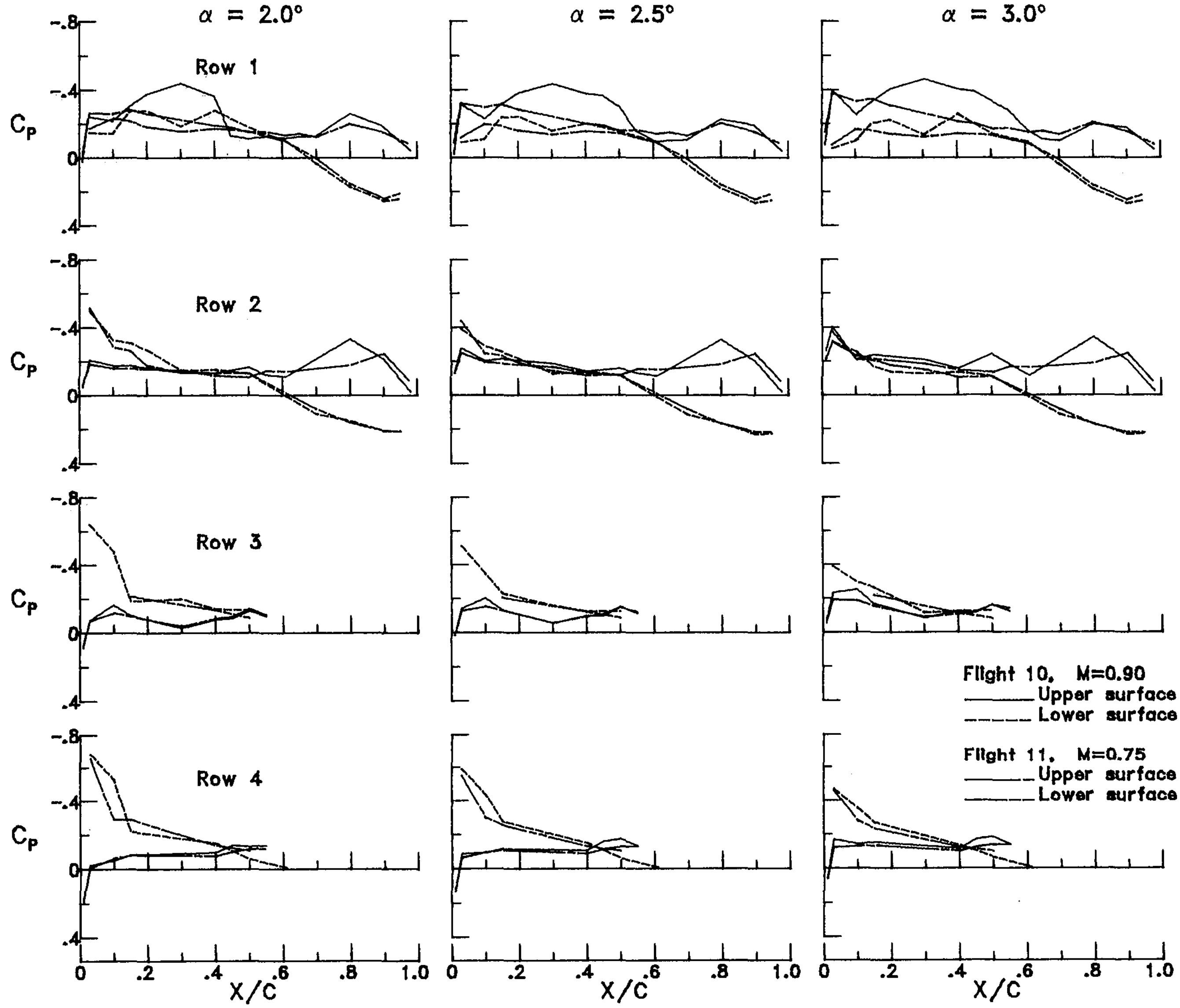

(b) M = 0.75; ($\bar{q}_\infty$ = 466 psf) and 0.90 ($\bar{q}_\infty$ = 456 psf).

Figure 15.- Concluded.

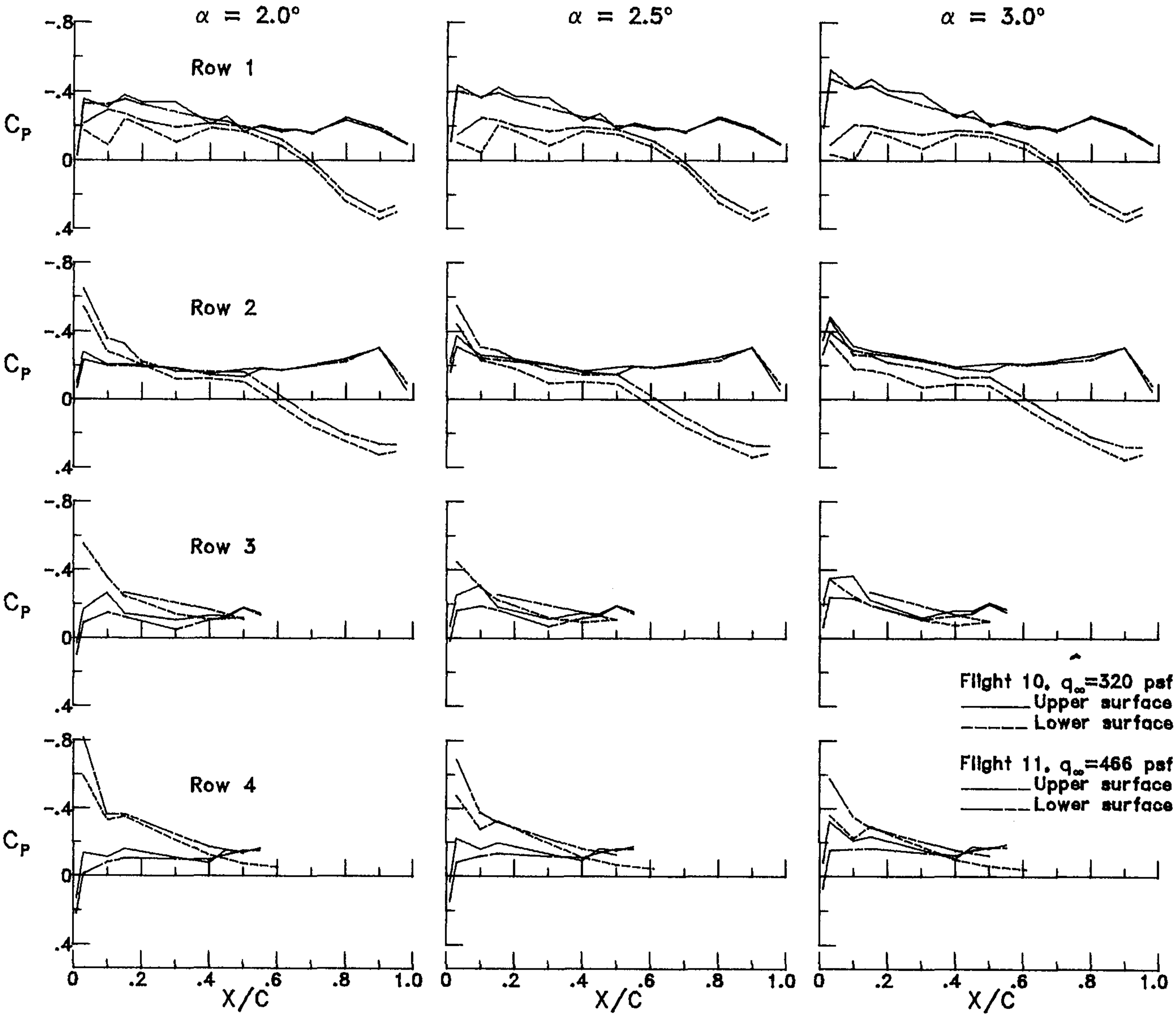

(a) M = 0.75.

Figure 16.- Variations of chordwise pressure distributions for equal Mach numbers but different dynamic pressures.

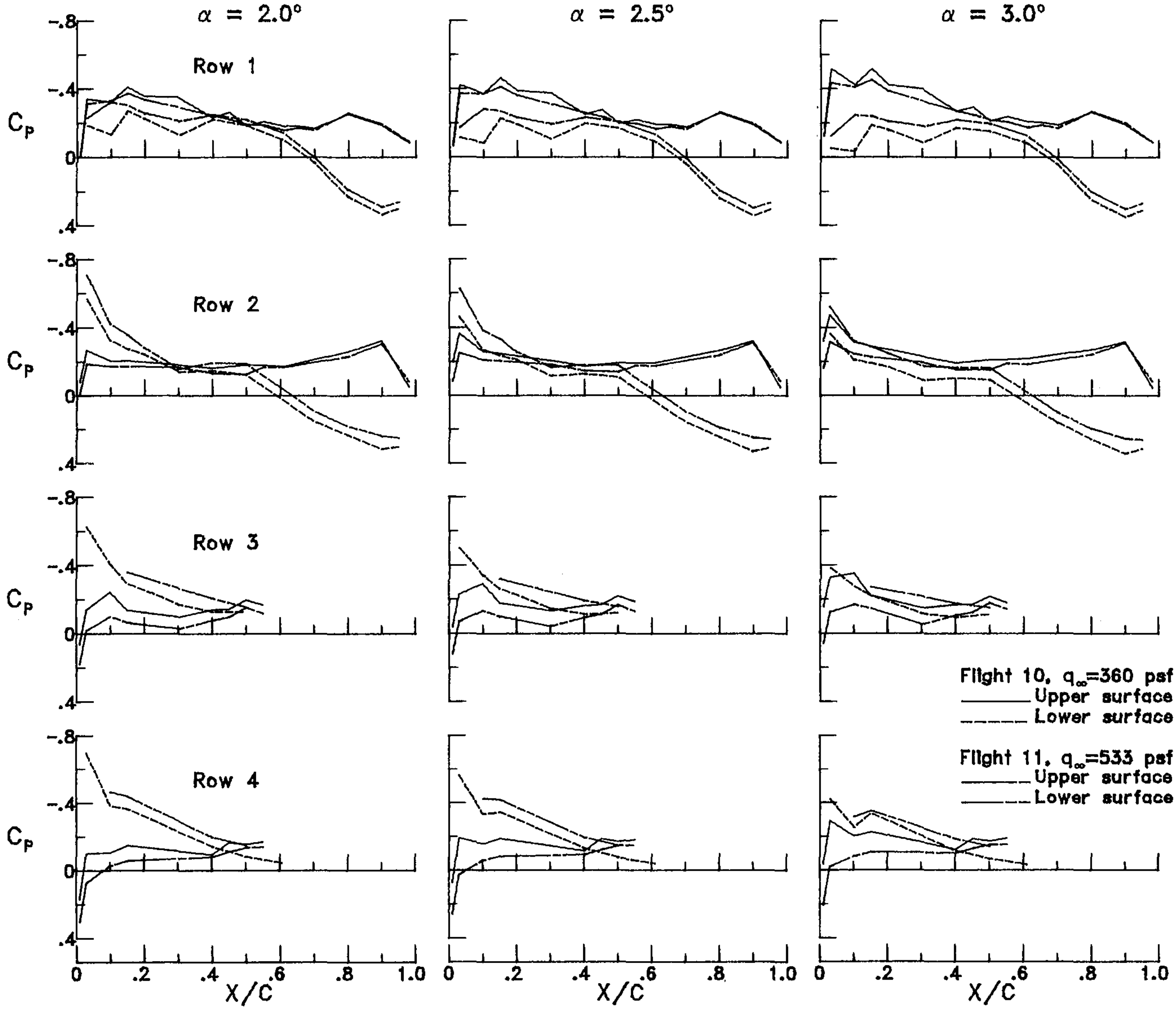

(b) M = 0.80.

Figure 16.- Concluded.

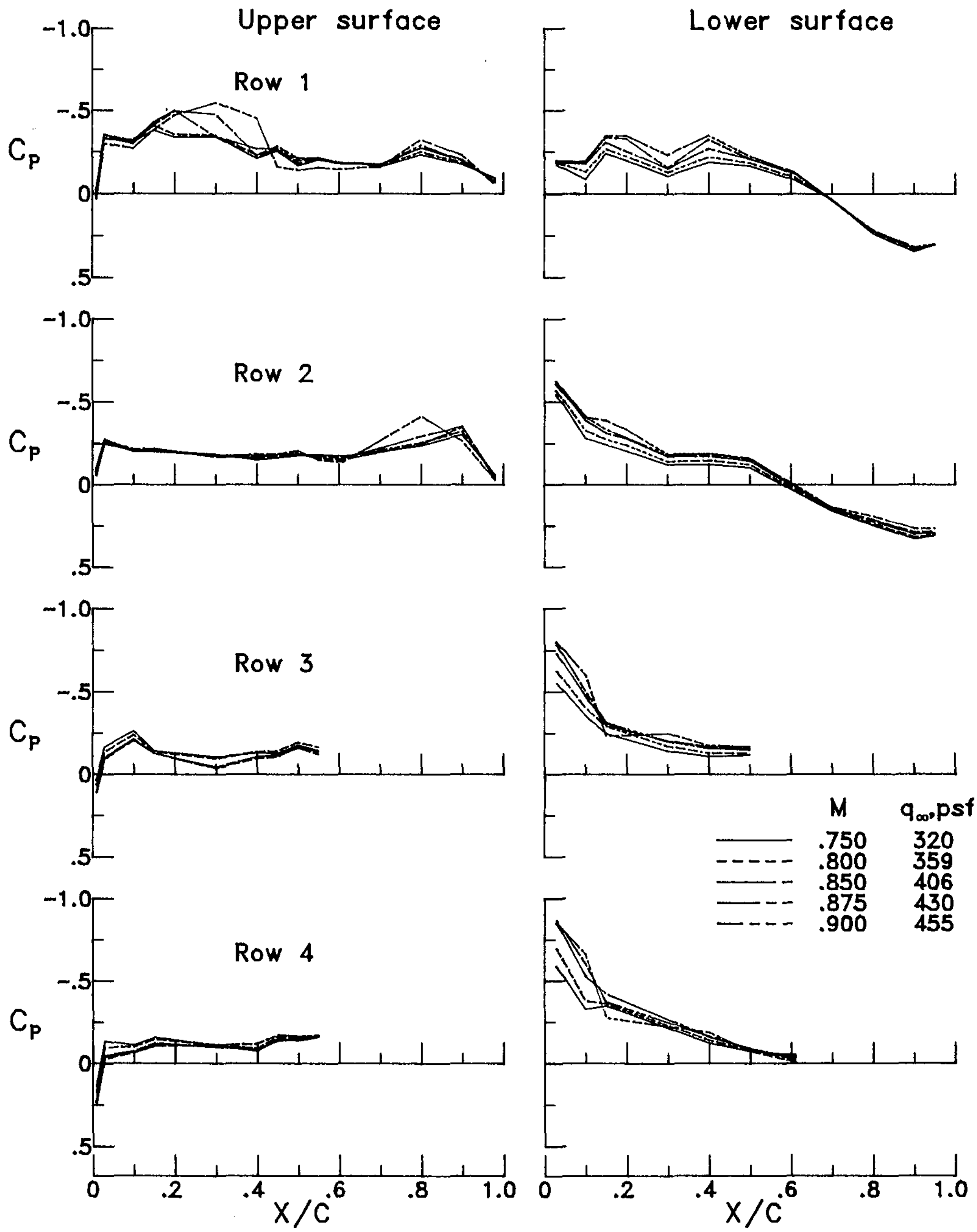

(a) α = 2.0°.

Figure 17.- Variations of chordwise pressure distributions with combined changes in Mach number and dynamic pressure for flight 10.

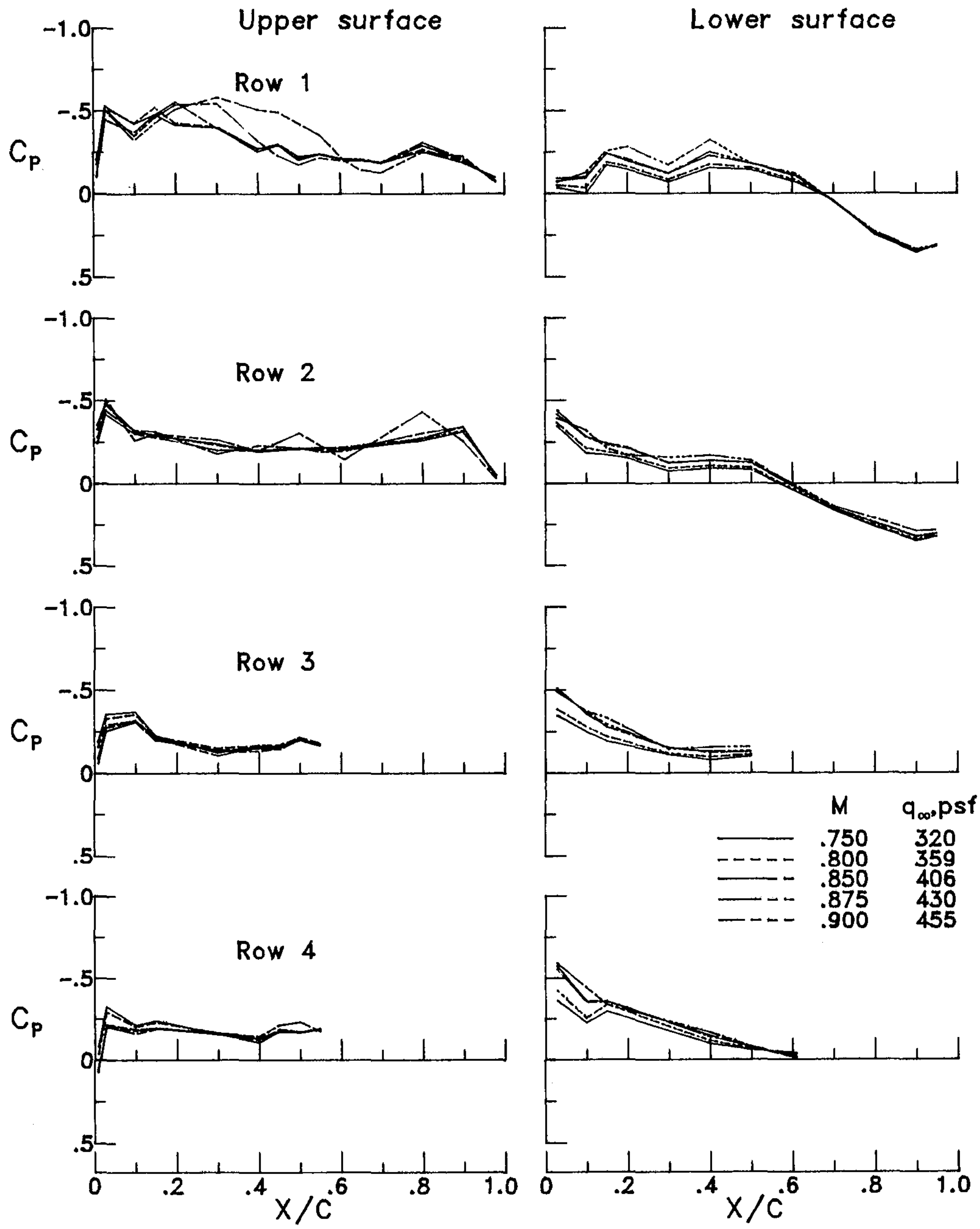

(b) α = 3.0°.

Figure 17.- Concluded.

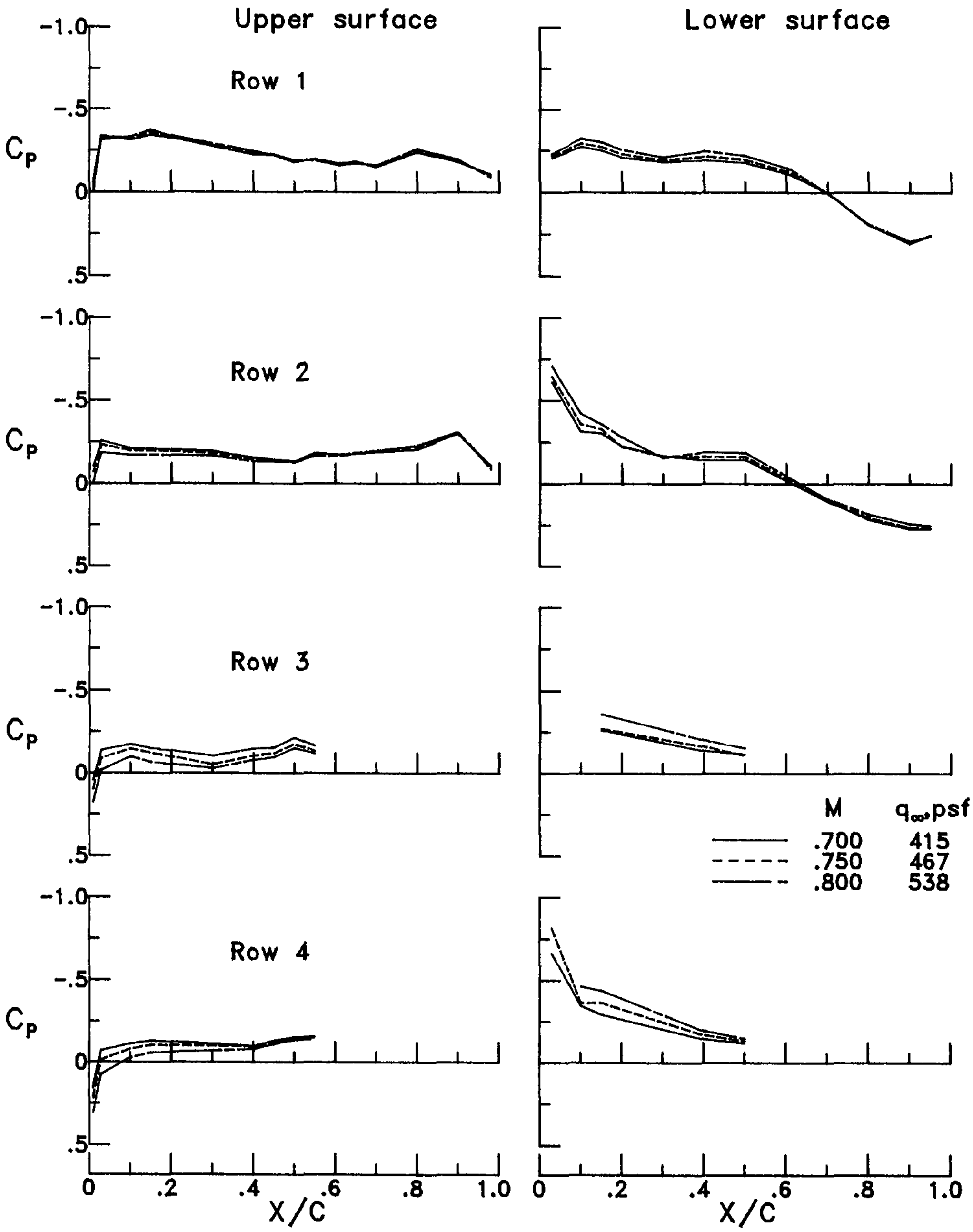

(a) α = 2.0°.

Figure 18.- Variations of chordwise pressure distributions with combined changes in Mach number and dynamic pressure for flight 11.

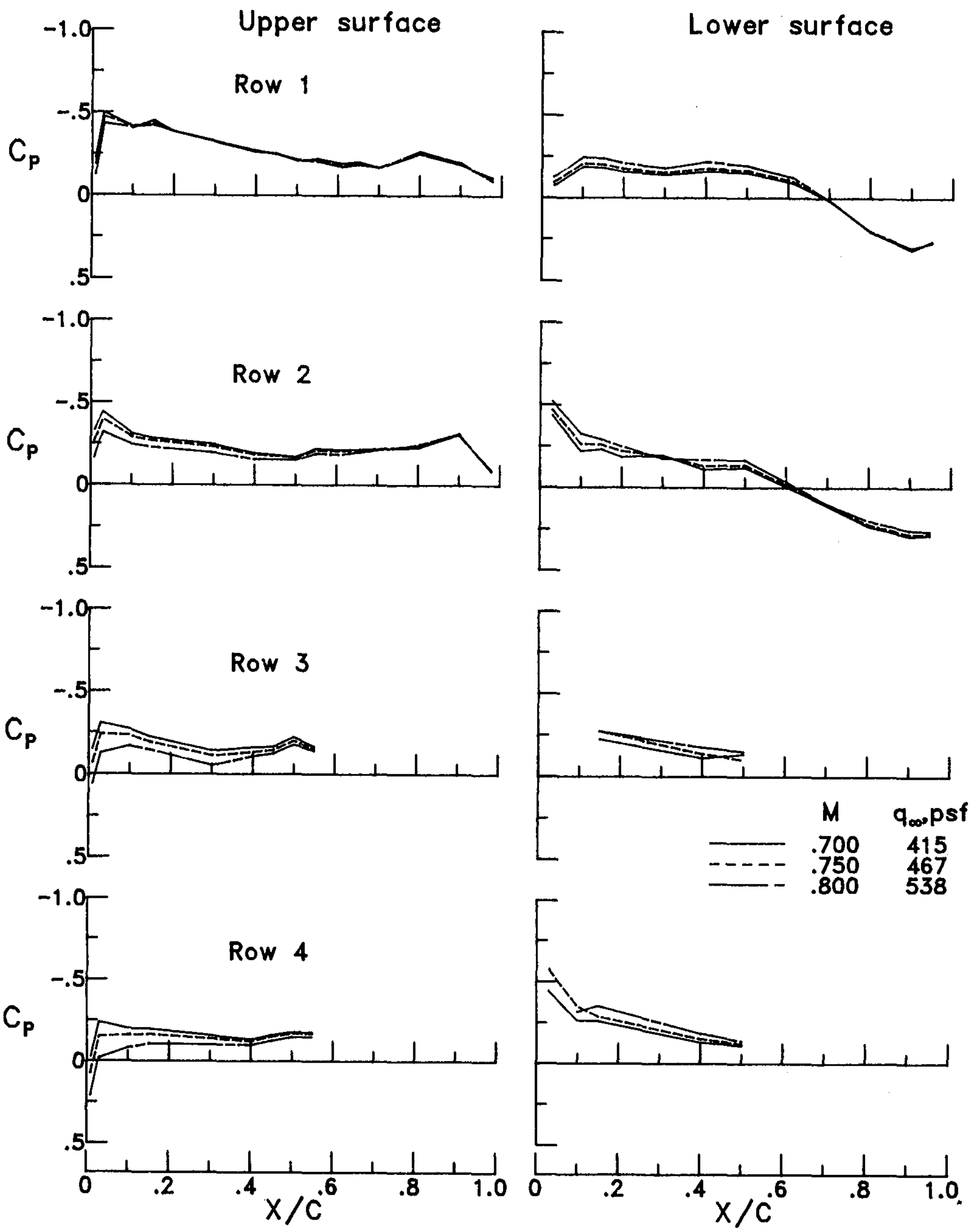

(b) α = 3.0°.

Figure 18.- Concluded.

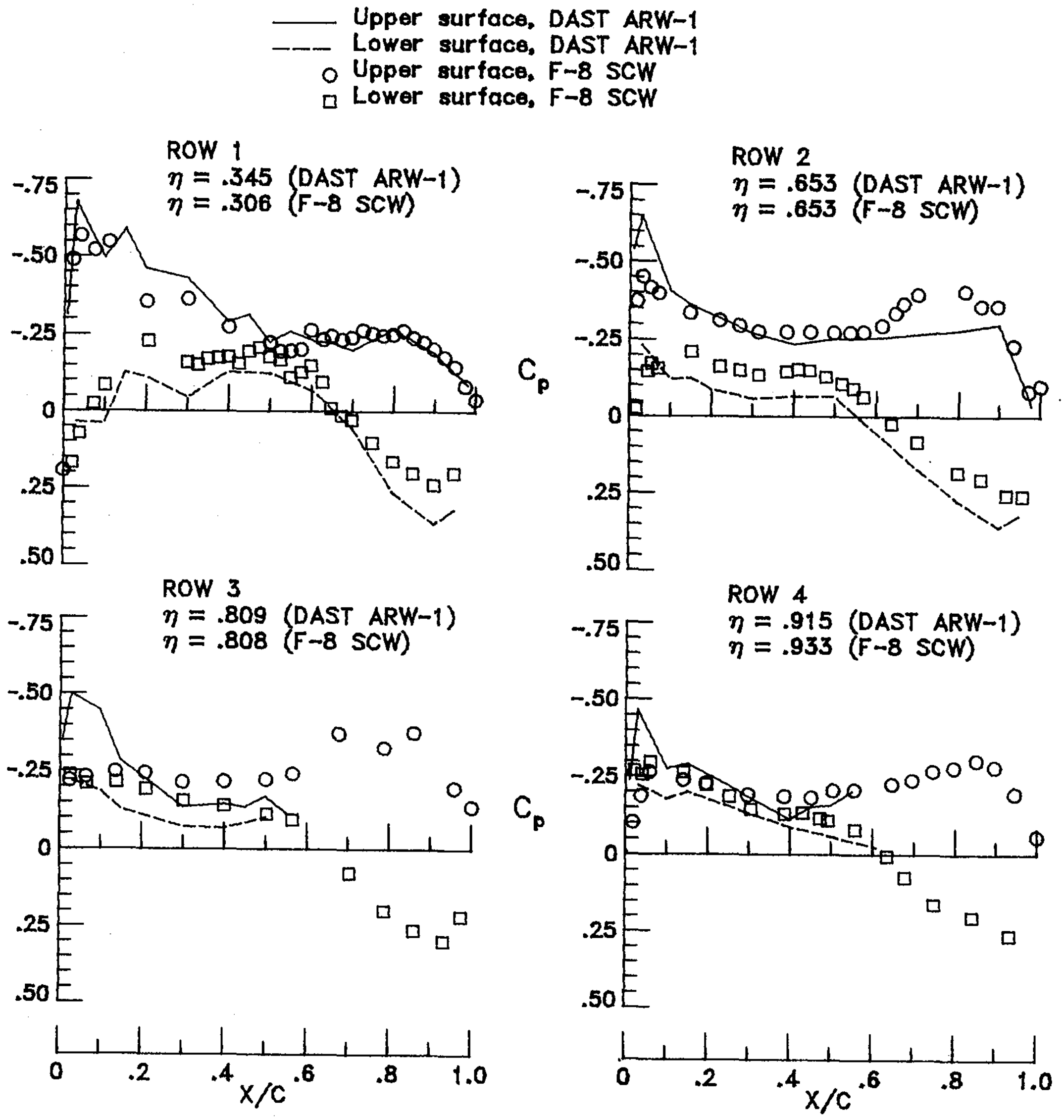

Figure 19.- Variations of chordwise pressure distributions from flight tests of DAST ARW-1 and F-8 SCW. M = 0.80; $\alpha = 3.73°$.

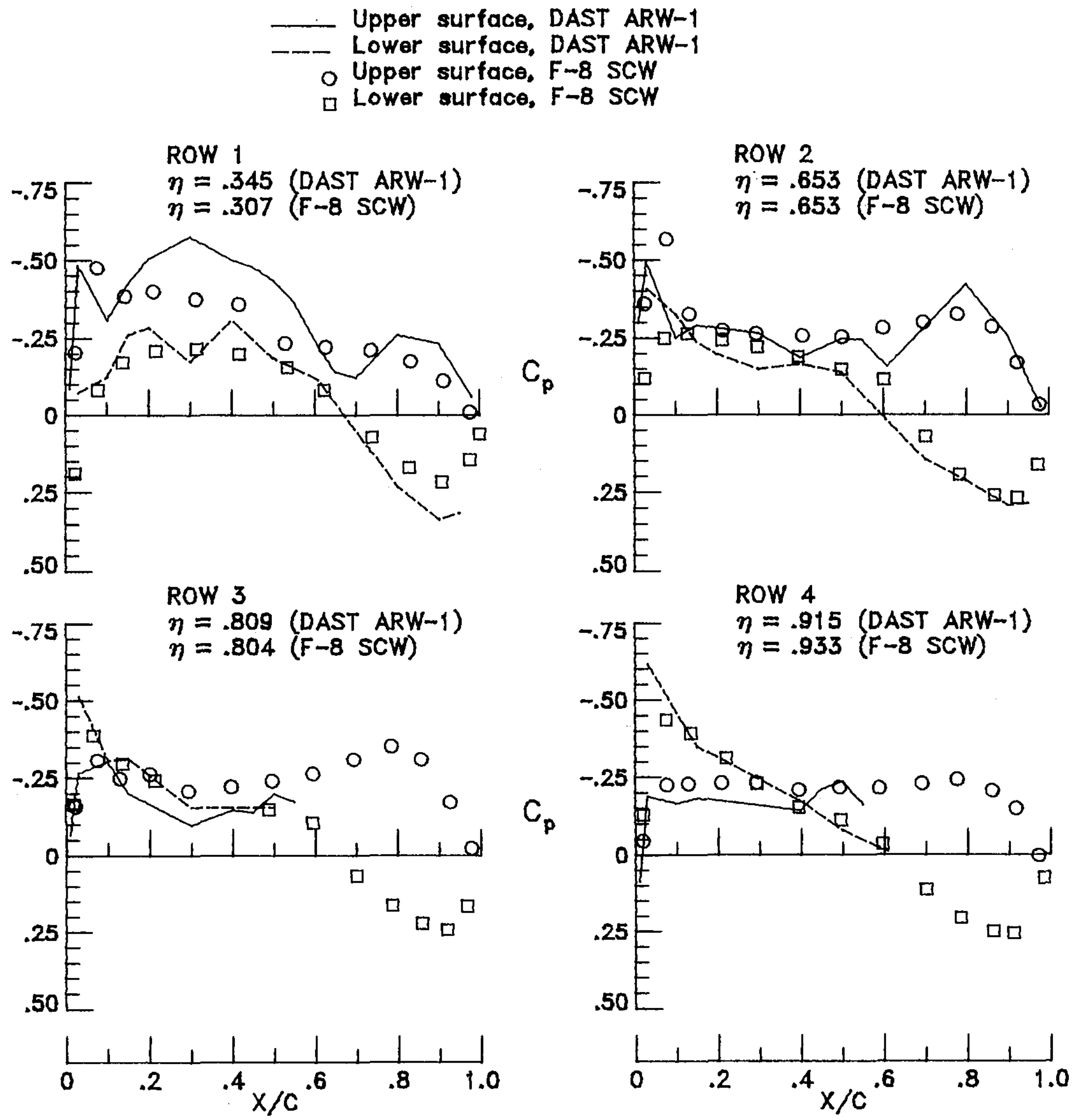

(a) M = 0.80; α = 2.90°.

Figure 20.- Variations of chordwise surface pressure distributions from DAST ARW-1 flight tests and F-8 SCW scaled-model wind-tunnel results.

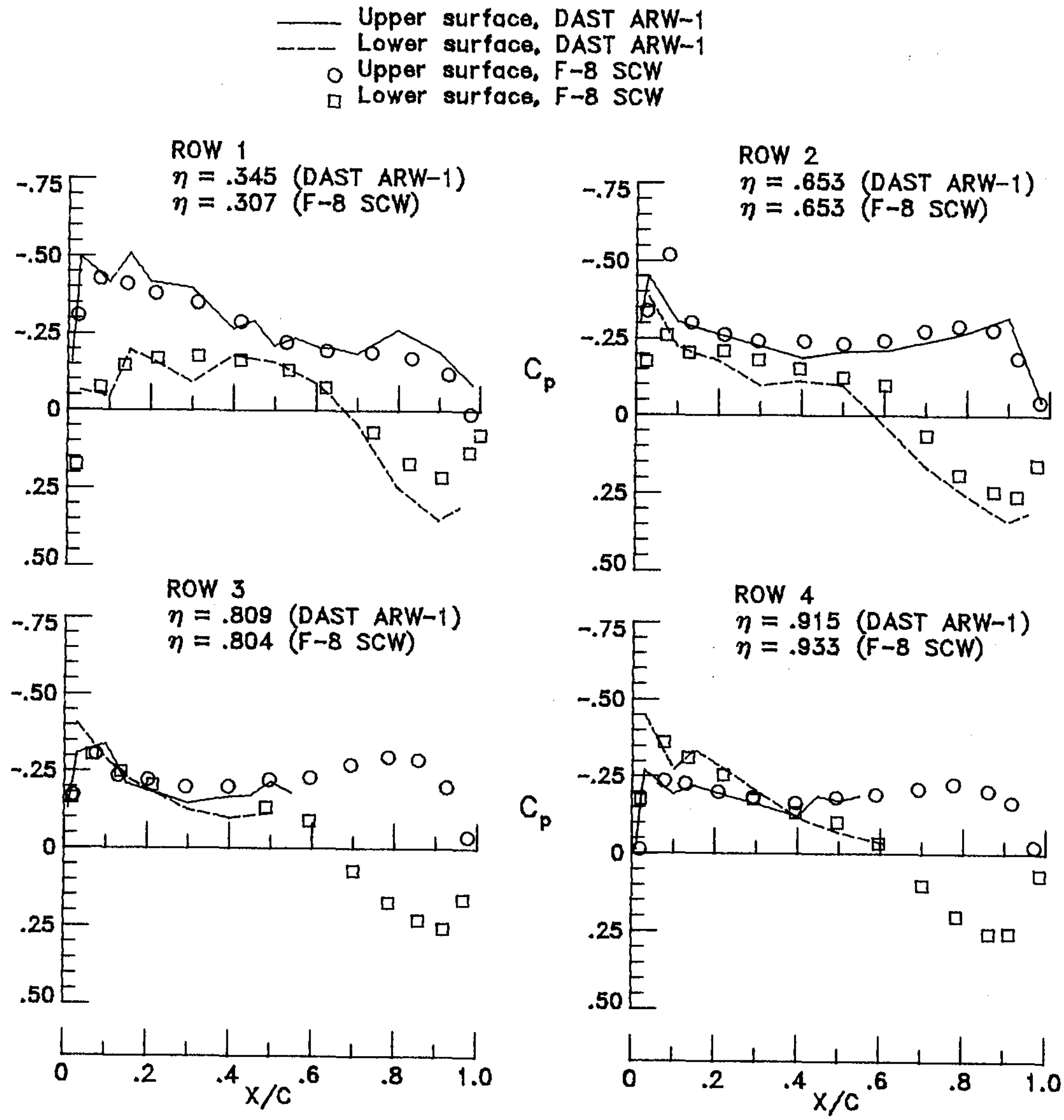

(b) M = 0.90; α = 2.91°.

Figure 20.- Concluded.

1. Report No. NASA TP-2501	2. Government Accession No.	3. Recipient's Catalog No.
4. Title and Subtitle Flight Measurements of Surface Pressures on a Flexible Supercritical Research Wing		5. Report Date December 1985
		6. Performing Organization Code 505-33-43-08
7. Author(s) Clinton V. Eckstrom		8. Performing Organization Report No. L-15877
9. Performing Organization Name and Address NASA Langley Research Center Hampton, VA 23665-5225		10. Work Unit No.
		11. Contract or Grant No.
12. Sponsoring Agency Name and Address National Aeronautics and Space Administration Washington, DC 20546-0001		13. Type of Report and Period Covered Technical Paper
		14. Sponsoring Agency Code

15. Supplementary Notes

16. Abstract

A flexible supercritical research wing, designated as ARW-1, was flight-tested as part of the NASA Drones for Aerodynamic and Structural Testing (DAST) Program. Aerodynamic loads, in the form of wing surface pressure measurements, were obtained during flights at altitudes of 15 000, 20 000, and 25 000 feet at Mach numbers from 0.70 to 0.91. Surface pressure coefficients determined from pressure measurements at 80 orifice locations are presented individually as nearly continuous functions of angle of attack for constant values of Mach number. The surface pressure coefficients are also presented individually as a function of Mach number for an angle of attack of 2.0°. The nearly continuous values of the pressure coefficient clearly show details of the pressure gradient, which occurred in a rather narrow Mach number range. The effects of changes in angle of attack, Mach number, and dynamic pressure are also shown by chordwise pressure distributions for the range of test conditions experienced. Reynolds numbers for the tests ranged from 5.7 to 8.4×10^6.

17. Key Words (Suggested by Authors(s))	18. Distribution Statement
Surface pressure measurements Supercritical wing Flight test results Flexible wing	Unclassified - Unlimited Subject Category 02

19. Security Classif.(of this report)	20. Security Classif.(of this page)	21. No. of Pages	22. Price
Unclassified	Unclassified	118	A06

For sale by the National Technical Information Service, Springfield, Virginia 22161

NASA-Langley, 1985

National Aeronautics and
Space Administration
Code NIT-4

Washington, D.C.
20546-0001

Official Business
Penalty for Private Use, $300

NASA

POSTMASTER: If Undeliverable (Section 158 Postal Manual) Do Not Return